PURDUE UNIVERSITY
SCHOOL OF ELECTRICAL ENGINEERING
ELECTRONIC SYSTEMS RESEARCH LABORATORY

THRESHOLD STUDY OF PHASE LOCK LOOP SYSTEMS

by

J. C. Lindenlaub and J. J. Uhran

Technical Report No. TR–EE 66–19
Sponsored by National Aeronautics and Space Administration
under Grant NsG–553

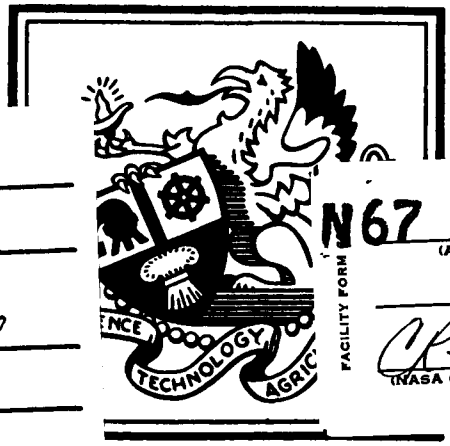

DECEMBER 1966
LAFAYETTE, INDIANA

Technical Report TR-EE 66-19

THRESHOLD STUDY OF PHASE LOCK SYSTEMS

An Interim Report Submitted to

NATIONAL AERONAUTICS AND SPACE ADMINISTRATION

WASHINGTON D.C.

Under
Grant NsG-553

by
John C. Lindenlaub, Principal Investigator
John J. Uhran

December, 1966

Electronic Systems Research Laboratory
School of Electrical Engineering
Purdue University
Lafayette, Indiana

FOREWORD

This report is an interim report which summarizes one phase of research that is being carried out at Purdue University in the area of communication theory under NASA Grant NsG-553.

TABLE OF CONTENTS

Page

Page

LIST OF TABLES

LIST OF FIGURES

Page

Figure

Figure Page

Appendix Figures

Page

ABSTRACT

This research has been concerned with the study of two aspects of phase lock loop systems. The first is the effect that the phase comparator, a non-linear device operating on the phase difference between reference and signal has on overall performance. The second directly related to the first, is the study and defining of the threshold phenomena.

Several comparators were chosen ad-hoc and analyzed using a Fokker-Planck model. Because the model is only approximate in the threshold region a carefully designed experimental evaluation of a first and second order sine, tanlock and tanlock squared comparator was undertaken.

It is shown that the additional complexity involved in using other comparators rather than the relatively simple sine comparators can be justified particularly when additional tracking range is required. For second order systems, it is shown that critical damping provides optimum performance in terms of tracking and threshold. The inclusion of a section on the limiter is given for comparison purposes.

The threshold is defined in terms of the rate of cycle slipping i.e., as output spikes/sec. It is an easily measurable quantity and

the acceptable level once chosen is independent of modulation, noise and loop filter. It also provides the easiest method of comparing the thresholds of various systems since the curves are all parallel to each other. It is also shown that in many cases of interest the output spikes follow a poisson time distribution.

I. INTRODUCTION

1.1. Problem Statement

For the most part past studies of phase lock loop systems have been constrained to analysis of systems employing a sine comparator. Approximate and exact loop models under various conditions of signals and noise have been considered and in some cases optimization procedures were applied. Despite such articles available in the literature and the frequent use of phase lock loops in communication systems, several problems associated with this device remain.

The purpose of this research has been to investigate two of these problems carefully so that fundamental behavior might be observed and design curves developed where appropriate.

One problem which has proven to be a fruitful area of research is the effect that the phase comparator, a non-linear device operating on the phase difference between reference and signal, has on overall performance. The second problem, directly related to the first, which has been given careful consideration in this research, is the threshold phenomena.

1.2. Previous Work

Though originally developed for commercial T. V. systems, phase lock loops now find wide use in present day communication systems. Because of its versatility the phase lock loop has found many

applications including

(1) Tracking systems where it is necessary to overcome the frequency uncertainties due to transmitter instabilities, doppler shift and rate of change of doppler,

(2) Demodulation of narrowband and wideband f. m. signals,

(3) Narrowband filtering to improve the carrier to noise ratio, CNR, providing a coherent carrier for synchronous detectors,

(4) Telemetry systems where PSK and FSK coded carriers are used and

(5) Signal Synthesis.

Though contributions to the study of phase lock loops are many and diverse, they can be categorized as considering the (1) signal with no noise case or (2) the signal with noise case. The latter problem being the most difficult has been attacked by using either (a) linear analysis, (b) quazi-linear analysis or (c) in a limited number of cases, exact solutions.

In the first case Gruen[1], Cahn[2], Baker[3], and Rey[4] found approximations for the capture range for second order systems under special conditions. A thorough analog computer analysis of the phase plane behavior of first, second and third order phase lock loops was done by Viterbi[5]. He also provides some design criteria for damping and synchronization times. Richman[6] made a significant contribution by establishing a series of design formulas interrelating damping, noise bandwidth and synchronization times for the second order (phase lag filter) case over a wide range of values. Byrne[7] and Goldstein[8] did an analysis similar to Richman's[6] for the sawtooth comparator over a wide range of values, while Robinson[9] did a

digital computer analysis of the second order case using a tanlock comparator. Other than the two latter papers all work has been done with the simple sine comparator. The difficulty of solving the non-linear equation precludes any exact solution except for the first order case.

When small signals and noise can be assumed, a linear analysis of the system is possible. Both Jaffe and Rechtin[10] and Gilchriest[11] optimized in a mean square sense, the loop filter for several types of signals and noise. They were able to conclude that a phase lock loop used with a limiter was an ideal combination for worst case design and showed that AGC was at best a poorer substitute.

By adding second and higher order terms using a perturbation technique, Margolis[12] was able to get a more accurate result for the phase variance than that obtained from a linear analysis. Schilling[13] studied the response of a second order system to a noisy f. m. signal using an iteration method, but gives no comparison with exact solutions. VanTrees[14] used the Volterra expansion technique to study the response to noise, but the result diverges for the high noise case as does the result of Margolis.

The quasi-linear technique of Booton[15] has permitted several authors such as Develet[16] and Robinson[9] to make a more direct attack on the threshold problem. The former has found the optimum demodulation curve for a phase lock loop for all CNR, but the gaussian assumption is not valid in the CNR region where the threshold actually occurs. The latter, studying the tanlock system also developed some threshold curves. However, the model as well as the gaussian assumption are not valid for low CNR leaving the results questionable.

Recently Viterbi[17] found the exact solution for the first order phase lock loop and established bounds for higher order systems, using Fokker-Planck techniques. Lindsey[18], in a very significant work, has built on this and found excellent approximate solutions for the second order sine system and demonstrated their validity with experimental results.

In conclusion it should be noted that Lehan and Parks[19] and Youla[20] demonstrated that the optimum, non-realizable estimation of a f. m. or p. m. signal required a system similar in form to the simplest phase lock loop. However, it has not yet been shown that the generally used loop is the optimum realizable demodulator or tracking system.

1.3. Content and Contributions

Considerable effort was spent in attempting various analytical approaches for the two stated problems for systems involving the more general phase comparators. Limited success was achieved. Thus it was decided that only a thorough and complete experimental analysis of a laboratory model as a complementary effort to the analytical work would shed light on the desired solutions. In this way a significant contribution has been made by this research effort and the sought after answers were resolved satisfactorily.

Chapter 2 includes the derivation of the exact and approximate equivalent circuits for the class of phase lock loop systems considered in this research. The criteria of performance listed are used for comparing the results presented in each of the succeeding chapters.

In Chapter 3, the evaluation of several comparators of interest was made using the Fokker-Planck Model. The failure of the model to be exact for all systems near threshold is carefully discussed. From this, the motivation for pursuing the experimental research was derived.

Since critical experimental evaluation was necessary, a thorough discussion of the important measurement and verification techniques is given in Chapter 4. It should be noted that some of these techniques are unique with this research. If necessary they are easily adaptable to computer simulations.

A set of universal design curves was established from the experimental results for all the first order systems evaluated in Chapter 5. A modified tanlock system was introduced which showed considerable improvement over the ordinary tanlock system of Chapter 2. Also, considerable attention is given to the threshold phenomena since it is typical of feedback systems with a periodic non-linearity.

Chapter 6 presents the results of second order systems using two types of filters in the forward path of the loop. Comparisons are given for these systems with comparable first order systems. Evidence is given to support the use of critical damping for such systems even when operation takes place in the highly non-linear regions.

Chapter 7 presents the performance of several phase lock loop systems when used in conjunction with a limiter. Comparisons with the results of Chapter 5 are discussed, since the threshold characteristics are different.

A thorough discussion of the threshold results along with a precise definition is given in Chapter 8. Statistical evidence is presented

to verify that the cycle slipping phenomena, the cause of threshold, has a poisson distribution.

II. THEORY AND CRITERIA

The basic models used for both the simple phase lock loop and the more general systems studied in this research are derived in this chapter. The criteria used are listed and the philosophy of this particular approach discussed. Definitions are given for the important terms so that no confusion will result with similar terms used in the literature. A table of the various loop filters used and their parameters are given for ready reference.

2.1. Basic Theory and Models

The widely used and simplest form of the phase lock loop is shown in Figure 2.1. The multiplication or cross-correlation of the input

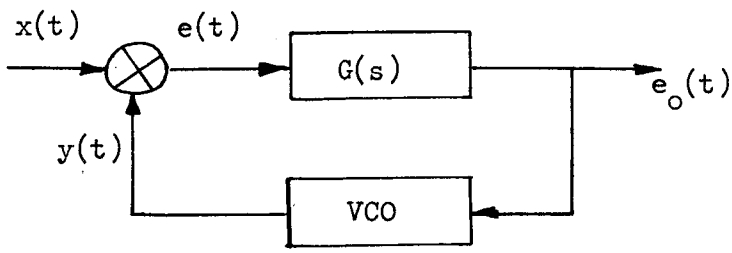

Figure 2.1. Block Diagram of Basic Phase Lock Loop

signal, x(t), with the reference, y(t), is passed through a low pass filter, G(s), and then used to control the VCO so that proper tracking takes place. With no noise at the input, the loop--if it is in a synchronous state--is capable of knowing the frequency of the input

exactly and the phase to a known static or dynamic error, called the degree of coherence. As noise increases, phase jitter appears and the estimating process degrades until random instability occurs.

The input signal, $x(t)$, is most generally represented as the sum of a fixed amplitude carrier with phase modulation, $\lambda_i(t)$, and narrow-band noise as in (2.1).

$$x(t) = \sqrt{2}\, A\, \mathrm{Sin}(\omega_o t + \lambda_i(t)) + n_1(t)\, \mathrm{Sin}\, \omega_o t + n_2(t)\, \mathrm{Cos}\omega_o t \tag{2.1}$$

The VCO output or reference signal

$$y(t) = \sqrt{2}\, \mathrm{Cos}\, (\omega_o t + \lambda_o(t)) \tag{2.2}$$

is a fixed carrier with unknown angle modulation, $\lambda_o(t)$. The VCO is ideally described as an integrator, i.e.,

$$\lambda_o(t) = \beta \int_{\infty}^{t} e_o(u)\, du \tag{2.3}$$

which by taking the two-sided Laplace Transform becomes

$$\lambda_o(s) = \frac{\beta}{s} E_o(s) \tag{2.4}$$

The gain, β, of the VCO is given in units of rad/volt. The detector output voltage

$$e(t) = A\, \mathrm{Sin}(\lambda_i - \lambda_o) + \frac{1}{\sqrt{2}} \left[n_2(t)\, \mathrm{Cos}\, \lambda_o - n_1(t) \mathrm{Sin}\, \lambda_o \right] \tag{2.5}$$

is found by multiplying (2.1) and (2.2) and neglecting the higher harmonics which are filtered out by $G(s)$. Using (2.1) and (2.5), an equivalent circuit such as shown in Figure 2.2 can be derived. Neglecting the modulation $\lambda_i(t)$ and rewriting (2.1) as

$$x(t) = A(t)\, \mathrm{Sin}\, (\omega_o t + \phi(t)) \tag{2.6}$$

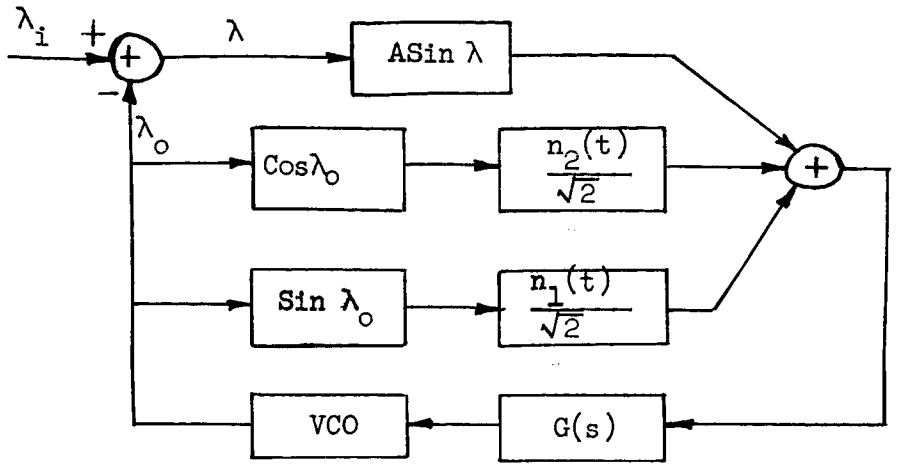

Figure 2.2. Exact Equivalent Circuit for a Noisy Phase Lock Loop

where

$$A(t) = \sqrt{\left(\sqrt{2}\,A + n_1(t)\right)^2 + n_2^2(t)} \tag{2.7}$$

$$\phi(t) = \tan^{-1} \frac{n_2(t)}{\sqrt{2}\,A + n_1(t)}\ , \tag{2.8}$$

a more useable form of the equivalent circuit results, where now

$$\lambda(t) = \phi(t) - \lambda_o(t) \tag{2.9}$$

as in Figure 2.3.

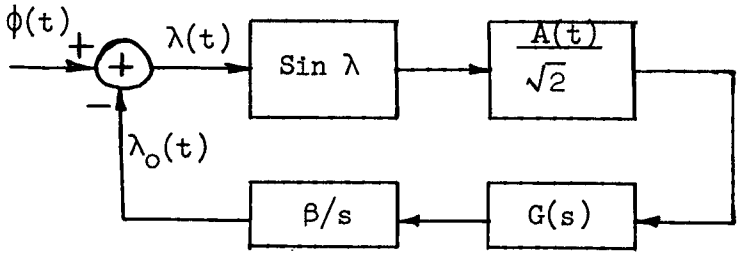

Figure 2.3. Exact Equivalent Circuit for a Noisy Phase Lock Loop.

The non-linear, randomly, time-varying nature of these systems do not lend themselves to easy analysis except in certain special cases.

Consider the input carrier to noise ratio (CNR) to be large, i.e.

$$\begin{aligned} \sqrt{2}\,A &\gg n_1(t) \\ \sqrt{2}\,A &\gg n_2(t) \end{aligned} \tag{2.10}$$

Then (2.1) can be approximated as

$$\begin{aligned} x(t) = \sqrt{2}\,A\ \mathrm{Sin}\ (\omega_o t + \phi(t)) \\ + n_2(t)\ \mathrm{Cos}\omega_o\ t \end{aligned} \tag{2.11}$$

Rewriting (2.11) in the same form as (2.6), we get

$$x(t) = A(t)\ \mathrm{Sin}(\omega_o t + \phi(t)) \tag{2.12}$$

where now

$$A(t) = \sqrt{\left(\sqrt{2}A\ \mathrm{Cos}\ \lambda_i\right)^2 + \left(\sqrt{2}A\ \mathrm{Sin}\ \lambda_i + n_2(t)\right)^2} \tag{2.13}$$

and

$$\phi(t) = \tan^{-1} \frac{\sqrt{2}\,A\ \mathrm{Sin}\ \lambda_i + n_2(t)}{\sqrt{2}\,A\ \mathrm{Cos}\ \lambda_i} \tag{2.14}$$

Further assuming that the carrier modulation is small such that

$$\begin{aligned} \mathrm{Cos}\ \lambda_i &= 1 \\ \mathrm{Sin}\ \lambda_i &= \lambda_i\ , \end{aligned} \tag{2.15}$$

we finally obtain

$$\begin{aligned} A(t) &= \sqrt{2}\,A \\ \phi(t) &= \tan^{-1}\left(\frac{n_2(t)}{\sqrt{2}\,A} + \lambda_i\right) \end{aligned} \tag{2.16}$$

which from (2.10) becomes

$$\phi(t) \doteq \frac{n_2(t)}{\sqrt{2}\,A} + \lambda_i \tag{2.17}$$

Therefore

$$x(t) = \sqrt{2}\,A\,\mathrm{Sin}\left(\omega_o t + \lambda_i + \frac{n_2(t)}{\sqrt{2}\,A}\right) \tag{2.18}$$

The output voltage of the detector e(t) is now

$$e(t) = A\,\mathrm{Sin}\left(\lambda_i - \lambda_o + \frac{n_2(t)}{\sqrt{2}\,A}\right) \tag{2.19}$$

which can be rewritten as

$$e(t) = A\,\mathrm{Sin}\,(\lambda_i - \lambda_o) + \frac{n_2(t)}{\sqrt{2}}\,\mathrm{Cos}\,(\lambda_i - \lambda_o) \tag{2.20}$$

Realizing that small modulation implies $\lambda_i - \lambda_o \ll 1$, we finally obtain,

$$e(t) = A(\lambda_i - \lambda_o) + \frac{n_2(t)}{\sqrt{2}} \tag{2.21}$$

Using (2.21) and (2.3), the small signal linear equivalent circuit of Figure 2.4 results.

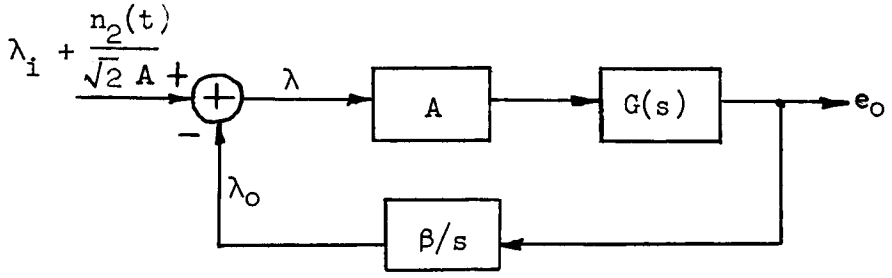

Figure 2.4. Small Signal, Large CNR, Linear Equivalent Circuit of Simple Phase Lock Loop.

If no input noise is present, Figure 2.2 reduces to the non-linear, time-invariant equivalent circuit of Figure 2.5 described by the equation

$$\dot{\lambda}_i(t) = \dot{\lambda}(t) + AKG(p)\ \mathrm{Sin}\lambda(t)$$

where $(\cdot)$ denotes differentiation with respect to t, $p=d/dt$ and $G(p)$ is the operator form of $G(s)$.

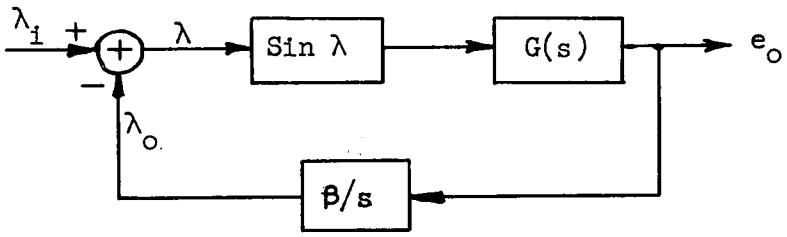

Figure 2.5. Exact Equivalent Circuit of Simple Phase Lock Loop with Noise Absent.

If $\lambda = \lambda_i - \lambda_o \ll 1$ as done above, Figure 2.5 reduces to the small signal linear equivalent circuit of Figure 2.4. The usefulness of the linear equivalent circuit lies in the ease of analysis. It can be reduced to a single input-output relation between $\lambda_i(t)$ and $\lambda_o(t)$, so that an equivalent small signal transfer function, $H(s)$, can be defined as

$$H(s) = \frac{K\ G(s)}{s+KG(s)} \qquad (2.23)$$

$$K = A\ \beta \text{ rad/sec}$$

2.2 General Phase-Lock Loop Systems

The previous section has provided the fundamental ideas, equations and circuit models for the commonly discussed phase lock loop system. Much of the analysis and present day design criteria are based on the models of Figures 2.4 and 2.5. There are other systems which operate in a similar fashion and are more general in form. The remainder of this research deals with these more general systems.

Suppose the non-linear element, Sin λ, of Figure 2.5 is replaced with an arbitrary, zero-memory, non-linearity $F(\lambda)$. Then a more general phase lock loop system is obtained, Figure 2.6, whose operation is described by the equation

$$\dot{\lambda}_i(t) = \dot{\lambda}(t) + K\, G(p)\, F(\lambda) \ . \qquad (2.24)$$

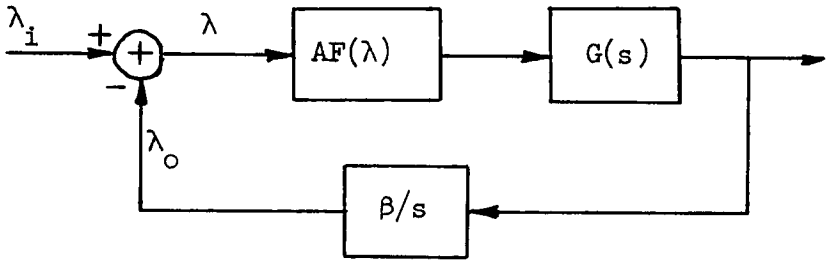

Figure 2.6. Exact Equivalent Circuit of General Phase Lock Loop with Noise Absent

$F(\lambda)$ is a non-unique transformation which is frequently referred to as a phase detector or phase-comparator since it operates on the difference

between the input and reference phases. Such comparators as tanlock, n^{th}-order tanlock, sawtooth and others (see Table 3.1) can be included in the study of phase lock loop systems of this type. The only constraints imposed on $F(\lambda)$ are it is (1) odd, and (2) periodic in 2π. A more general $F(\lambda)$, modulo $2\pi n$, has not been considered here.

The n^{th}-order tanlock system, shown in Figure 2.7, is of particular

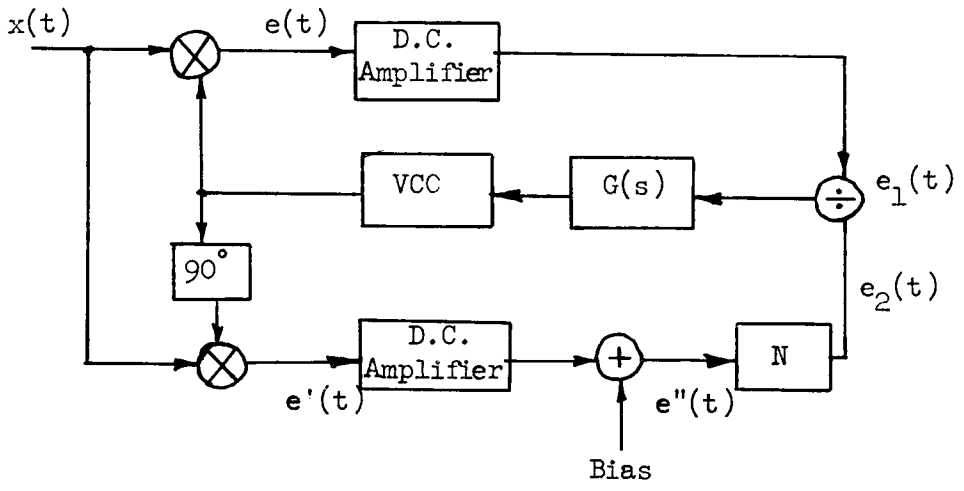

Figure 2.7. Block Diagram of n^{th} Order Tanlock System

interest because it includes many systems. The element, N, is a zero memory, non-linear device whose transfer function is

$$e_2(t) = [e''(t)]^n \tag{2.25}$$

With no noise present and using previous equations, Figure 2.7 can be reduced to the model of Figure 2.5. The phase comparator is now

$$F(\lambda) = \frac{(1+k)^n \sin \lambda}{(1+k \cos\lambda)^n} \quad 0 \leq k < 1 \tag{2.26}$$

With noise, the equivalent circuit of Figure 2.8 can be derived. It

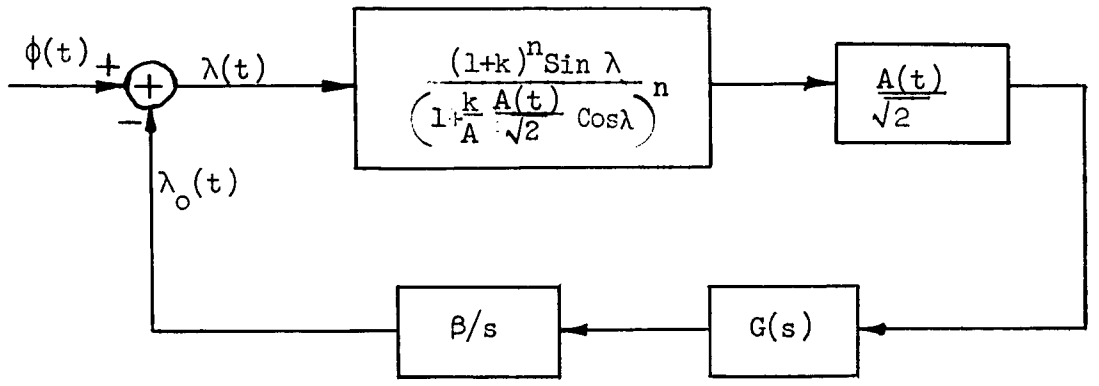

Figure 2.8. Exact Equivalent Circuit of General Tanlock System with Noise Present

should be noted that it is very similar to the circuit of Figure 2.3, except for the additional A(t) term which is not present in the denominator of the phase comparator box.

When k=o, the system reduces to the simple phase lock loop of Figure 2.1 for any value of n. In this case the output of the second or quadrature multiplier, e'(t), when properly filtered, can be used as an estimation of the carrier amplitude A. For n=1, (2.26) reduces to the tanlook comparator.

Figure 2.9 is a plot of (2.26) for several values of the parameter k and n. The shape changes from a sine wave at k=o to an approximate sawtooth to a highly non-linear shape as k varies from zero to one. It should be noted that for any non-zero value of k and n, the stability range of the system (the region of positive slope) is increased while for certain values of k and n, the linear operating range is extended. As n

increases the characteristic becomes more non-linear for a given value of k, but for all values of k and n the slope at zero is equal to unity. This fact enables results obtained from the linear equivalent circuit to hold true for any n^{th} order tanlock phase comparator. A sawtooth or linear characteristic has been plotted on Figure 2.9 for comparison purposes.

2.3. Criteria

Since one of the purposes of this work is to study the effect of the phase comparator on system performance, it is necessary that a set of criteria or performance indices be established. This allows easy comparisons to be made amongst systems of the same order. The criteria used to evaluate performance were:

(a) f_N – Equivalent linear noise bandwidth.

(b) C_{max} – Normalized lock range. (Lock range when open loop gain is unity.)

(c) T_s – Synchronization time.

(d) σ_λ^2 – Error variance of λ due to noise only.

(e) P_e – Probability of the error voltage exceeding a specified value.

(f) Threshold

To make any comparisons meaningful, each system considered should maintain fixed, one of the above criteria. In this research both the analytical and experimental values of f_N were constrained to a fixed value, since it is the simplest to apply to all cases and seems to be one of the most significant parameters. However, in some instances

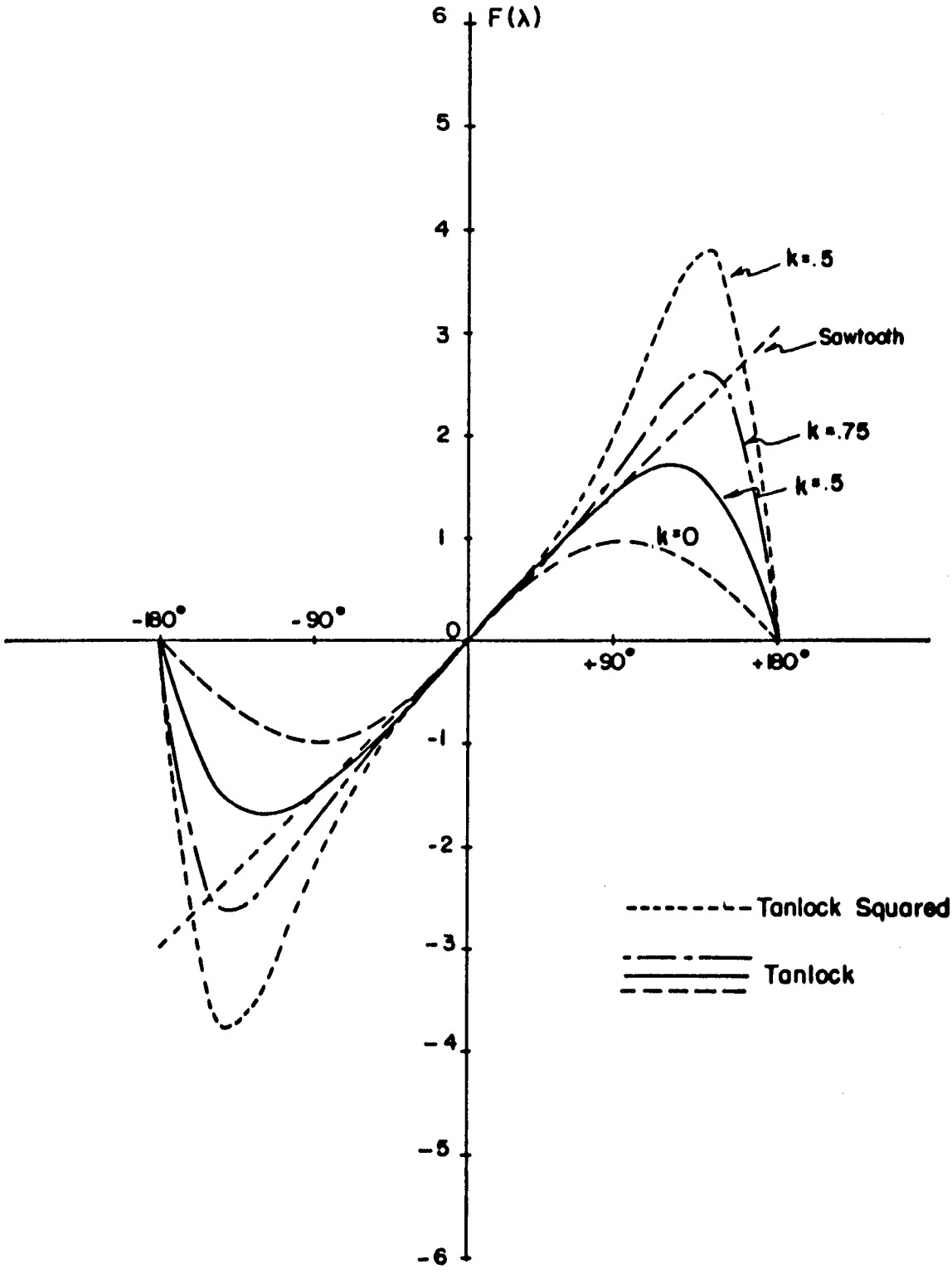

Figure 2.9. Phase Comparator Plots for Several Tanlock and Tanlock Squared Characteristics

this is not necessarily the most meaningful normalization procedure as will be shown in Chapter 5.

From a theoretical point of view these seemed to be the most useful indices of performances. However, in an actual experimental system, the phase error is not a physically accessible point, so no measurements can be made directly. The results that were found can, however, be related to these criteria in meaningful ways.

2.4. Definitions

With the basic systems and theory established it is appropriate to introduce some basic definitions of terms which will be used throughout this work.

(a) Equivalent linear noise bandwidth (f_N) is the bandwidth of an ideal rectangularly shaped filter which passes the same output power for white noise input as does the given network. It is analytically found as

$$f_N = \frac{1}{|H(\omega)|^2_{max} 2\pi} \int_{-\infty}^{\infty} |(H(\omega)|^2 d\omega \qquad (2.27)$$

(b) Synchronization time (T_s) - Starting from an initial state of zero carrier at the input to the loop, the time it takes the loop output signal (VCO input) to reach 90% of the difference between its initial value and its final value.

(c) Lock range (LR) - The maximum fixed frequency difference between the input carrier and the frequency of the VCO when the input to the loop is zero (VCO reference frequency) which the system can synchronously track at a rate much lower than f_N.

(d) Capture range (CR) - The maximum fixed frequency difference between a suddenly applied carrier and the VCO reference frequency with which the system can become synchronous. Depending on the type of filter used for G(s), we find the following inequality.

$$CR \leqslant LR \qquad (2.28)$$

(e) Cycle slipping — This is the phenomena where the system is forced to momentary lose synchronism due to noise and will proceed to stabilize itself in an adjacent stable point $\pm 2\pi$ radians

Table 2.1

Tabulation of Loop Filters and the Corresponding Loop Parameters

Type	G(s)	H(s)	f_N	ζ
I	1	$\frac{K}{s+K}$	$\frac{K}{2}$	—
II	$\frac{1}{sT_1+1}$	$\frac{K}{T_1 s^2+s+K}$	$\frac{K}{2}$	$\frac{1}{2\sqrt{T_1 K}}$
IIa	$\frac{1}{K}\left(\frac{\sqrt{2}\,B_o s+B_o^2}{s}\right)$	$\frac{\sqrt{2}\,B_o s^2+B_o s}{s^2+\sqrt{2}\,B_o s+B_o^2}$	$\frac{\sqrt{2}}{4}B_o$	$\frac{1}{2}$
III	$\frac{T_1 s+1}{\gamma T_1 s+1}$	$\frac{K(T_1 s+1)}{\gamma T_1 s^2+s(1+KT_1)+K}$	$\frac{K}{2\gamma}\frac{(KT_1+\gamma)}{(KT_1+1)}$	$\frac{1+K T_1}{2\sqrt{\gamma K T_1}}$
IIIa	$\frac{T_1 s+1}{\gamma T_1 s+1}$	$\frac{K(T_1 s+1)}{\gamma T_1 s^2+s(1+KT_1)+K}$	$\frac{K}{2\gamma}$	$\frac{1}{2}\sqrt{\frac{T_1 K}{\gamma}}$

away. As seen from the differential equation the system has an infinite number of stable points due to the 2π periodicity of the phase comparators.

(f) Threshold – The value of input signal to noise ratio at which the rate of cycle slipping or spike activity at the output exceeds a specified level.

(g) Open loop gain (K) – This is the total gain expressed in rad/sec. between the input and output phase with the loop opened. The open loop gain is always equal to the lock range for the simple phase lock loop.

2.5. System Order

The order of any non-linear system of this type is generally found from the small signal linear transfer function such as H(s) in (2.23). Any practical phase lock loop system will always be one order higher than the order of the loop filter. It should be noted in this analysis that the filter which is necessary to get rid of the higher order terms in (2.5) has no response to any signals in the loop range and thus can be neglected.

For easy reference, a list of the several types of loop filters used in this research is given in Table 2.1 along with some previously defined parameters. Type IIa is included for completeness, since it is the filter which minimizes the mean square phase error due to a step signal and white noise as found by Jaffe and Rechtin[10]. Type IIIa is derived from III by assuming that

$$K T_1 \gg \gamma$$

and (2.29)

$$\gamma \gg 1$$

III. EVALUATION OF FIRST ORDER FOKKER PLANCK MODEL

Chapter three presents a theoretical analysis of the first order general phase lock loop systems. A new model (Fokker-Planck Model) is introduced. The results from this model are evaluated for the criteria established in Chapter 2. Finally the use of this model for higher order systems is discussed along with the use of experimentation in obtaining useful results.

3.1. Theoretical Analysis

Consider the general loop differential equation (2.24). With a type I filter, G(s)=1, the first order differential equation

$$\frac{d\lambda}{dt} + KF(\lambda) = \lambda_i(t) \tag{3.1}$$

is obtained. Suppose the phase of the received signal is

$$\lambda_i(t) = \Delta\omega t + \theta \tag{3.2}$$

where $\Delta\omega$ is the frequency difference (rad/sec.) between the signal and reference carriers and

θ is a fixed but arbitrary phase.

If (3.2) is substituted into (3.1), the result is

$$\frac{d\lambda}{dt} + KF(\lambda) = \Delta\omega \tag{3.3}$$

Dividing (3.3) by K and letting

$$\tau = Kt \tag{3.4}$$

the normalized form of (3.3) is

$$\frac{d\lambda}{d\tau} + F(\lambda) = C \tag{3.5}$$

where $C = \frac{\Delta\omega}{K}$ is defined as the normalized frequency difference.

The previously stated requirement that each system has the same linear noise bandwidth is equivalent to requiring that the initial slope of $F(\lambda)$ be unity. As a result the small-signal linear equation becomes

$$\frac{d\lambda}{d\tau} + \lambda = C \tag{3.6}$$

for each phase comparator.

The various comparators, $F(\lambda)$, to be considered in this chapter are listed in Table 3.1. Some are widely reported in the literature. However, several are modified forms, giving improved performance in certain situations but only recently reported[27] as part of this research. The results for the normalized system of (3.5) are now given in terms of the criteria of Chapter 2.

Table 3.1

Comparator Functions

	Name	$F(\lambda)$
A.	Sine	$\text{Sin}\ \lambda$
B.	Sawtooth	$\lambda \qquad -\pi > \lambda > \pi$
C.	Tanlock	$\frac{(1+k)\text{Sin}\ \lambda}{(1+k\text{Cos}\ \lambda)}$
D.	Tanlock Squared	$\frac{(1+k)^2\text{Sin}\ \lambda}{(1+k\ \text{Cos}\ \lambda)^2}$
E.	Trig Function #1	$\frac{(A^2+B^2+2AB)^2\text{Sin}\lambda}{(A^2+B^2+2AB\text{Cos}\lambda)^2}$
F.	n^{th} Order Tanlock	$\frac{(1+k)^n\text{Sin}\lambda}{(1+k\text{Cos}\lambda)^n}$
G.	Trig Function #2	$\frac{(1+B+A)\text{Sin}\lambda(B+2A\text{Cos}\lambda)}{(2A+B)(1+B\text{Cos}\lambda+A\text{Cos}^2\lambda)}$

3.1.1. Equivalent Linear Noise Bandwidth

As a result of (3.6) and using (2.23), the linear noise bandwidth of each normalized system is $\frac{1}{2}$ rad/sec.

3.1.2. Normalized Lock Range

C_{max} is the maximum normalized value of $\Delta\omega$ which will still permit the loop to remain synchronous. It corresponds to the peak positive and negative values of the plots of $F(\lambda)$ in Figure 2.9. It is most easily found by solving the equation

$$F'(\lambda) = 0 \tag{3.7}$$

for λ and substituting the result back into the steady state solution of (3.5). A graph of C_{max} vs. k for tanlock and tanlock squared is given in Figure 5.7 and values for special cases of the others are given in Table 3.2.

From these results it is clear that with no noise present considerable improvement in lock range is obtainable by altering the phase comparator in the manner shown. Also, the necessity of the system to handle the large control voltages generated is implied.

3.1.3. Synchronization Time

For the first order system of (3.5), the normalized synchronization time, τ_s, is easily found as

$$\tau_s = \int_{\lambda_1}^{\lambda_2} \frac{d\lambda}{C-F(\lambda)} \tag{3.8}$$

where λ_1 is the initial value of the phase,

and λ_2 is a value of λ close to but not equal to λ_f, the final or steady state value.

Exact solutions of (3.8) can only be found for Cases A and B of Table 3.1. For Case A, the solution is

$$\tau_s = \frac{1}{\sqrt{1-C^2}} \log \left| \frac{C\tan \lambda/2 - 1 - \sqrt{1-C^2}}{C\tan \lambda/2 - 1 + \sqrt{1-C^2}} \right|_{\lambda_1}^{\lambda_2} \quad C \neq 0 \tag{3.9}$$

For most $F(\lambda)$ of interest, no direct solutions of (3.8) or (3.9) are available. Thus numerical techniques were applied to (3.5) for different $F(\lambda)$ and typical plots appear in Figures 3.1 and 3.2. For simplicity only values of $\lambda_1=0$ are given while C took on the values of .5 C_{max} and .95 C_{max}. From these curves values of τ_s and thus T_s can be easily found according to the definition given in Section 2.4.

It is apparent that considerable improvement in synchronizing can be obtained by the use of other comparators as compared to the simple phase lock loop. As k approaches one for the tanlock cases, τ_s decreases. This effect can be attributed to the very steep negative and positive slopes of the phase comparator, despite the constant slope at zero. Other cases for $\lambda_1 \neq 0$ produce similar results. The scale change between Figures 3.1 and 3.2 should be noted.

3.1.4. Phase Variance

The exact solution of the phase variance of a phase lock loop with a noisy input has proved to be a challenging and formidable problem. Recently, however, Viterbi[17] was able to find the exact solution of a first order system by applying Fokker-Planck techniques.

Suppose the input consists of a fixed carrier signal with no modulation and additive, white, gaussian noise whose single-sided spectral

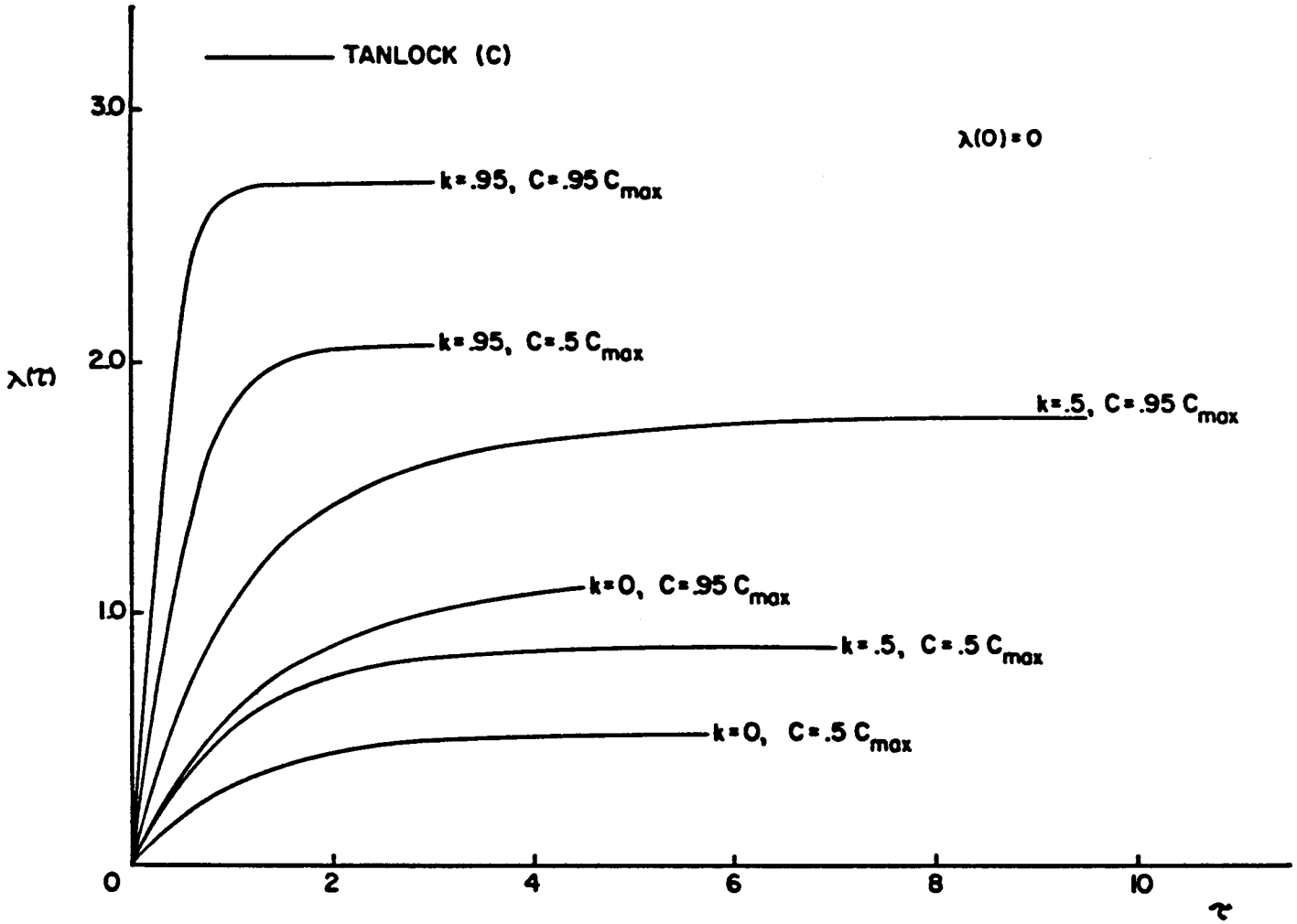

Figure 3.1. Transient Response Curves of a First Order Phase Lock Loop Using a Tanlock Comparator — No Noise

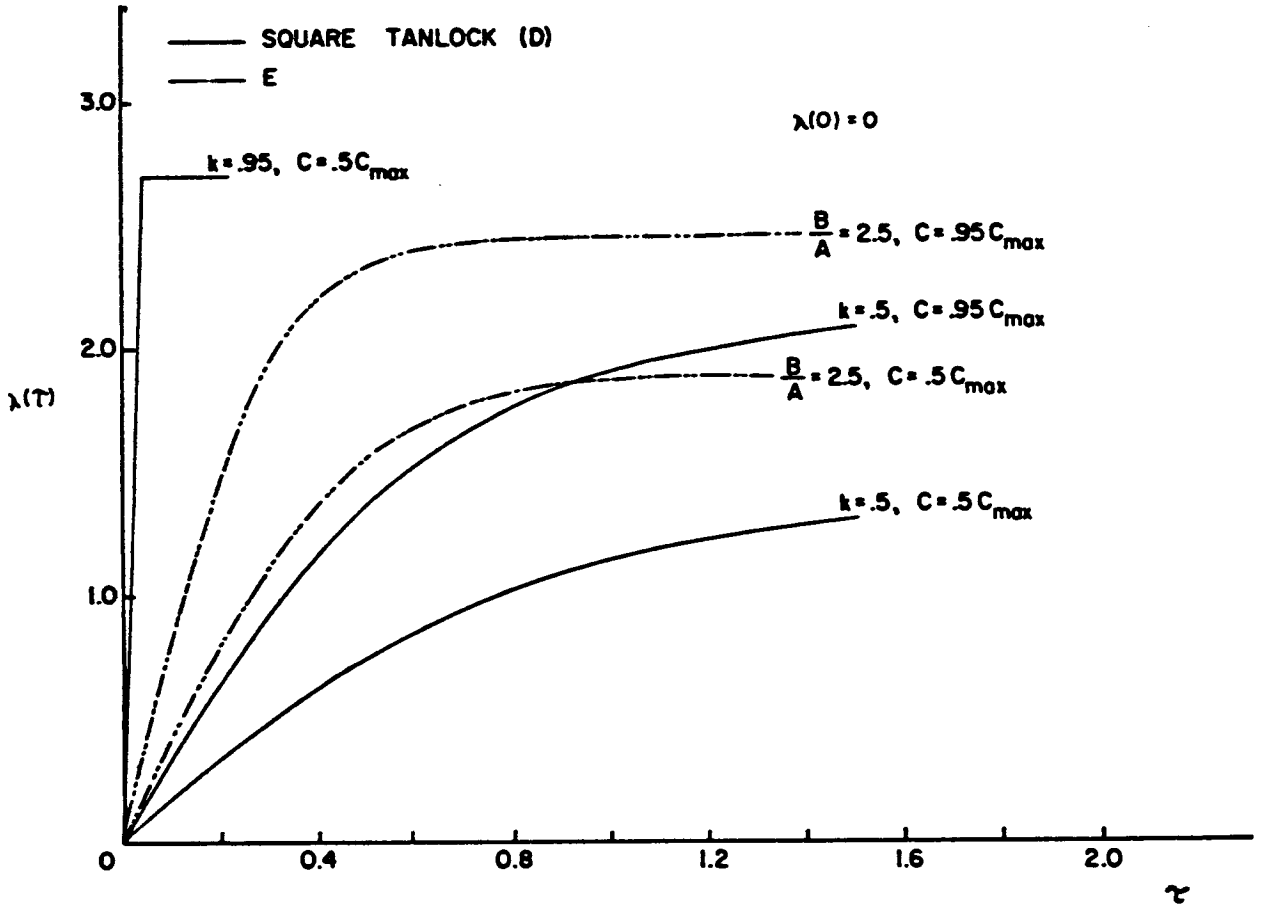

Figure 3.2. Transient Response Curves of a First Order Phase Lock Loop Using Tanlock Squared and Trig Function #1 Comparators — No Noise

density is N_o. The exact steady state probability density function of the phase error is

$$p(\lambda)=De^{[-\alpha g(\lambda)+\epsilon\lambda]}\cdot\left\{1+\frac{(e^{-2\epsilon\pi}-1)\int_{-\pi}^{\lambda}e^{-(-\alpha g(x)+\epsilon x)}dx}{\int_{\pi}^{\pi}e^{-(\alpha g(\lambda)+\epsilon\lambda)}d\lambda}\right\} \qquad (3.10)$$

$$-\pi < \lambda < \pi$$

where D = Constant which makes $\int_{-\pi}^{\pi} p(\lambda)\,\lambda = 1$

α = CNR referred to equivalent noise bandwidth

$\epsilon = C\alpha$

$g(\lambda) = \int_{\lambda} F(u)\,du$

If C = 0, then (3.10) reduces to

$$p(\lambda) = \frac{e^{-\alpha g(\lambda)}}{\int_{-\pi}^{\pi} e^{-\alpha g(\lambda)}d\lambda} \qquad (3.11)$$

The phase variance immediately follows from (3.11) as

Table 3.2

Tabulation of Criteria of a First Order Loop for Several Comparators

Comparator	f_N	τ_s	$\sigma_\lambda^2(\alpha = 1)$	$P_e(\alpha = 1)$		C_{max}
A	$\frac{1}{2}$	2.52	1.60	.65	$\pm$	1.0
B	$\frac{1}{2}$	2.30	.98	.28	$\pm$	3.14
C(k = .5)	$\frac{1}{2}$	2.35	1.1	.478	$\pm$	1.732
C(k = .95	$\frac{1}{2}$	1.1	.815	.313	$\pm$	6.26
D(k = .5)	$\frac{1}{2}$	1.37	.759	.36	$\pm$	3.81
D(k = .95)	$\frac{1}{2}$	.032	.577	.21	$\pm$	161.
E(A/B=2.5)	$\frac{1}{2}$	.62	.651	.420	$\pm$	8.8

$$\sigma_\lambda^2 = \frac{\int_{-\pi}^{\pi} \lambda^2 e^{-\alpha g(\lambda)} d\lambda}{\int_{-\pi}^{\pi} e^{-\alpha g(\lambda)} d\lambda} \qquad (3.12)$$

The phase density and thus the variance from the above is exact for any phase lock loop system whose equivalent circuit is similar to that of Figure 2.3 and whose $F(\lambda)$ satisfies the previously imposed restrictions. This can be called the Fokker-Planck Model. Figure 3.3 is a plot of (3.12) for the various comparators listed in Table 3.1. All show improvement over the ordinary sine comparator (k=0). Tanlock is better than the sawtooth comparator for some values of the parameter k and reaches its best performance for k=1 which is a lower bound. Other comparators such as tanlock squared have improved even further due to the heavy weighting given to large values of λ in (3.12).

If $C \neq 0$, the phase variance can be found from (3.10). Calculations indicate that the variance gets larger as $\Delta\omega$ increases for a given α. The ordering of various systems remains the same for similar values of C. A plot of the tanlock comparator (k=0, .5, .95) for several values of C is given in Figure 3.4.

In all cases the asymptotic value of the variance is $\frac{\pi^2}{3}$, the same as the variance of a phase distribution uniform between $-\pi$ and π. This is not unexpected due to the fact that as CNR approaches zero, all values of phase are equally probable.

These results are exact for the sine and sawtooth comparators. However, the equivalent circuit derived for the general tanlock system, Figure 2.8, is not quite the same as Figure 2.3, though for the

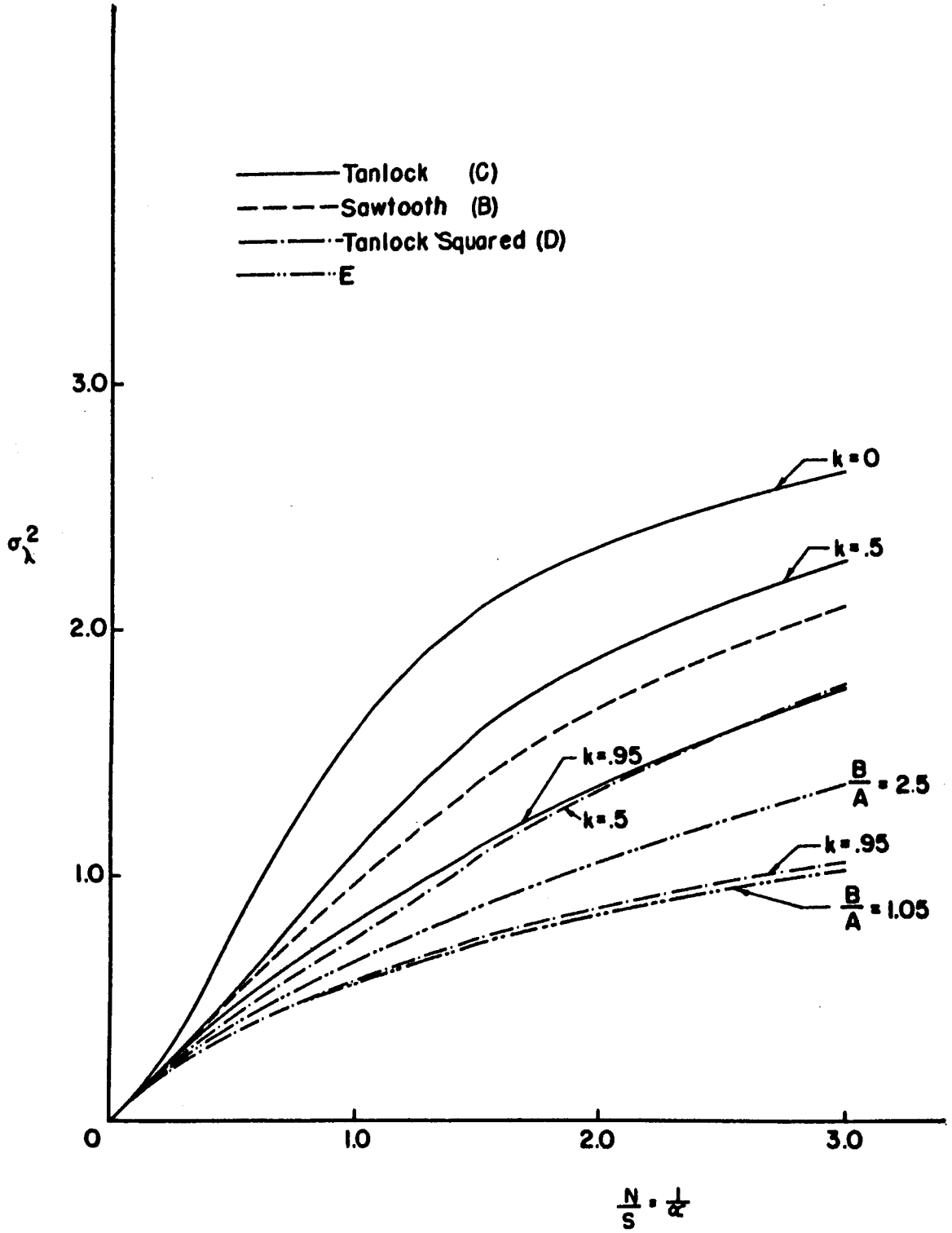

Figure 3.3. Phase Variance Due to Noise Alone of a First Order Phase Lock Loop Using Several Comparators ($\Delta\omega=0$)

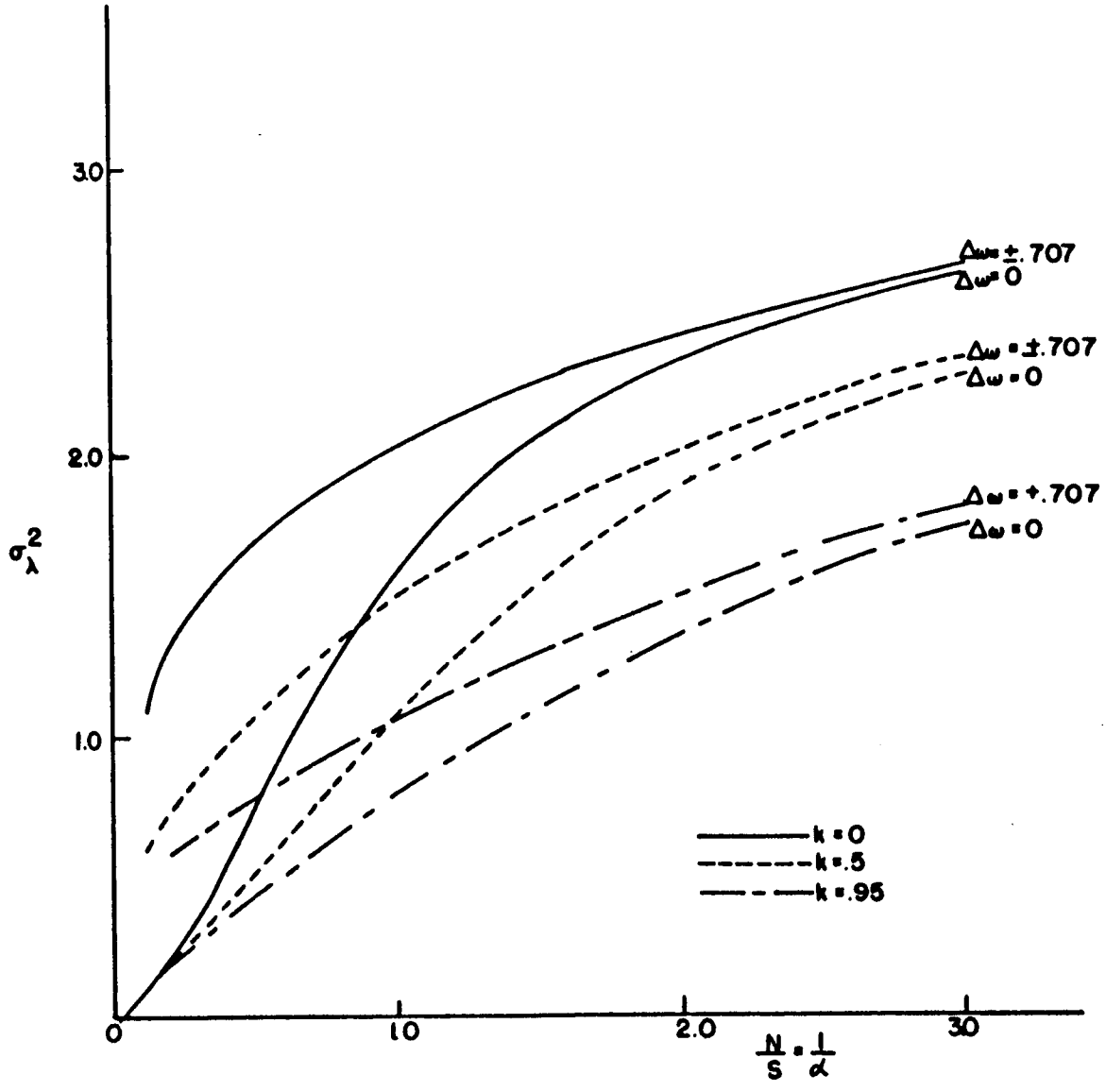

Figure 3.4. Phase Variance Due to Noise Alone of a First Order Phase Lock Loop Using a Tanlock Comparator ($\Delta\omega \neq 0$)

noiseless case they are identical. The difference is due to the additional A(t) term in the denominator of the forward path non-linearity. For small values of noise, the circuits are approximately equivalent, but as noise increases, the undesired A(t) term becomes dominant. The result is that the model analyzed above fails to be realistic at some CNR and the stated conclusions are questionable below this value.

An attempt was made to solve the exact general system model using Fokker-Planck techniques. However, division by a stochastic process occurs in the partial-differential equation and the technique is no longer applicable because the resulting process is not Markov. The problem is not tractable as far as can be determined.

Extension of methods such as linear[21], quazi-linear[15], and perturbation[14] analysis for finding the phase variance of the tanlock system were investigated. However, in each case not only is the A(t) term of the equivalent circuit neglected, but apriori knowledge of the phase density must be assumed over the entire CNR range. The phase density was thus assumed to be gaussian, a fact which Viterbi[17] and Lindsey[18] have shown to be incorrect. As a result these approaches fail to be valid at a higher CNR in general than the analysis of the preceding Fokker-Planck model.

3.1.5. Probability of Error

The probability of the phase error voltage exceeding some arbitrary value, called the probability of error, P_e, follows immediately from (3.11).

$$P_e = P\left\{\lambda_a \leq |\lambda|\right\} = 1 - \frac{\int_{\lambda_a}^{\lambda_a} e^{-\alpha g(\lambda)}\, d\lambda}{\int_{-\pi}^{\pi} e^{-\alpha g(\lambda)}\, d\lambda} \qquad (3.13)$$

Plots of (3.13) for several comparators of Table 3.1 appear in Figure 3.5. The order of improvement in P_e follows that of the variance curves. The value of λ_a in each case was chosen to be 1/3 of the largest stable value of λ. A larger choice of λ_a will give a lower P_e for any given value of α.

3.1.6. Threshold

Assuming that the threshold is proportional to phase variance, then from Figure 3.3, it may be concluded that the threshold improves as k increases. But the taking into account of the A(t) term, indicates that a different conclusion must be drawn as will be subsequently shown in Chapter 5. Thus because the Fokker-Planck model is approximate, no prediction of the threshold has been made.

3.1.7. Summary

A tabulation of the results obtained from the Fokker-Planck Model in this section is given in Table 3.2. A quick comparison of performance can be made and it is seen that the higher order non-linearities do extremely well.

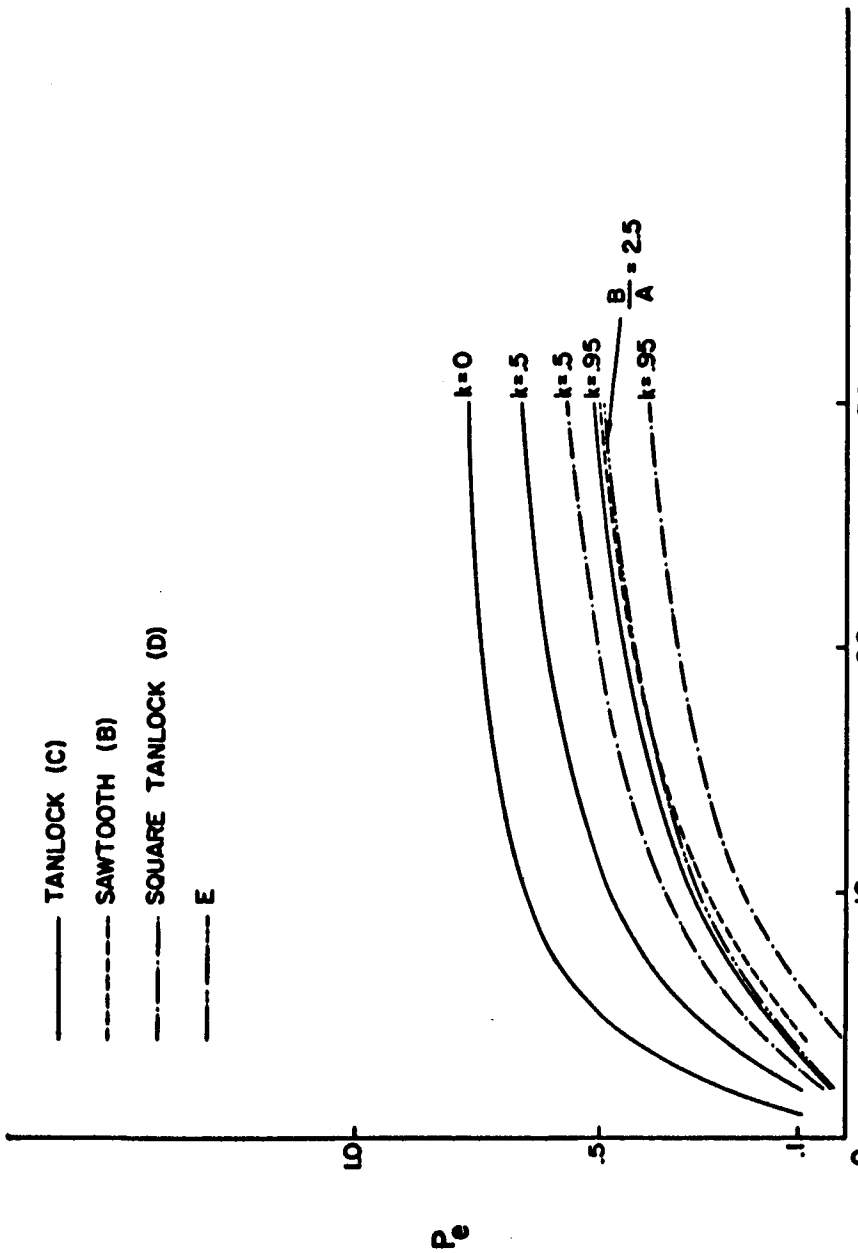

Figure 3.5. Probability of Error Curves Due to Noise Alone of a First Order Phase Lock Loop Using Several Comparators ($\Delta\omega$=0)

3.2. Discussion of Results and Extensions

The use of an analog divider in the physical model proved to be the major block to exactly analyzing the general tanlock system in the presence of noise. However the Fokker-Planck method gives a better approximation than the other methods over a larger range of CNR. Though the threshold could not be predicted from these results, the ordering of the various systems above threshold for certain criteria was correctly established. It should be noted that the improvements obtained for the noiseless case are exact.

When one goes to higher order systems, the theoretical problems increase many fold. Lindsey[18] found an approximate solution for the phase variance of a sine comparator using an extension of the Fokker-Planck equation in two dimensions. This author attempted to find the exact solution using a similar approach with little success. Extensions to other comparators were not possible at all.

The failure of analytical methods to give a clear understanding of the general phase lock loop problem and reasonable design criteria led this investigation to an experimental research effort. Though analog or digital computer simulation could have been used, it was felt that an actual laboratory model would provide better insights into the problems being investigated. The remainder of this research is a report of the experimental phase of the problem.

IV. MEASUREMENTS AND TECHNIQUES

In this chapter an introduction to the experimental system is given with attention centered on the overall performance of the most important circuits of the receiver. The methods used in measuring the criteria of Chapter 2 are also discussed.

4.1. Introduction

The general tanlock system of Figure 2.7 was the only one considered in the experimental part of this research, but it covers a large class of non-linearities. Certain comparators such as the sawtooth type, though interesting, were not considered because of the different experimental implementation required. However, the experimental procedures, measurements and data display would all be the same.

A block diagram of the entire experimental system appears in Figure 4.1. Transmitter and channel as well as the receiver are shown. The system has proven very versatile since most of the subsystems were constructed as plug-in boards for easy removal and replacement. The limiter was designed to be switched in and out of the system. The gate was included so that criteria such as synchronization time and capture range could be checked.

The only specialized equipment used in the experimentation was a General Radio Noise Generator, Model 1390-B, a Ballantine True RMS

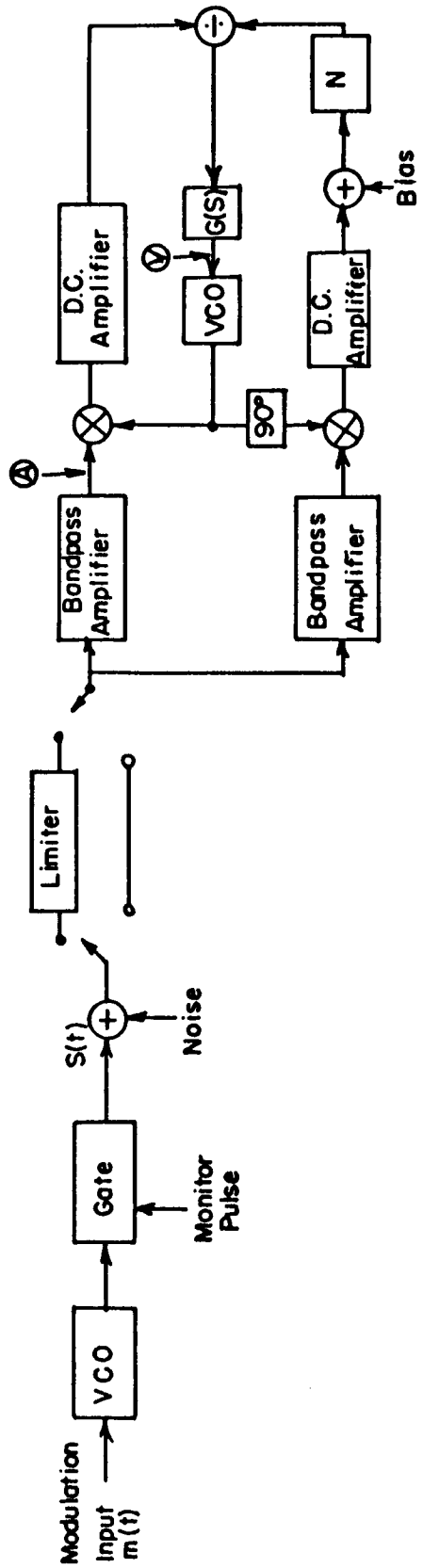

Figure 4.1. Block Diagram of Experimental System

Meter, Model 320, a Hewlett-Packard Wave Analyzer, Model 302A, a Singer Panalyzor, Model SB-126, and a Hewlett-Packard True RMS Meter, Model 3400A. All other items used such as scopes, voltmeters and signal generators are generally found in any experimental laboratory.

4.2. Tanlock Model Subsystems Verification

The performance of the tanlock model, especially in the threshold region, is not known very well due to a lack of any exact theoretical results. Thus it was necessary that each subsystem in the receiver operate properly. To insure this, the characteristics of each subsystem were carefully checked before being used in the overall system. A discussion of the results of these tests and the measurement techniques used will now follow.

4.2.1. Voltage Controlled Oscillator

The operation of the VCO was shown to be ideally characterized by (2.3). To perform in this fashion a VCO must possess three qualities: (1) the variation of frequency vs. D.C. input voltage should be linear, (2) the overall frequency response should be much larger than the spectrum of the input signals and (3) the device should be frequency stabilized. The VCO circuit used in the experimental work is shown in Figure 4.1. The degree to which the VCO satisfied these criteria was excellent.

The VCO had a large adjustable gain factor equal to 43kc/volt. and was linear over at least 5% of the center frequency, 450kc. To reduce the effective gain of the loop, the control signal passes thru a resistive divider to the VCO. A typical gain curve of this combination is

shown in Figure 4.2 and the gain is 2.4 kc/volt. This combined gain remained fixed throughout the work and will henceforth be referred to as β.

The small signal frequency response of the VCO was measured over 160kc, at least 16 times greater than the bandwidth of any information or control signal. Short time stability of the oscillator was 2 parts in 10^4 while the longer term stability was no greater than 5 parts in 10^4.

For this work, the small non-linearities of the VCO are no problem, though they might cause serious trouble in a study of intermodulation distortion. Both VCO's in the system had identical characteristics.

4.2.2. Multiplier

The multipliers used in the system are of the full-wave rectifier type which effectively eliminates any higher order harmonics. However, a filter must be used to get rid of the carrier at the output. It should also be noted that in order to multiply correctly, it is required that the total input signal plus noise be 50% or less of the peak of the reference.

A static test of the device, Figure 4.3, indicated that the normalized characteristic closely follows the ideal cosine curve, Cos $(\lambda_i - \lambda_o)$ between the two input signals. A small unbalance voltage existed which shifted the curve 10°, but this was effectively compensated for in the system by biasing it out. Dynamic multiplication indicated results similar to the static curve and the frequency response was over 150kc.

Correct performance of these detectors in a noisy environment was a crucial requirement for this research. Performance of the multipliers in noise was checked by multiplying the signal plus noise with signal

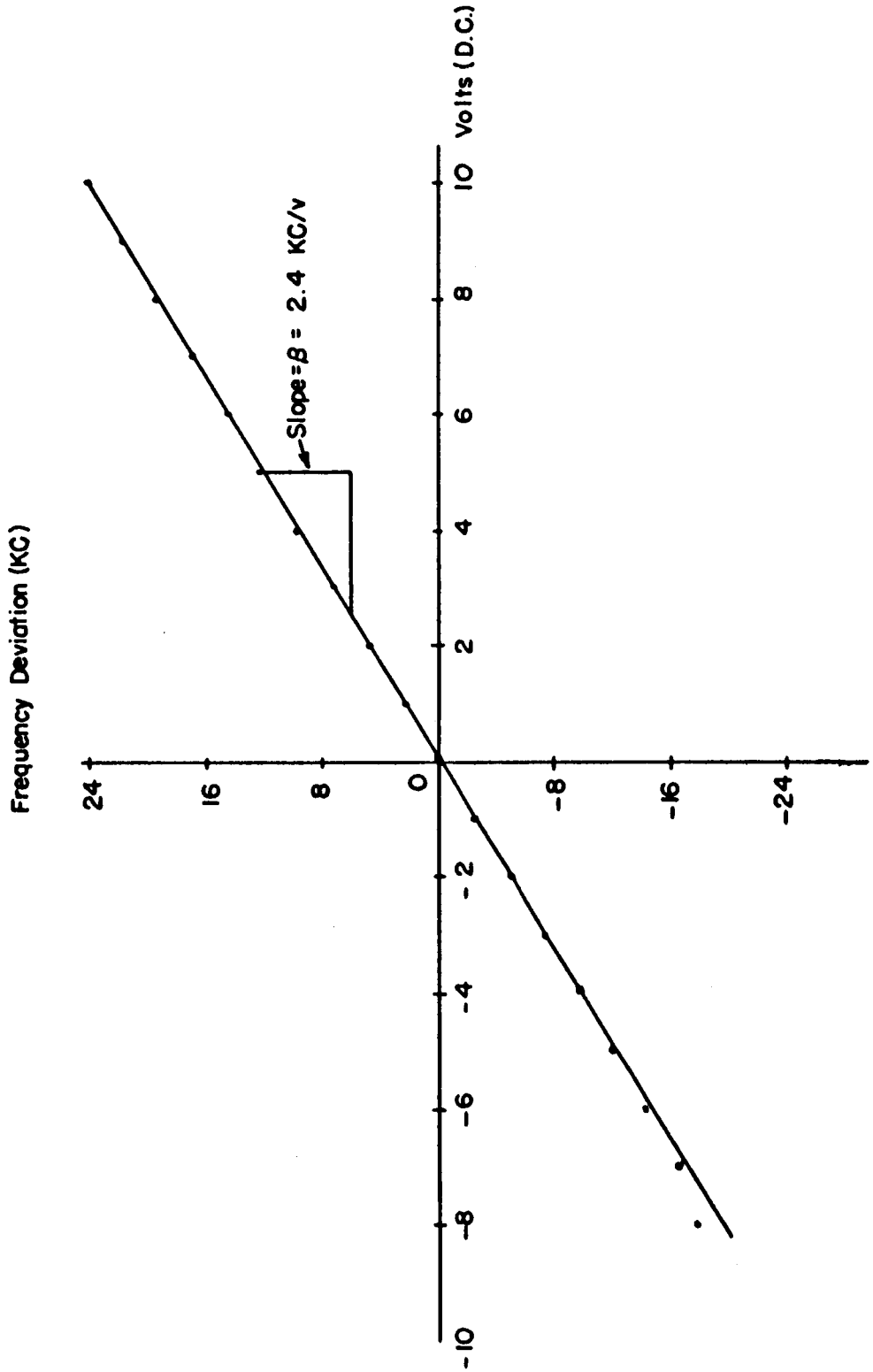

Figure 4.2. Typical Characteristic of Transmitter and Receiver VCO

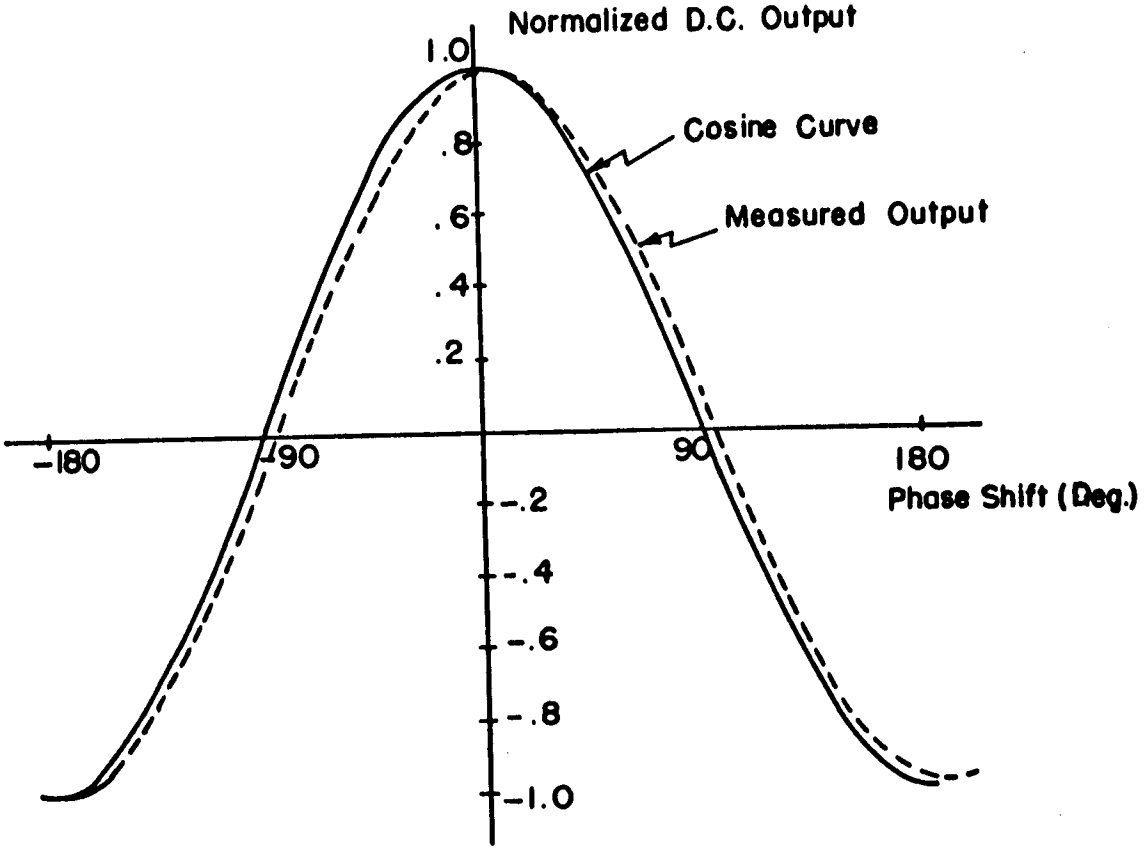

Figure 4.3. Static Phase Characteristic of Carrier Multipliers

and measuring the signal and noise power in the product as a function of CNR for various values of the input signal. Figure 4.4 shows the

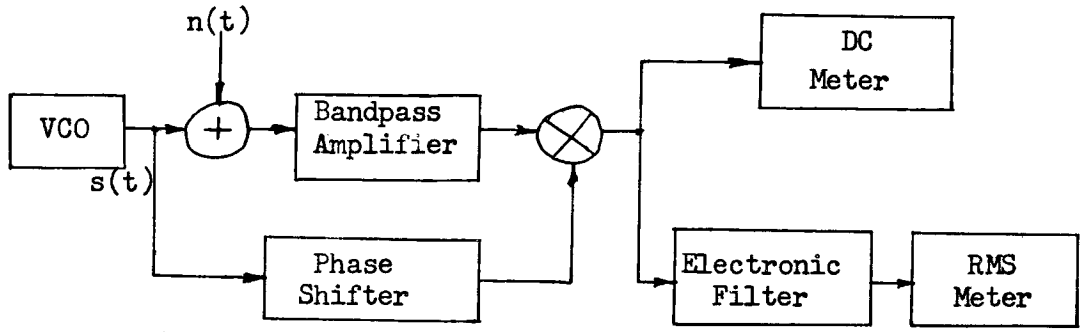

Figure 4.4. Block Diagram of Multiplier Test Setup.

test setup used.

Assume that the signal is a fixed carrier with no modulation and the noise is narrowband, white and gaussian with zero mean. If $\phi=0$ and the multiplication is ideal, then the average (D.C.) value of the output will be a constant, $\frac{A^2}{2}$, and the variance of the output, $\frac{A^2}{4} + \sigma^2$, where $\sigma^2=\overline{n^2}$

Plots of the test are given in Appendix A and summarized here.

(1) A plot of the d.c. output of the detector vs. CNR shows that the d.c. value decreases sharply below a certain CNR. The location of this threshold effect depends on the signal amplitude. The lower the signal, the larger the range of accurate multiplication. Thus, in the experimental measurements care must be taken to ensure that the multipliers are operating above threshold. (See Figure A.1)

(2) A plot of the output noise power in a 100cps band vs. input noise power is a straight line. Thus, the multipliers cause no distortion of the noise component regardless of signal level. (See Figure A.2)

(3) A plot of the D.C. output vs. total input power indicates that the threshold occurs at about the same place regardless of CNR. Thus it is the value of the peaks exceeding $\frac{1}{2}$ the reference peak which causes distortion. (See Figure A.3)

In conclusion, as long as the reference signals are large, about

40 volts p-p and the signal level is in the range of .4 volts rms, ideal performance of the multiplier can be assumed for the ranges of CNR used.

4.2.3. Analog Multiplier-Divider

Two Philbrick Q3-MlP analog multiplier-divider units were used in the experimental system. One was used in the divide mode and the other in the multiply mode to square the inphase or denominator signal.

The linearity of the multiply mode was excellent, but in the divide mode saturation effects were present under certain conditions. For a given value of e_2, the denominator, there is a tendency to give low readings for $e_1 < 0$ and high values for $e_1 > 0$. (See Figure 4.5 for notation.) The saturation distortion is poor for e_2=.1 volt d.c., but as e_2 increases the linearity improves and for $e_2 > 1.0$ volt d.c. no problem exists. These effects are shown in Figure A.4

The Table A-1 in Appendix A also indicates the frequency response for both modes of the unit. The response is affected by the magnitudes of e_1, e_2 and E, the scale factor. To operate the divider as ideally as possible as far as frequency response and linearity are concerned let $E > 2$ and $|e_2| > 1.0$ volts. The frequency response of the device in the multiply mode is about twice that of the divide mode for similar operating conditions.

A dynamic test of the divider in a noisy environment was made by using it in the tanlock model for the case k=0. (See Figure 4.5). The noise output of the divider was measured as a function of CNR for several values of the d.c. voltage e_2. In each case the open loop gain of the system was kept constant by adjusting the attenuation of the

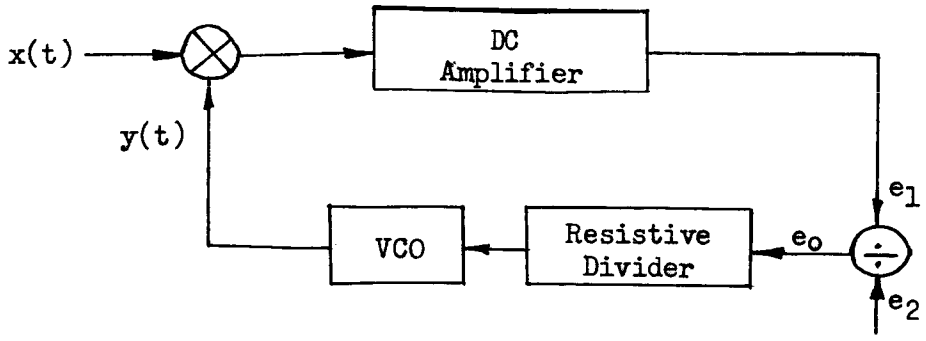

Figure 4.5. Block Diagram for Testing Divider Response to A Noisy Signal.

resistive divider as e_2 varied. E and e_1 were kept constant throughout the test.

As e_2 varied from .1 to 1.0 volt d.c., there was no significant change in a 200 or 600 cps band of the output noise over a complete range of CNR. Operation with noise was thus concluded to be satisfactory.

Measurements of the small signal frequency response of the general system (k=0) with and without the divider indicate this device to be the weak link in our system. It was concluded, however, that for the conditions under which measurements would be made, no significant problems due to the divider should occur.

4.2.4. Miscellaneous

All the remaining circuits in the system performed properly in the context of the signal specifications. Linearity was excellent and the

frequency response was more than adequate to make the model a valid one for all systems considered. A discussion of the model in Chapter 5 demonstrates this fact.

4.3. Measurements

It is helpful in understanding or interpreting the results of experimental work to have a clear idea of the techniques and knowledge of all the conditions under which the experiments were run. An elaboration and discussion of certain procedures considered unique with this research follow so that any future evaluation is made easier.

4.3.1. Verification of Tanlock Characteristic

In order to have any confidence in the measured performance of the general phase lock system in noise, measurements have to be taken to determine the degree to which the mathematical and physical models agree. Furthermore, it is desirable that the phase detector characteristic be checked both statically and dynamically in order to assure proper performance.

Figure 4.6 is a block diagram of the static test setup. The loop has been partially disabled by opening the feedback path and locking the system instead to a phase shifted version of itself. By observing the two signals A and B on a dual beam scope and operating the external trigger from A, the traces can be made stationary allowing the relative phase shift between A and B to be measured in time units. As the phase is varied, e_o is measured and a plot of the Tanlock characteristics obtained. A static curve for k=0 has already been shown in Figure 4.3. Curves for n=1,k=.5 and .75 were also obtained. The results

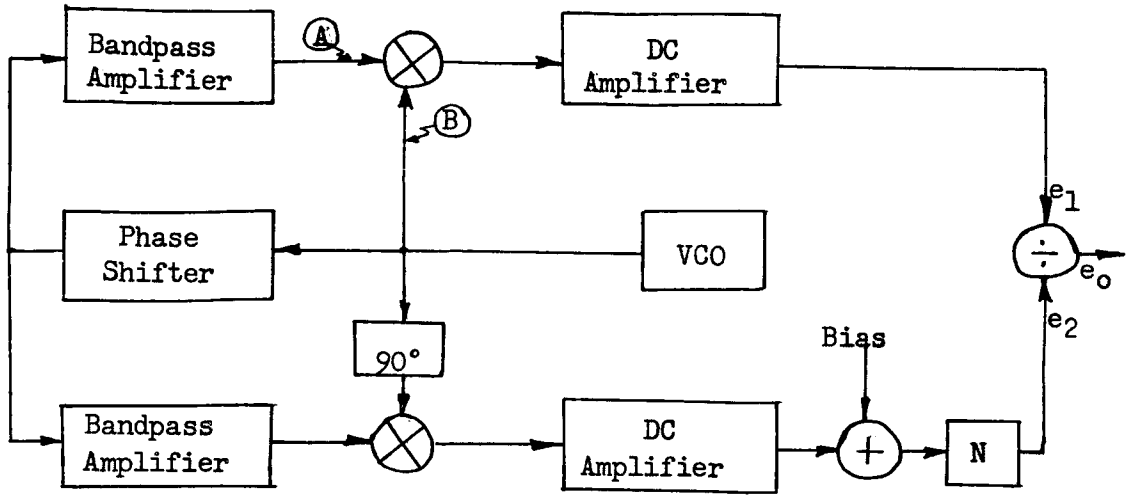

Figure 4.6. Block Diagram of Test Setup Used to Statically Measure Phase Comparator Characteristic

compared favorably with the theoretical curve. In the latter cases, the stable region was slightly smaller than it should have been as were the values of the peaks. This saturation effect was attributed to the divider, but only seems to take place at d.c. and very low frequencies.

The dynamic shape of the comparator characteristic can be obtained by simply opening the feedback loop of the entire system when an unmodulated carrier is present at the input and observing the output of the divider. Since the system will be asynchronous, one multiplier produces a sine wave output and the other a cosine output both at the same rate, thus allowing any tanlock derived characteristic to be displayed. The rate of this periodic output is equal to $\Delta\omega$. The method provides a quick way of adjusting the phase relations of the loop and also of observing the system frequency response.

A series of scope pictures taken of the loop non-linearity is shown in Figure 4.7a for n=1, k=0, .5, .75, .9 and Figure 4.7b n=2, k=.25, .5,

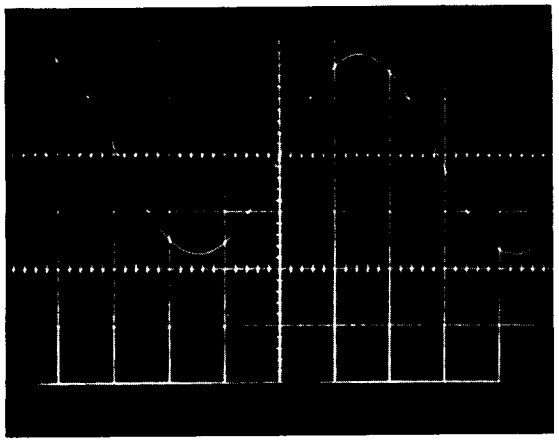

k =0

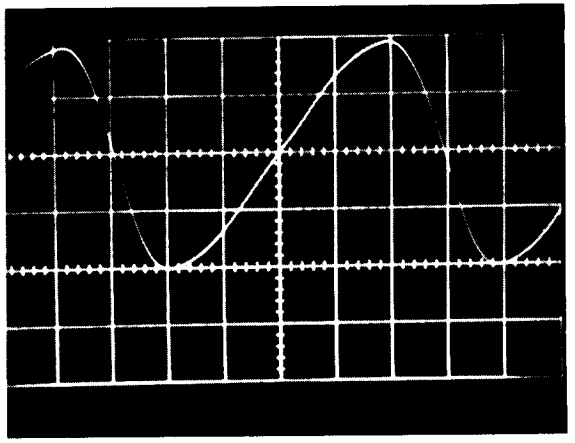

k =.5

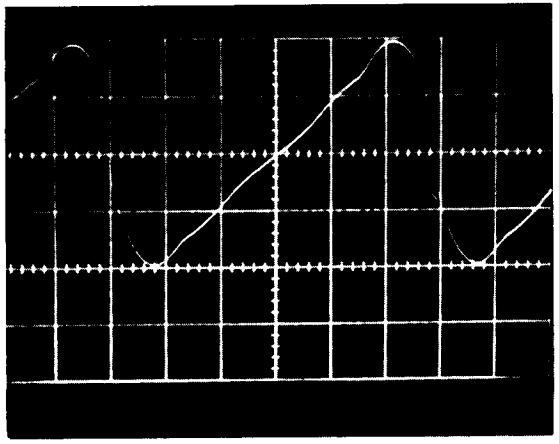

k =.75

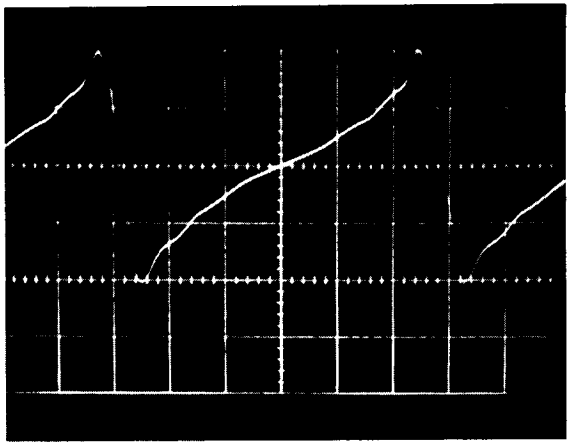

k =.9

Figure 4.7a. Scope Pictures of Tanlock Characteristic

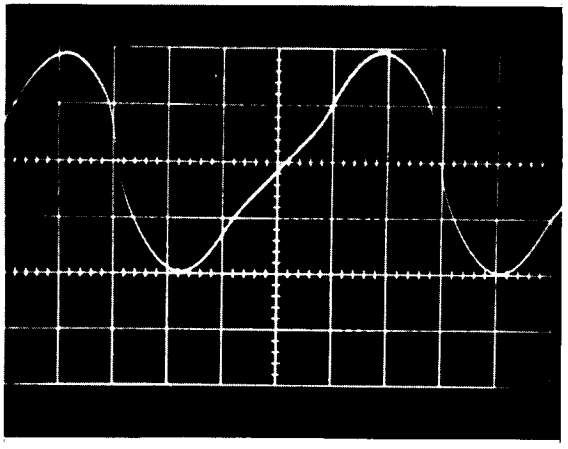

k =.25

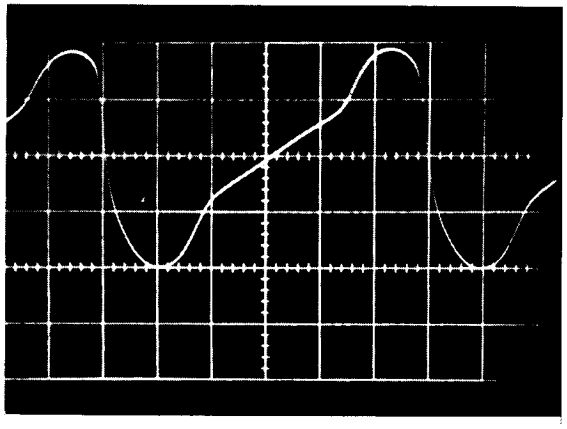

k =.5

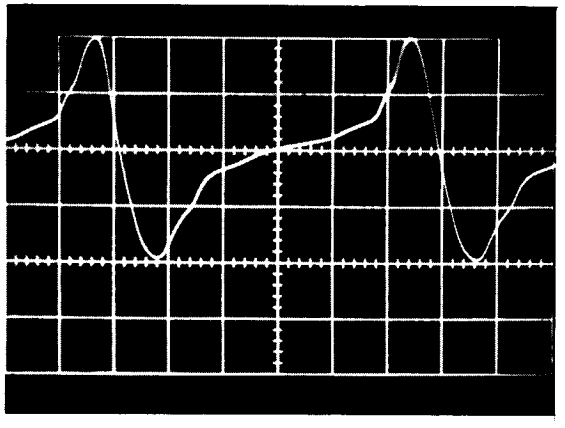

k =.7

Figure 4.7b. Scope Pictures of Tanlock Squared Characteristic

.7. By comparing these with Figure 2.9, it is seen that the dynamic performance is quite good. The horizontal scaling is the same in each case and the peaks approach $\pm 180^{\circ}$ as k approaches one for both values of n. To accommodate the picture in the entire frame, the vertical scaling was reduced as k approached one, thus the slopes are shown to get progressively smaller.

4.3.2. Signal and Noise Measurements

A. Measurement of Input Signal and Noise

In order to prevent any loading effects on the system an emitter follower is connected between the phase detector input (point A, Figure 4.1) and the external meter (rms). Since the system is linear to this point, superposition holds and no measurement difficulties are experienced if the phase detector is not overdriven.

The amplifier preceding the phase detector band limits the signal and noise with a single tuned circuit. Its response curve, Figure 4.8, indicates a 3db. bandwidth of 56.4kc , and a corresponding equivalent noise bandwidth of F_N=81.5kc . The amplifier input noise is white as is the detector input noise whose single sided spectral density N_o can be found as

$$N_o = \frac{N_p}{F_N} \tag{4.1}$$

where N_p = Total output Noise Power of the Bandpass Amplifier. The noise power in the equivalent noise band of the loop is then

$$N_{Band} = \frac{f_N}{F_N} N_p \tag{4.2}$$

Because the bandwidth of the bandpass amplifier is much greater than

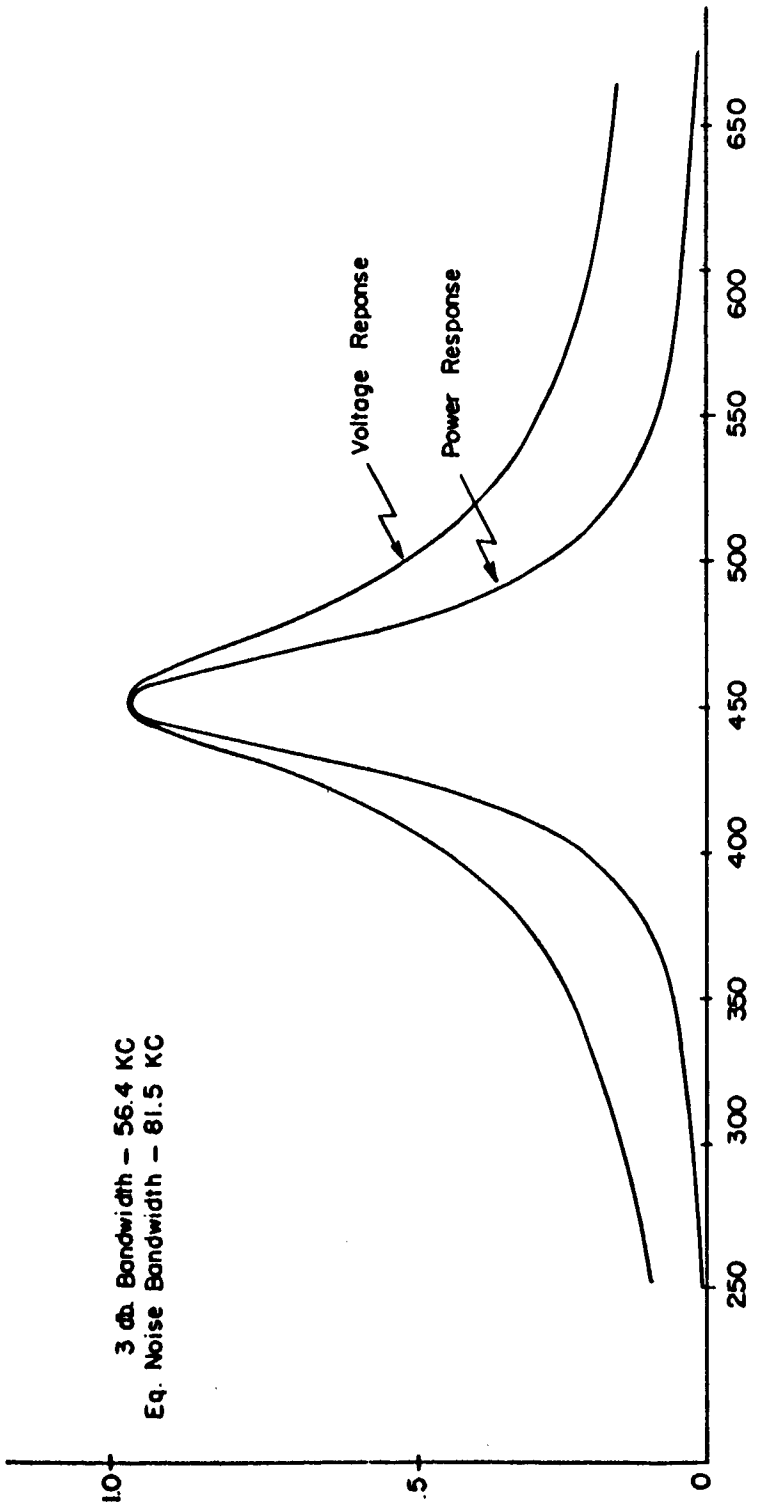

Figure 4.8. Voltage and Power Response of Bandpass Amplifier

that of the loop, the input noise to the receiver is considered to be essentially white.

B. Measurement of Output Noise — No Signal Modulation

The output noise is measured at the VCO input (point V on Figure 4.1). External meters were effectively isolated from this point by a d.c. coupled emitter follower. With no signal present, the output noise is easily measured by a true rms meter provided all 450 kc components are filtered out. If noise of a specific band is desired then an electronic filter with a variable bandwidth is inserted between the VCO and meter.

This noise is neither white or in general gaussian. In the high CNR region, the noise is gaussian and the output spectral density is parabolic. In the low CNR region, neither of these properties hold.

A measurement of the output noise spectral density was made for a high CNR. A block diagram of the method is shown in Figure 4.9.

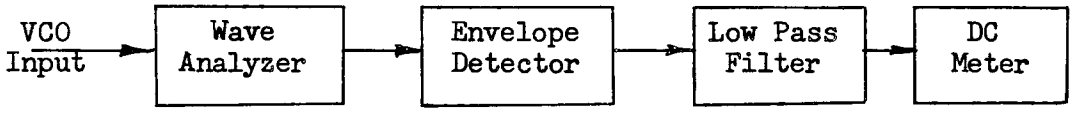

Figure 4.9. Block Diagram for Measuring Noise Spectral Density

The Wave Analyzer has a very narrow bandwidth — 3cps. Though the noise passing into it is not necessarily gaussian, the output will be approximately gaussian. It is then envelope detected, the current passed through a very low pass filter to reduce the variance and the d.c.

value detected. Since the noise from the Wave Analyzer is gaussian, the envelope detected signal is rayleigh. Thus the mean or d.c. value of this signal when squared is proportional to the total power in the 3cps band. By making this measurement at distinct frequencies, a good representation of the spectral density can be obtained. The resultant wave came out very close to a parabolic curve for the frequency range of interest.

C. Measurement of the Output Signal With No Noise

This presents no problem and is exactly the same as mentioned in B for the noise alone.

D. Measurement of the Signal and Noise Together

The measurement of the signal and noise components at the output (pt. V, Figure 4.1) is difficult to make. It is also necessary to define what is meant by output signal, above and below the threshold.

In the high CNR region, the signal component predominates over the noise in the information band, is observable on a scope and easily measurable. Below threshold, the loop randomly loses synchronism, each loss of synchronization causing the output signal to become discontinuous. The effect is to spread the signal energy out into adjacent bands. A measurement of signal power under these conditions requires defining. For our purposes, measurement of the fundamental was considered sufficient.

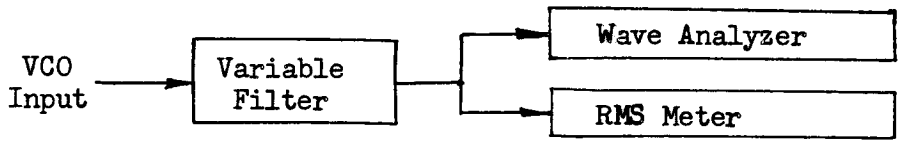

Figure 4.10. Block Diagram for Measuring Output Signal and Noise

The actual measurement setup is shown in Figure 4.10. The Wave Analyzer with its narrow bandwidth is used to measure the true signal component, while the rms meter measures the total signal and noise power.

By subtracting the mean square values of the two outputs $\overline{(S+N)^2} - \overline{(S)^2}$, the noise power alone is obtained.

In the high CNR region, very little difference between the two readings occur so that accuracy is lost. This is overcome by measuring the signal and noise separately with the other turned off, a valid method where linearity holds.

For the low CNR region a significant portion of the wave analyzer reading is noise in the 3cps band, so that the true signal power is obscured. The signal component can then be found in 3 steps. Turn off the signal and measure the noise in the 3cps band, then measure the total power due to signal and noise, and finally subtract the noise-power of the first measurement from the noise plus signal power of the second. This is a valid method since the difference in noise power in a 3cps band with and without signal present is negligible. The total output noise power is then found as before. The measurement in between these regions is as described.

4.3.3. Synchronization Time

The measurement of the time it takes a system to reach a steady state condition after a fixed carrier signal is applied is difficult to make. If mechanized, a great deal of auxilliary equipment is necessary, otherwise a lot of patience is required by the experimentor.

The sync time (3.8) is a function of the offset frequency $\Delta\omega$, λ_1, and λ_2 . Since no control is easily had over the initial phase, a distribution of times has to be obtained for fixed values of $\Delta\omega$ and λ_2, thus requiring many samples.

The system was designed to be gated on and off either by using a variable pulse rate device or a manual switch. If the scope is triggered from zero each time the system is activated, the transient at the VCO input can be displayed on a scope and a measurement of the sync time for any particular λ_2 can be made. If the system is stable this is fairly easy, if instabilities such as oscillators and power supplies cause changes in $\Delta\omega$ then more careful control must be exerted. By fixing $\Delta\omega$ and then observing the number of times out of the total sync is achieved for each value of time, a distribution of sync time is found. As $\Delta\omega$ increases towards the maximum lock range, the curves will shift and also spread out. There is a practical minimum unit of time necessary to achieve sync and so a dead space shows up.

The value of λ_2 (3.8) is extremely critical since if $\lambda_2 = \lambda_f$, the final state, the time will be infinite. Thus a judicious choice of λ_2 say within 5% of λ_f is necessary so that the experimental and theoretical results may be compared.

A plot of (3.9) vs. λ_1 is shown in Figure 4.11 for several values of $\Delta\omega$. A value of λ_2 within 5.0° of λ_f was chosen. These sync curves can easily be converted to the experimental distribution curves by assuming that any value of λ_1 is equally probable and using the relation.

$$P\left\{T_s \leq t_1\right\} = P\left\{-\lambda' < \lambda < \lambda_f\right\} + P\left\{\lambda_f < \lambda < \lambda''\right\} \qquad (4.3)$$

where λ' and λ'' are coordinates corresponding to t_1.

It would be desirable to measure sync time when noise is present. However, this is extremely difficult as the noise preceding the VCO completely masks any transient. It is possible to assume that the

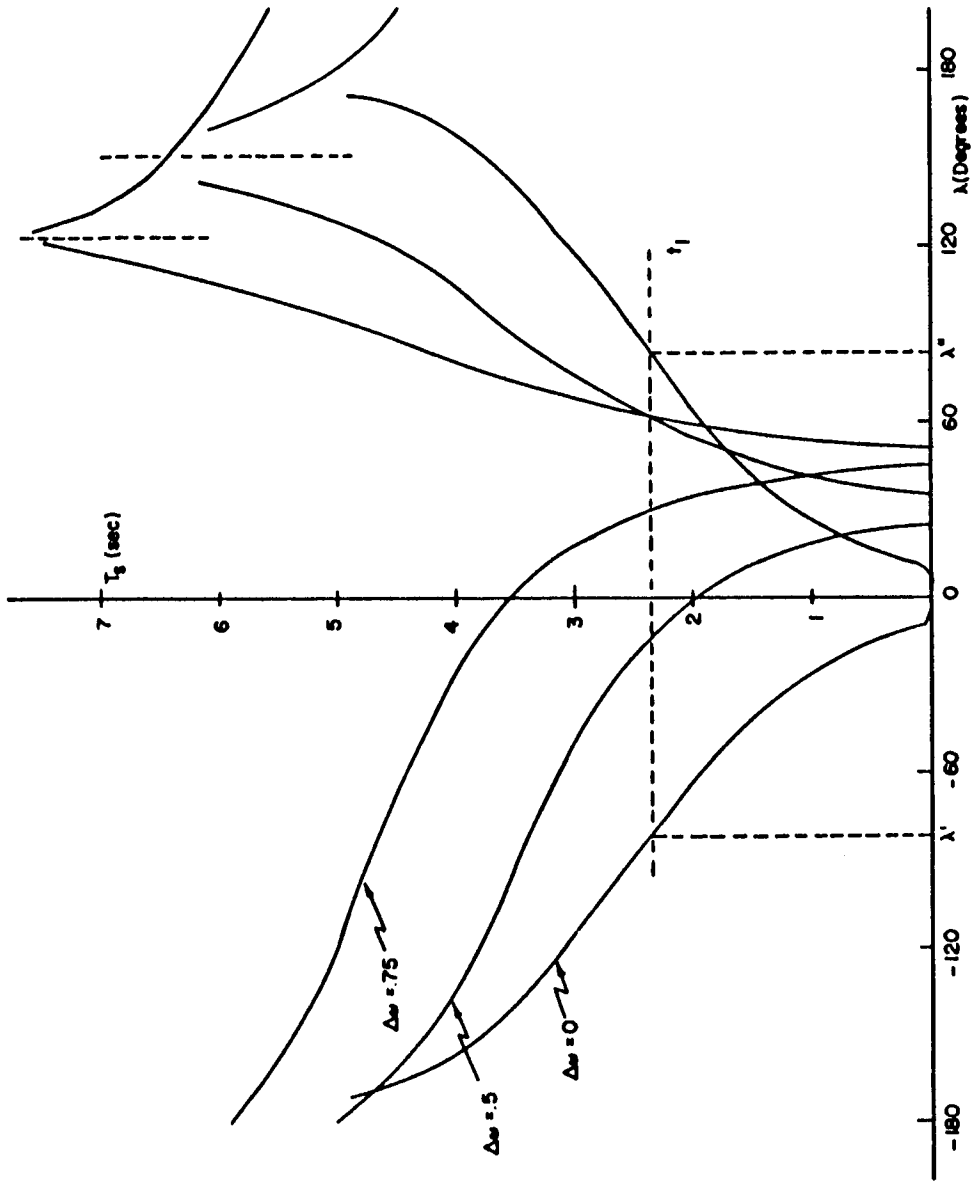

Figure 4.11. Synchronization Curves of a Simple First Order Loop

average sync time is inversely proportional to the lock range, then the average sync time can be extrapolated from the lock range curves as a function of CNR. As will be seen the lock range decreases with noise and so the sync time will increase. This result may be observed qualitatively in the laboratory.

4.3.4. Cycle Slipping Measurement

For a fixed bandwidth system and a given frequency offset, $\Delta\omega$ (with or without modulation), any phase lock loop system will remain synchronous until the input noise reaches a certain level. It will then go out of sync a certain percentage of the time, depending on the CNR. Conversely, the CNR for a fixed percentage of asynchronous operation is a function of $\Delta\omega$. This momentary loss of synchronization or cycle slipping phenomena produces a high energy pulse or spike which can be used to detect cycle clipping.

The test system used in measuring and counting these spikes is shown in Figure 4.12.

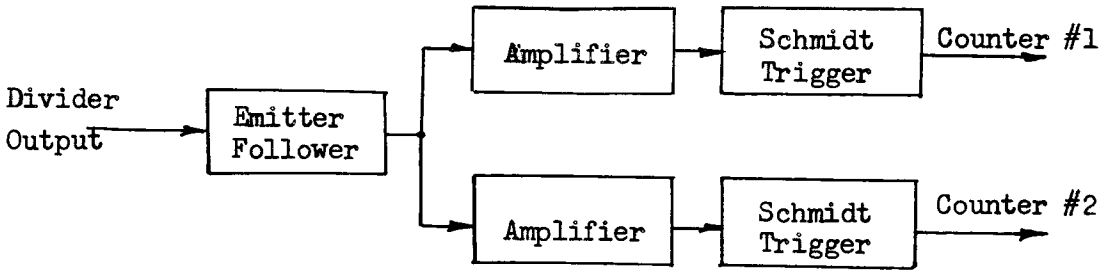

Figure 4.12 Block Diagram for Measuring Cycle Slipping Pulses

The schmidt triggers were used to discriminate the positive and negative spikes, and their outputs then counted. Figure 4.13 is a typical picture

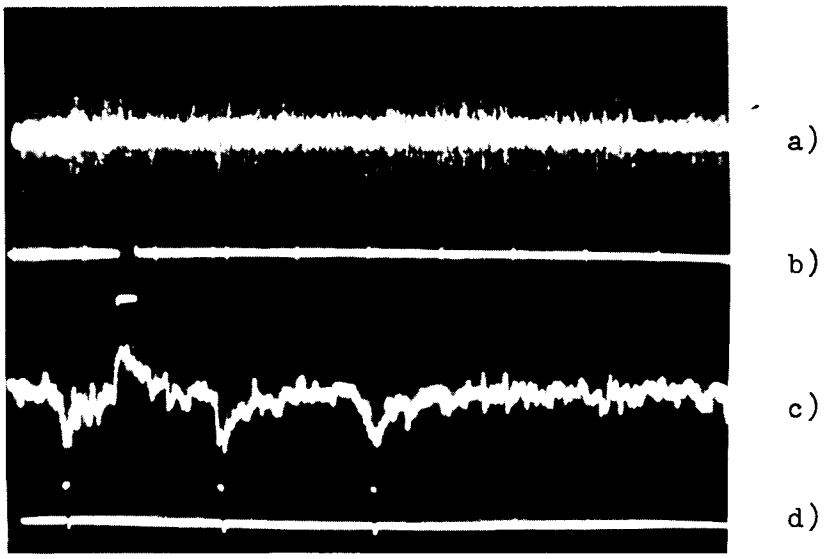

Figure 4.13 Scope Picture of Cycle Slipping Pulses

a) Unfiltered Divider Output
b) Positive Pulse Detector
c) Filtered Divider Output
d) Negative Pulse Detector

of the filtered and unfiltered divider output and the detected spikes for a first order system.

4.3.5. Lock Range Measurement

The measurement of lock range when no noise is present is easily done by slowly shifting the frequency of the carrier until synchronism is lost. The total shift in frequency from the VCO steady state value is the lock range and it should be symmetrical. As noise is added, this value of $\Delta\omega$ cannot be reached because the noise will cause cycle slipping

spikes to occur first. Increasing noise causes the lock range for a given spike rate to decrease until the system is out of sync even for $\Delta\omega=0$ (see Figures 5.8 and 5.9). For a given CNR the lock range was measured as the total VCO shift causing a specified spike rate.

4.3.6. Measurement of Equivalent Linear Noise Bandwidth

The importance of the parameter f_N in this research required that it be easily measurable before taking any data. For a first order loop, the small signal transfer function from the input phase to VCO input (Figure 2.4) is

$$E_o(s) = \frac{K}{\beta} \frac{s}{s+K} \tag{4.4}$$

If the input carrier is f.m. modulated by a signal m(t), then

$$\lambda_i(s) = \frac{m_f}{s} M(s) \tag{4.5}$$

where m_f = modulation index of transmitted signal, and M(s) is the Laplace Transform of m(t).

Combining (4.4) and (4.5) we obtain

$$E_o(s) = \frac{Km_f}{\beta} \frac{1}{s+K} M(s) \tag{4.6}$$

By using a low frequency generator as m(t), the frequency response of the system can be easily checked. Since the 3db point is equal to the open loop gain K, f_N can be found from

$$f_N = K/2 \tag{4.7}$$

Rewriting (4.4) for the other filters of Table 2.1 permits an easy check of the frequency response and f_N for these systems also.

V. EXPERIMENTAL RESULTS — FIRST ORDER SYSTEM

After a brief discussion of the methods used to check system operation, the remaining part of Chapter 5 is devoted to the experimental results for the first order systems. The order of presentation follows the list of criteria given in Chapter 2. Particular attention is devoted to the threshold section since the definitions along with the measurements are unique with this research. A final section is devoted to a discussion of design criteria.

5.1. Experimental System Verifications

Once all system components were performing properly and the correct comparator function incorporated into the system, several simple experimental measurements were taken. These final checks, as indicated below, were generally made before the loop criteria were evaluated.

Figure 2.5 is the exact equivalent circuit of the general phase lock loop of Figure 4.1 when the noise is zero. If this system is synchronized to an unmodulated fixed carrier, the d.c. control voltage of the loop , e_o, is proportional to $\Delta\omega$ in the following way,

$$e_o = AF(\lambda) = \frac{\Delta\omega}{\beta} \tag{5.1}$$

A typical experimental plot of (5.1) for a fixed A is shown in Figure 5.1 and as can be seen, linearity is excellent.

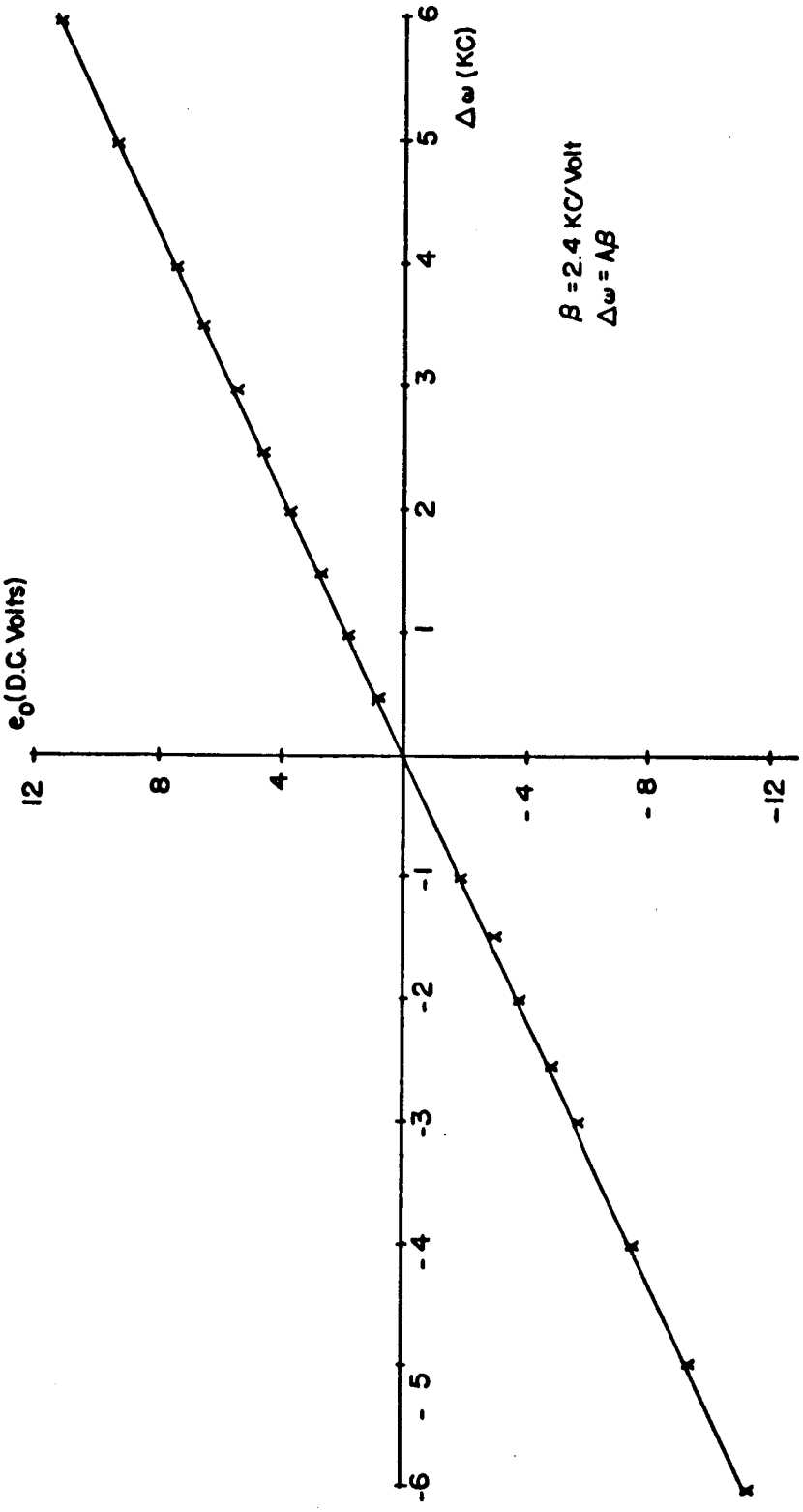

Figure 5.1. Experimental Graph of e_o vs. Δm(eq. 5.1)-First Order System

A dynamic counterpart of the above measurement can also be made. Suppose that the fixed carrier is modulated by

$$m(t) = \sqrt{2}\, e_i \operatorname{Cos} \omega_m t \tag{5.2}$$

where $\omega_m < K$

and $\Delta\omega = 0$.

Then

$$e_o(t) = \sqrt{2}\, e_i \frac{K_t}{\beta} \operatorname{Sin} \omega_m t = AF(\lambda) \tag{5.3}$$

where K_t = Transmitter constant.

Again the relationship is linear and will hold as long as the loop is capable of tracking the instantaneous frequency of the input carrier. An experimental plot of (5.3) for n=1, k=0, .5, .75, and.9 is given in Figure 5.2. The graph is linear as expected for each system until tracking stops. It should be noted that the linear portion is extended as k approaches one. This is consistent with the fact that the tracking (lock range) capability of tanlock increases as k approaches one as shown in Chapter 3. Though not shown, measurements for n=2, k=.25, .5 and .7 produced similar results.

Finally it should be noted that the maximum offset frequency, $\Delta\omega_{max}$, or lock range is linearly related to the input signal level A by the relation

$$\Delta\omega_{max} = A\beta \tag{5.4}$$

A typical plot for k=0 appears in Figure 5.3 and again performance is shown to be good.

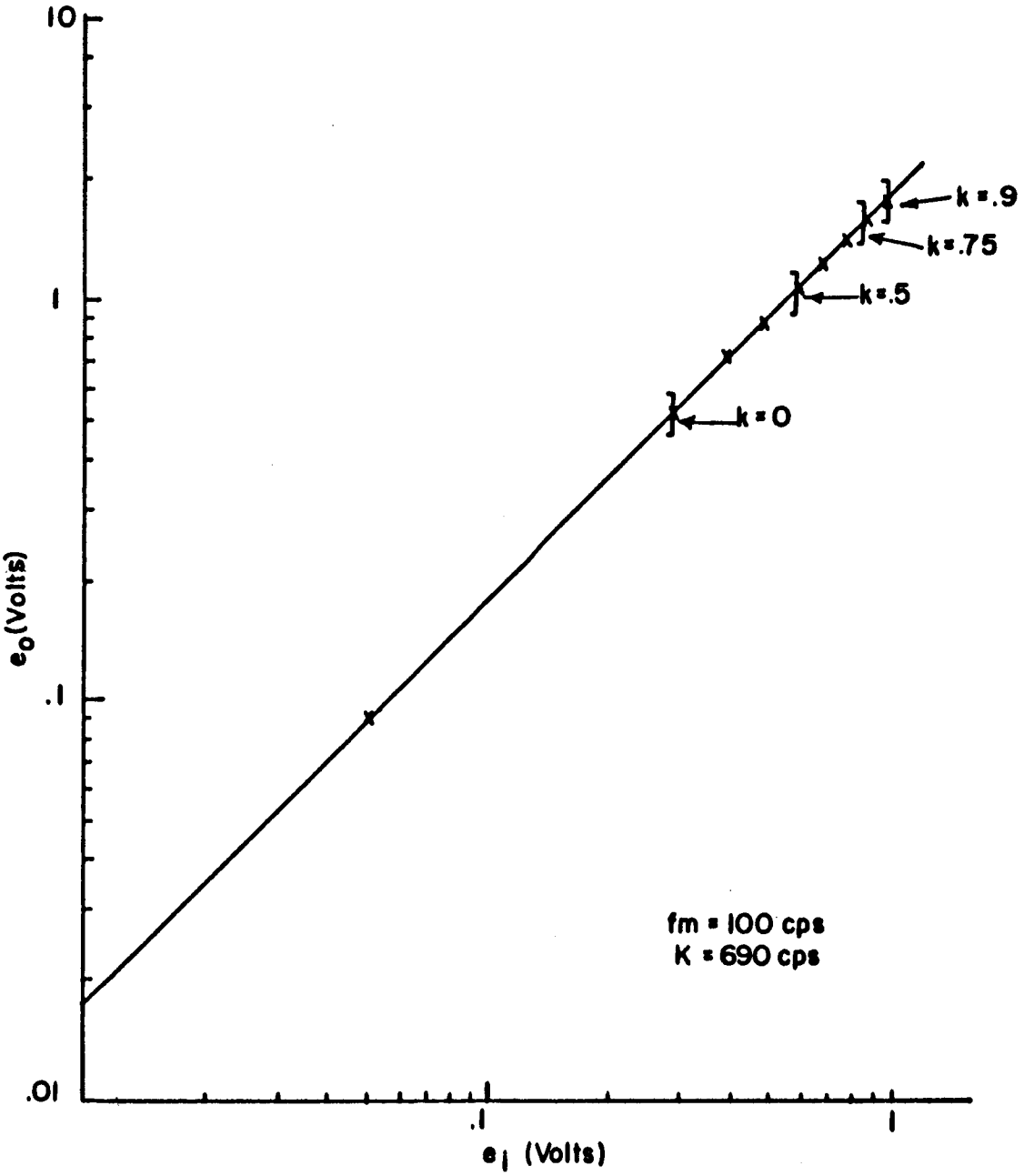

Figure 5.2. Experimental Graph of e_o vs. e_i (eq. 5.3)-First Order System

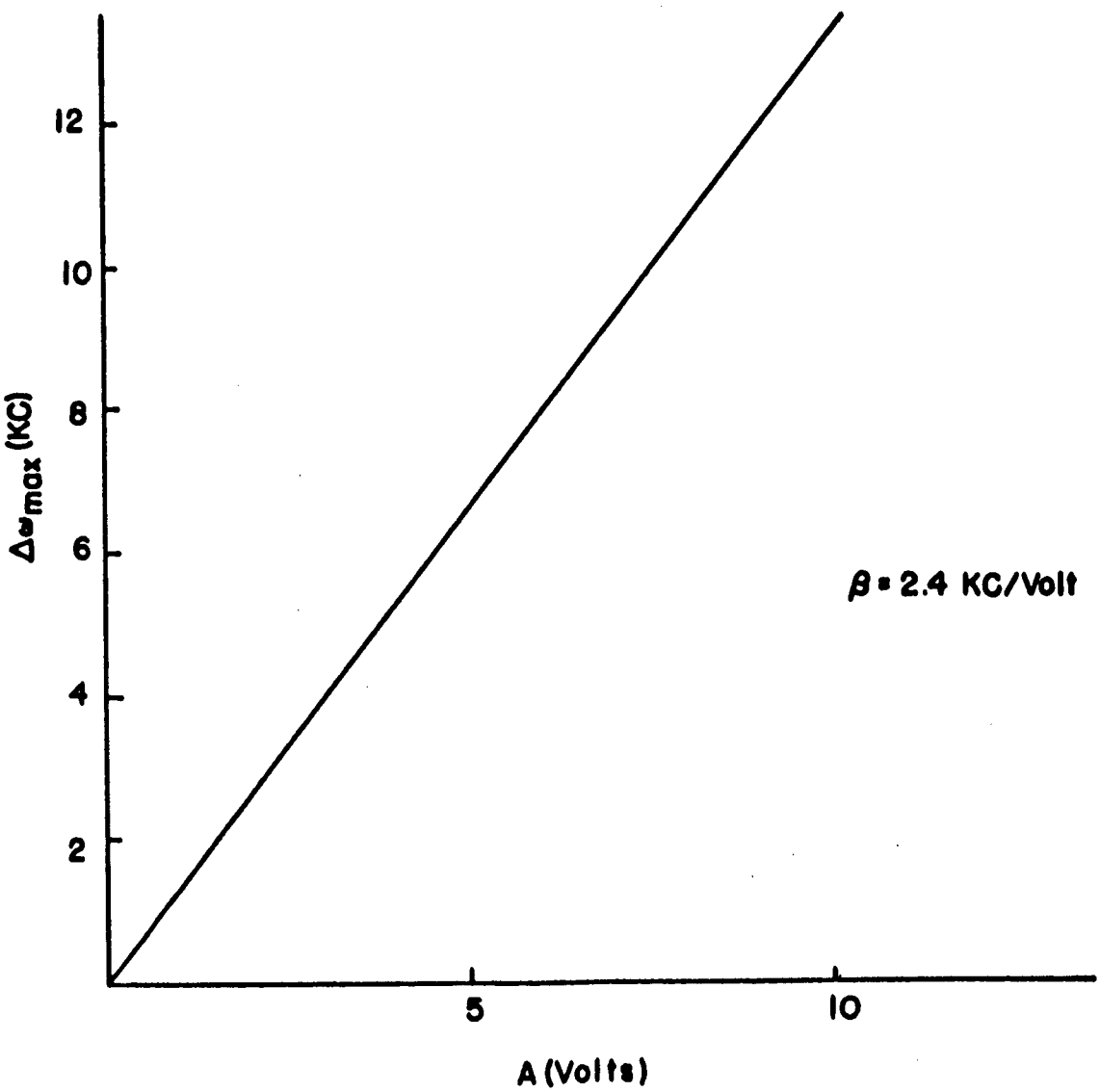

Figure 5.3. Experimental Graph of $\Delta\omega_{max}$ vs. A (eq. 5.4)-First Order System

5.2. Tanlock Modification

It was noted in Chapter 3, that the A(t) term in the denominator path of the general tanlock system prevented any exact noise analysis. When the noise peaks of the denominator approach or go through zero for tanlock, or simply approach zero for tanlock squared, large pulses occur at the VCO input causing momentary cycle slipping. Thus, as expected the physical system performs poorer than that predicted by the Fokker-Planck model.

A modified tanlock system was developed to overcome part of the difficulty. Two diode clamps were used to limit the range of the denominator to $C^n(1\pm k)^n$, Figure 5.4, where the bias is equal to C volts.

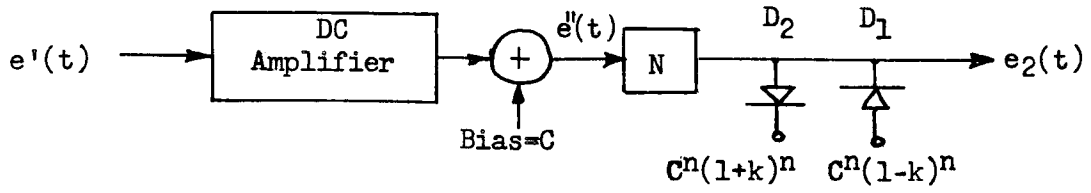

Figure 5.4. Block Diagram of Modified Signal Path for Tanlock Systems.

The noise peaks are effectively hard limited to this fixed range. As a result the performance significantly improves. It is essential to note that because of the clamping or limiting levels chosen, the signal characteristics are preserved. With little or no noise present, the diodes do not switch, only the threshold performance is affected.

An effective demonstration of the distortion introduced by misadjustment of the diodes is shown in Figure 5.5 and Figure 5.6. The first picture, Figure 5.5 shows the dynamic tanlock squared characteristic (k=.25). In the top trace the diodes have been properly adjusted. In the bottom trace distinct distortion appears because D_1 has been biased too high and D_2 biased too low.

a.

b.

Figure 5.5. Scope Picture of Diode Distortion of Tanlock Squared Characteristic (k=.25)
a. Undistorted
b. Distorted — Diodes Misadjusted

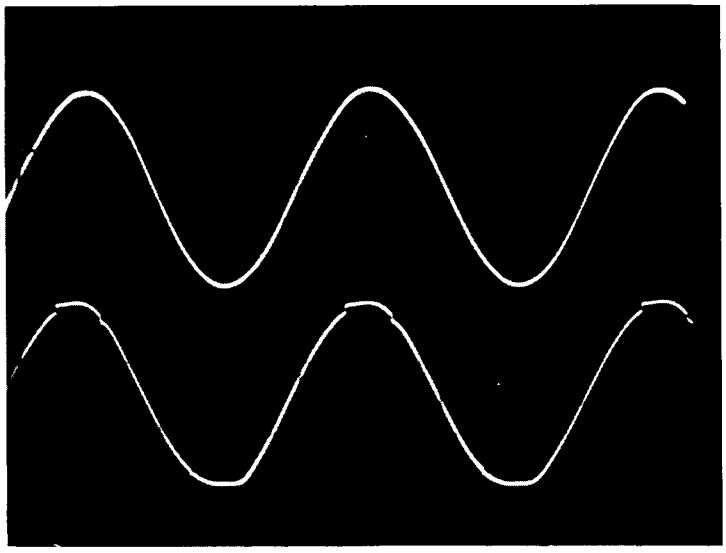

a.

b.

Figure 5.6. Scope Picture of Diode Distortion of Output Signal
a. Undistorted
b. Distorted — Diodes Misadjusted

Figure 5.6 is the output of the divider when the carrier is f.m. modulated with a 50 cps sine wave. While the top trace is distortion free, the bottom indicates some distortion due to the misadjustment of the diodes.

The output noise power was measured for the modified and unmodified versions of the general system so that a comparison could be made. However, all the other criteria were measured for the modified system only, due to its superior performance.

5.3. Equivalent Linear Noise Bandwidth

As mentioned in Chapter 2, it was decided to compare all systems both theoretically and experimentally on the basis of the same equivalent linear noise bandwidth. For convenience a value of f_N=345 cps was chosen for all the experimental work involving a first order system and was measured as indicated in Section 4.3.7.

In order to permit the use of the experimental results for design purposes and future comparisons, all measurements made with CNR as the independent variable have been plotted using a normalized input signal to noise ratio, R_i

$$R_i = \frac{S_p}{N_p}\frac{F_N}{f_N} = \frac{A^2}{N_o f_N} \qquad (5.5)$$

where $\frac{S_p}{N_p}$ = Measured Signal to Noise Ratio at the detector input (CNR)

R_i is a more practical parameter because the lock range and threshold curves become universal. For check purposes, other values of f_N were used in some measurements and the normalized curves were always the same. A similar parameter is used by authors such as Viterbi[17], Lindsey[18] and Van Trees[14]. It should be noted that since only part of the output noise power was measured, these curves are not

universal. However, if the measuring band such as 600 cps is normalized by f_N, then these curves too can be considered universal.

5.4. Lock Range

A static test of the lock range of the generalized tanlock system for n=1 and n=2 indicated excellent correlation with the theoretical values. Figure 5.7 is a plot of the normalized lock range, C_{max}, vs k for n=1 and 2. The normalized experimental values of lock range are also shown. For the various values of k used, the largest deviation of the experimental values is 8%. These static results are valid for both the first and second order systems tested.

Though it was expected that the lock range would degrade as R_i decreased, it was hoped that the improvements of the no noise case could be maintained as k increased. Figure 5.8 and Figure 5.9 are plots of the lock range vs R_i based on a criterion of 30 spikes/sec. for the modified system.

The improved lock range for larger k is maintained for both tanlock and tanlock squared until the threshold occurs. The slopes both above and below threshold get larger as k increases, indicating a sharper threshold. If a lower slip rate is used, then all of these curves will be a little lower.

5.5. Synchronization Time

Since synchronization time could not be easily measured with noise present, only several distribution curves of T_s for the no noise case were found. These were used to test both the system and the measurement technique.

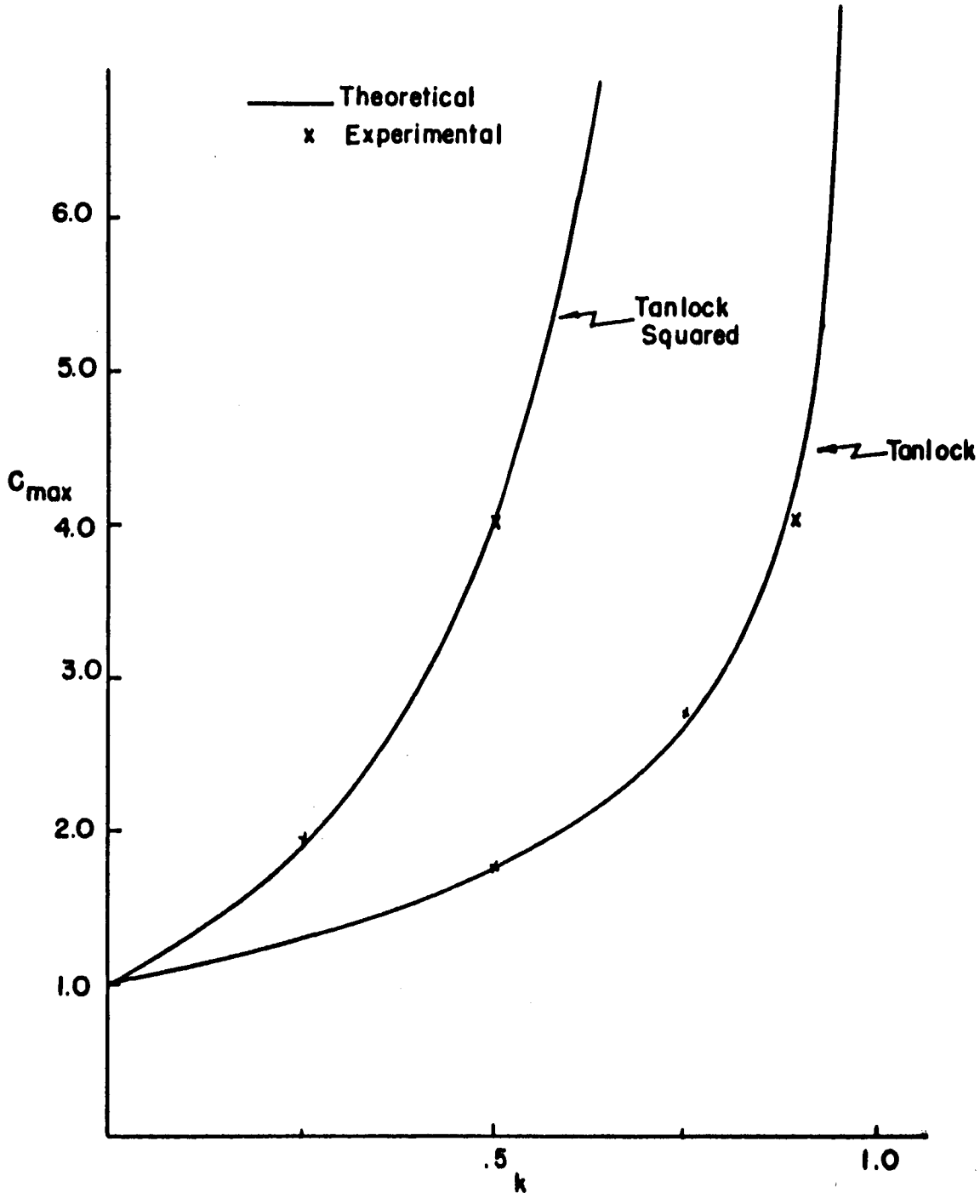

Figure 5.7. Normalized Lock Range Curves

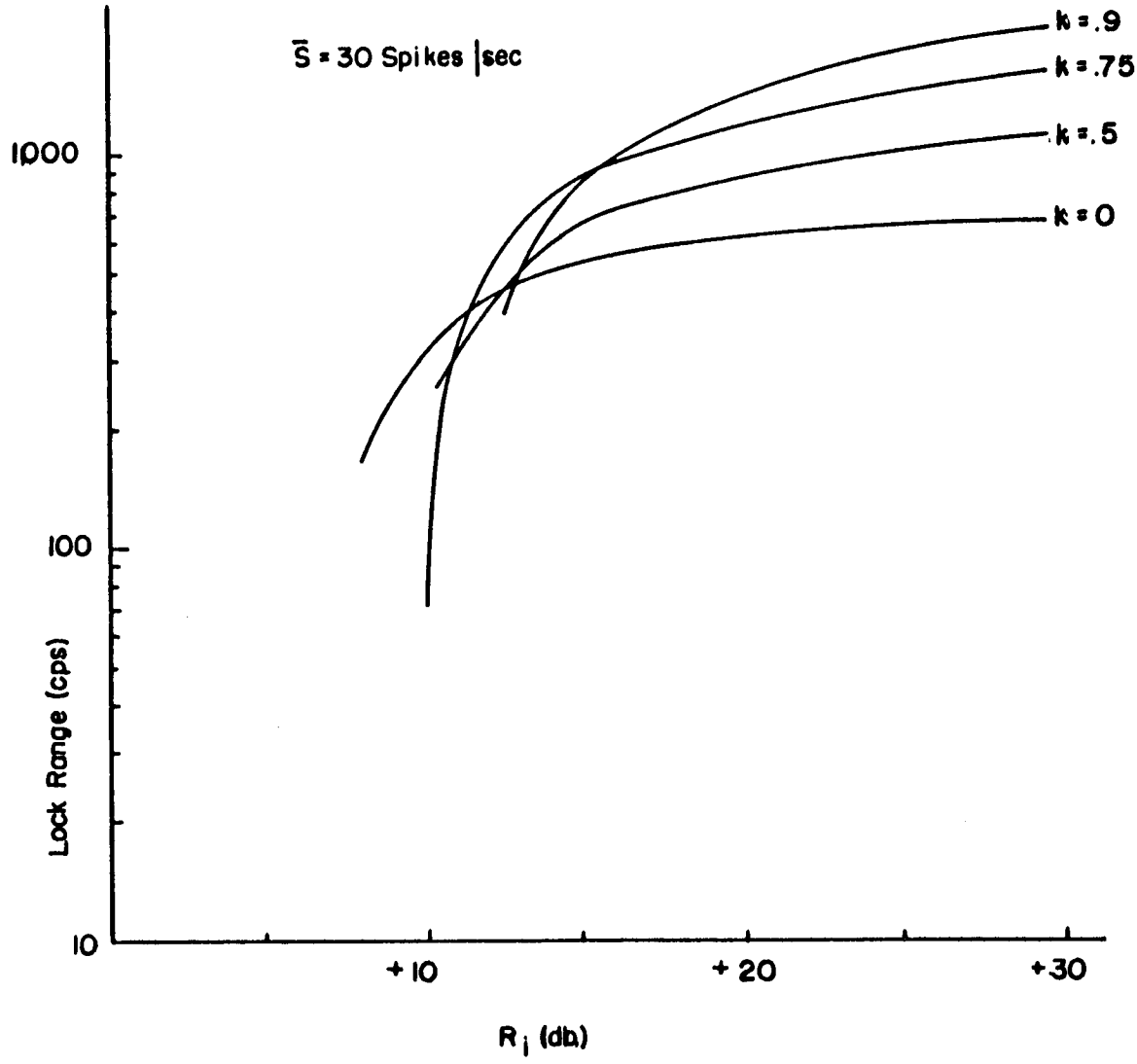

Figure 5.8. Dynamic Lock Range Curves for First Order Tanlock System

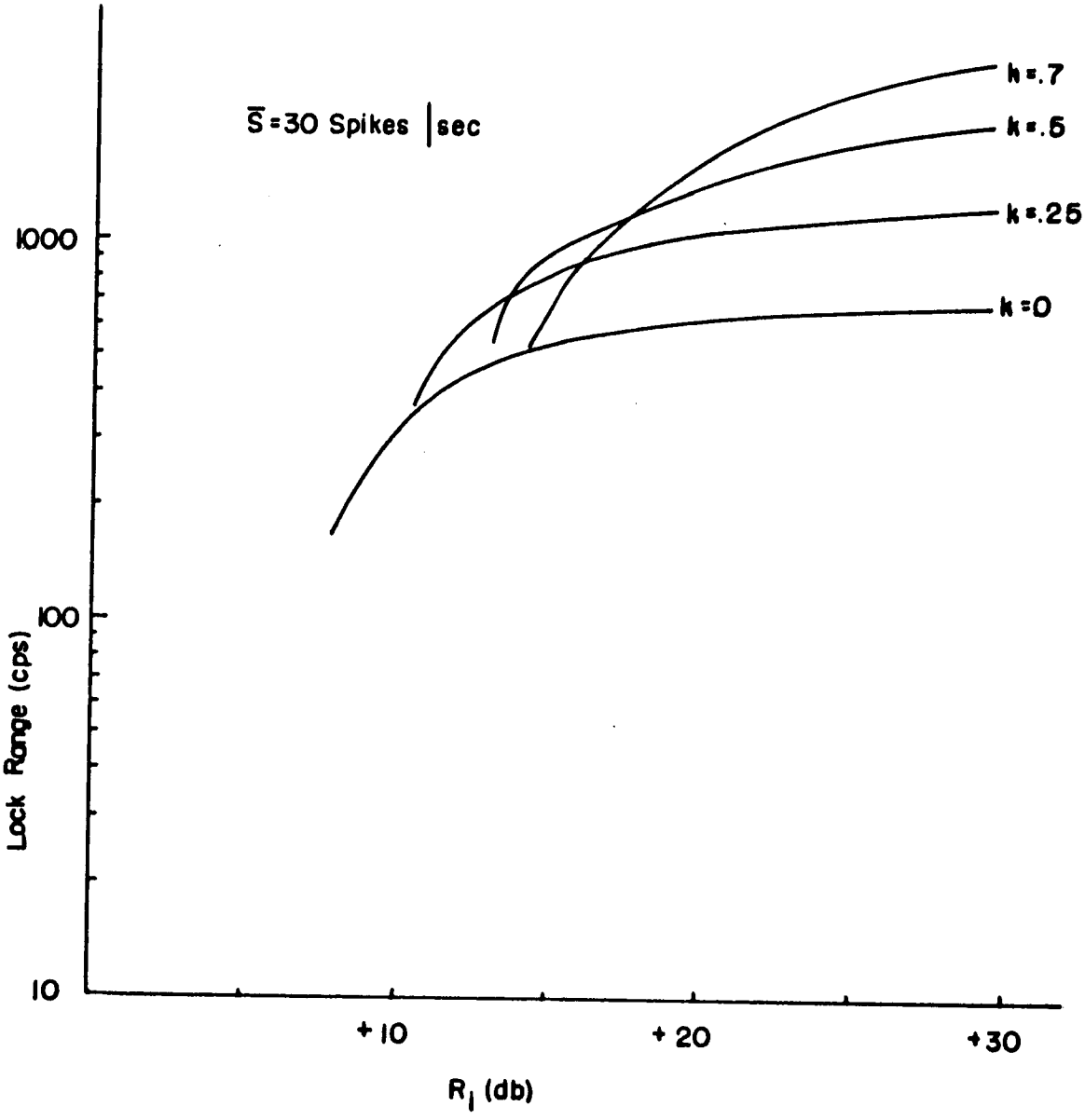

Figure 5.9. Dynamic Lock Range Curves for First Order Tanlock Squared System

For the case k=0, a typical set of synchronization distribution curves are plotted in Figure 5.10. Three values of $\Delta\omega$ were chosen: 0, $\frac{1}{2}\Delta\omega_{max}$ and $\frac{3}{4}\Delta\omega_{max}$. The open loop gain was 3.3 kc. As previously noted for increasing $\Delta\omega$, the curves spread out due to the larger phase plane trajectories required.

Figure 5.11 is the plot of both theoretical and experimental distribution curves whose open loop gain is 610 cps. In both cases $\lambda_2 = 2.5^\circ$ and $\Delta\omega = 0$. Under the stated conditions the correlation between experimental and theoretical results is excellent and thus the technique is proven.

No distribution curves were found for other values of k. However, a qualitative check indicated that as k increased, the average value of T_s decreased as prescribed by the results in Chapter 3.

5.6. Output Noise Power

Though it was desired to know the phase error voltage under various noisy conditions, such a measurement cannot be directly made in the physical system. As a result, the noise power into the VCC (filter output), was measured. A noise measurement at this point gives considerable insight into the fundamental behavior of the loop.

In measuring output signal to noise ratios, the noise power is typically measured in an ideal band only as wide as the information band. Such a band can be equal to or less than the loop bandwidth. A qualitative look at the output power in various information bands for a loop (k=0) of fixed bandwidth is clearly seen in Figure 5.12. Here the output power was measured in four different bandwidths of 100, 600, 1000

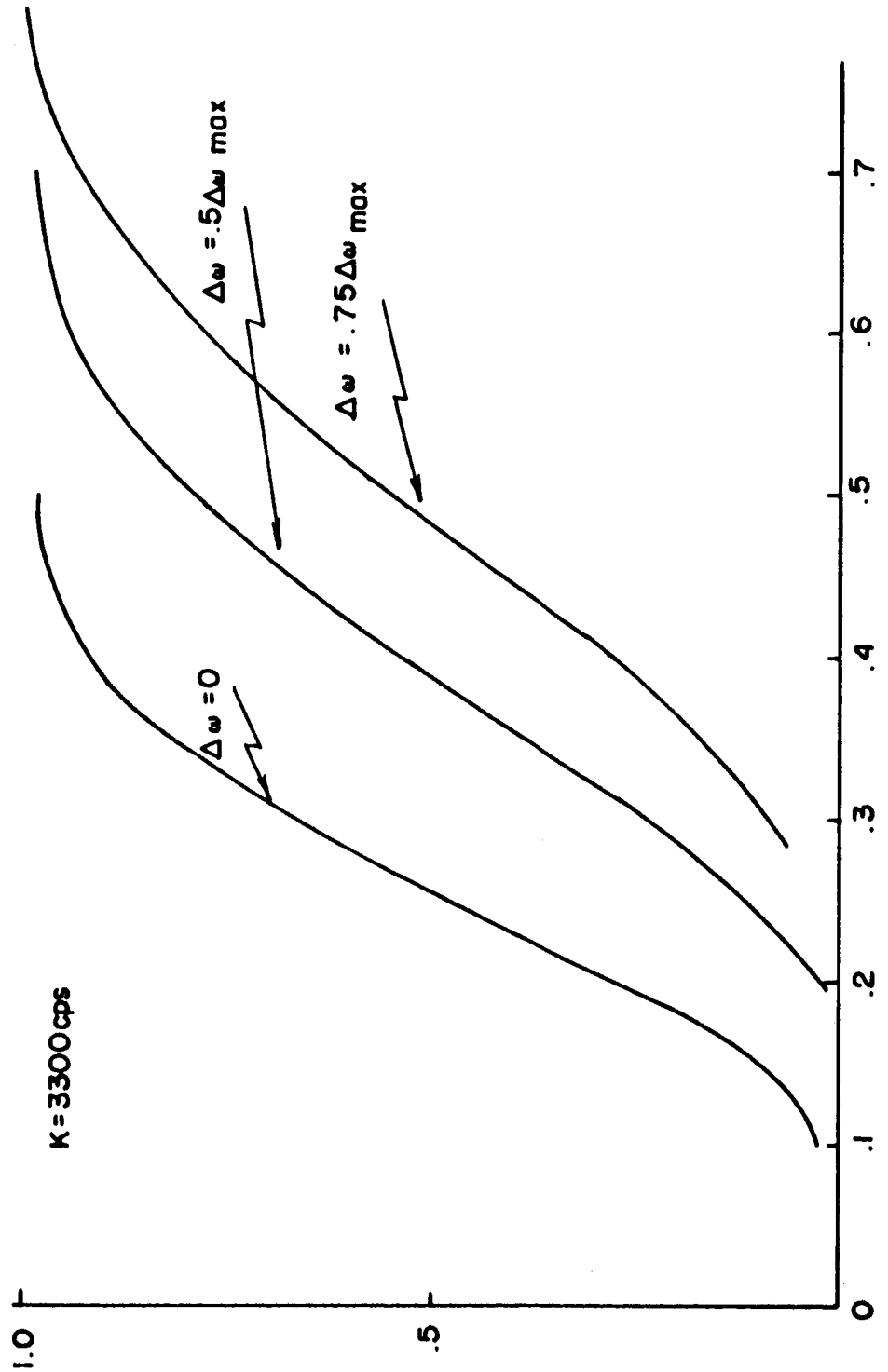

Figure 5.10. Synchronization Distribution Curve for a Simple First Order System

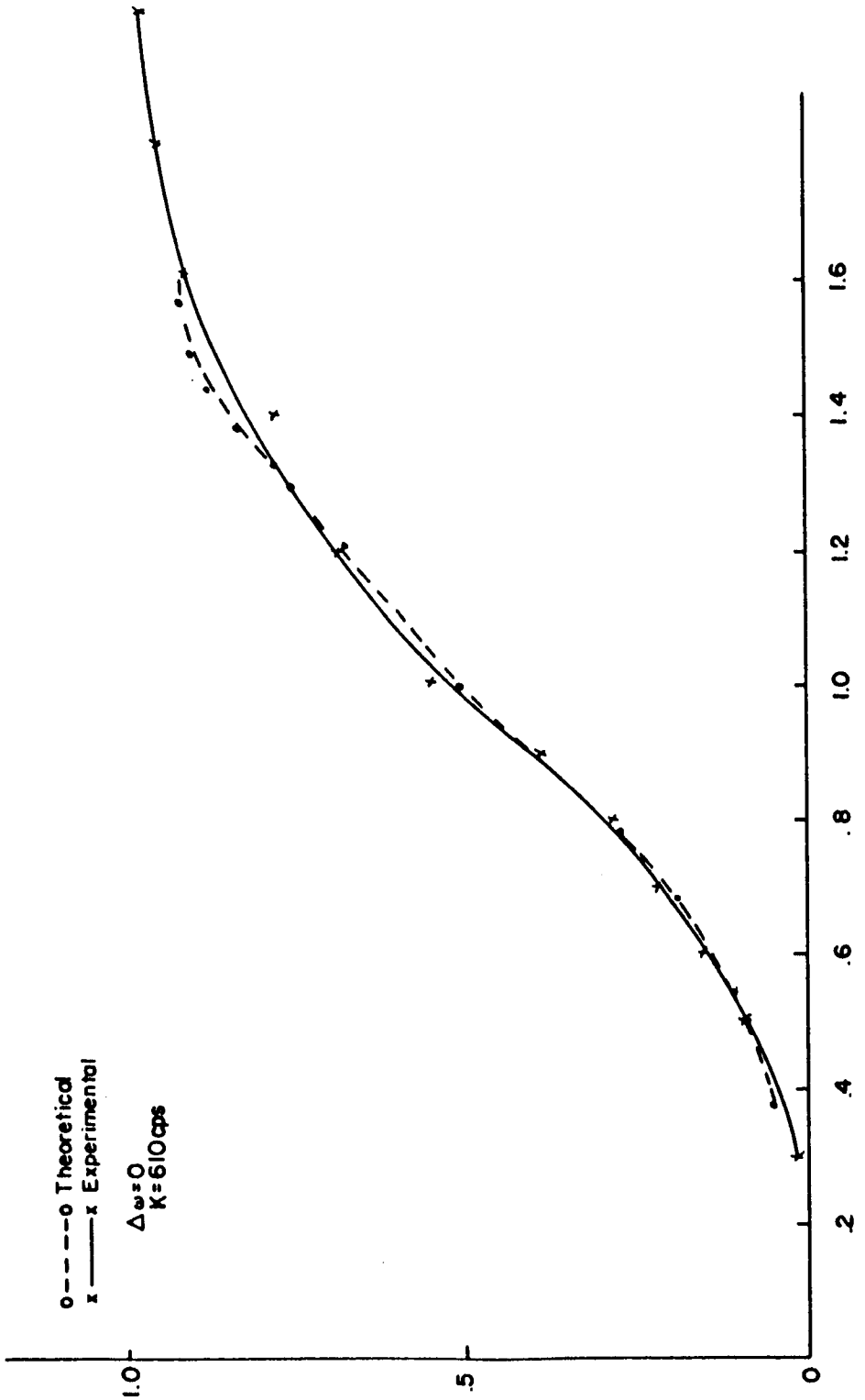

Figure 5.11. Synchronization Distribution Curves for a Simple First Order System

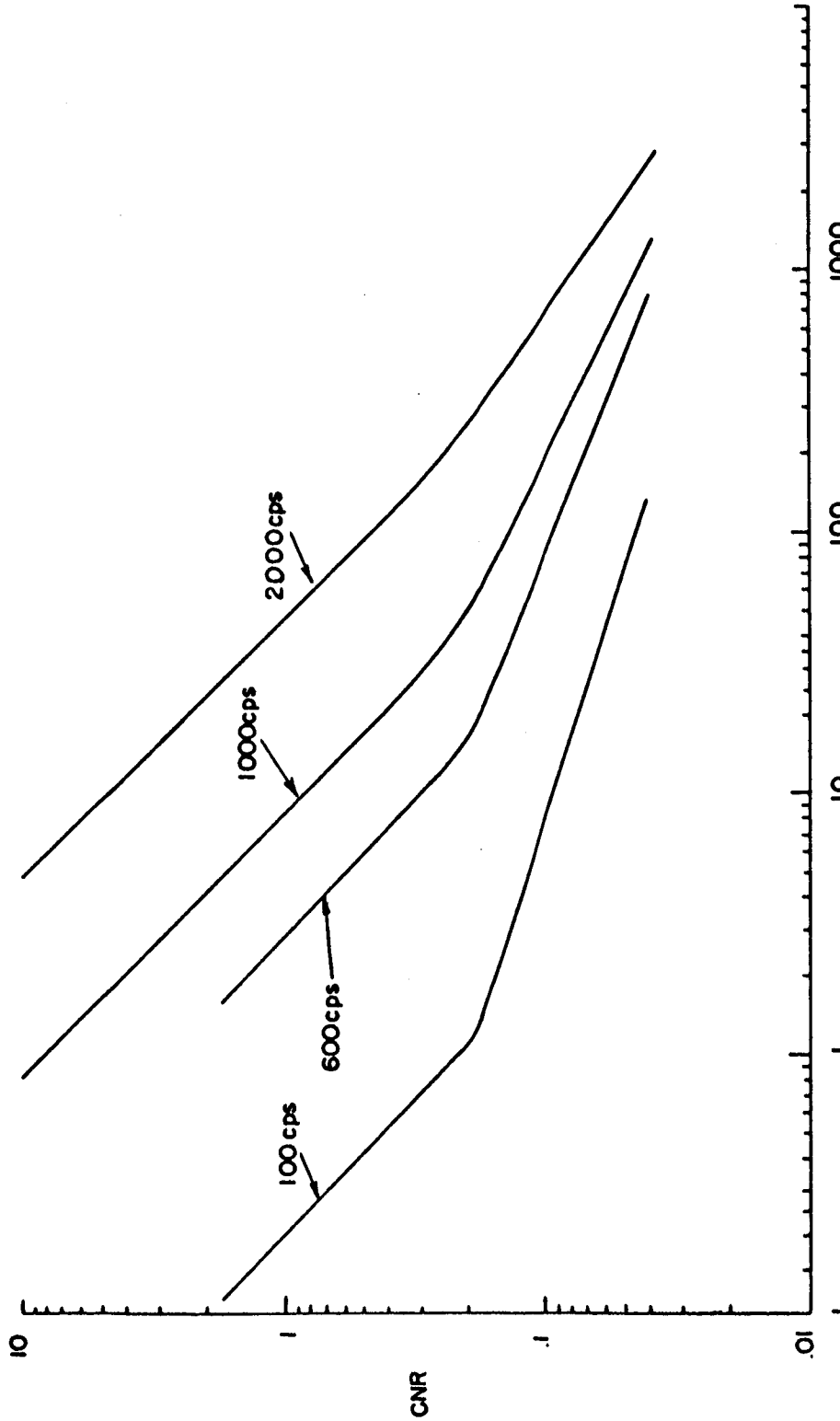

Figure 5.12. Output Noise Power of a Simple First Order Loop for Several Information Bands ($\Delta w=0$)

and 2000 cps. In the high CNR region, the output noise power in any band increases linearly with the input noise power and each curve has the same slope. In the lower CNR region a sharp break takes place and the output noise power increases much faster than the input noise power. This additional power is attributable to the noise spikes which begin to occur at threshold. The slope of this increase is much larger for the smaller bandwidths. Thus the spikes have a relatively low frequency spectrum of the order of f_N.

It should also be noted that the change in slope becomes smaller and the identification of the threshold becomes harder as the measuring band increases. A family of curves such as shown in Figure 5.12 may be used to obtain a graphical plot of the output power spectral distribution.

Plots of the total output noise power in a 600 cps band are shown in Figure 5.13 and Figure 5.14 for various tanlock and tanlock squared detectors respectively (no modulation). It is clear that each system has the same output power for high CNR indicating that the value of f_N was identical for all. As k approaches one, the thresholds occur at a higher CNR. Clearly, the modified systems have a better threshold than the unmodified ones.

A comparison of the figures shows that the behavior of tanlock for k=.5 is essentially the same as tanlock squared for k=.25. Similarly, tanlock, k=.9, is equivalent to tanlock squared k=.5. This is interesting inasmuch as the lock ranges of these respective cases are comparable for the same f_N.

It should also be noted that a significant difference between the

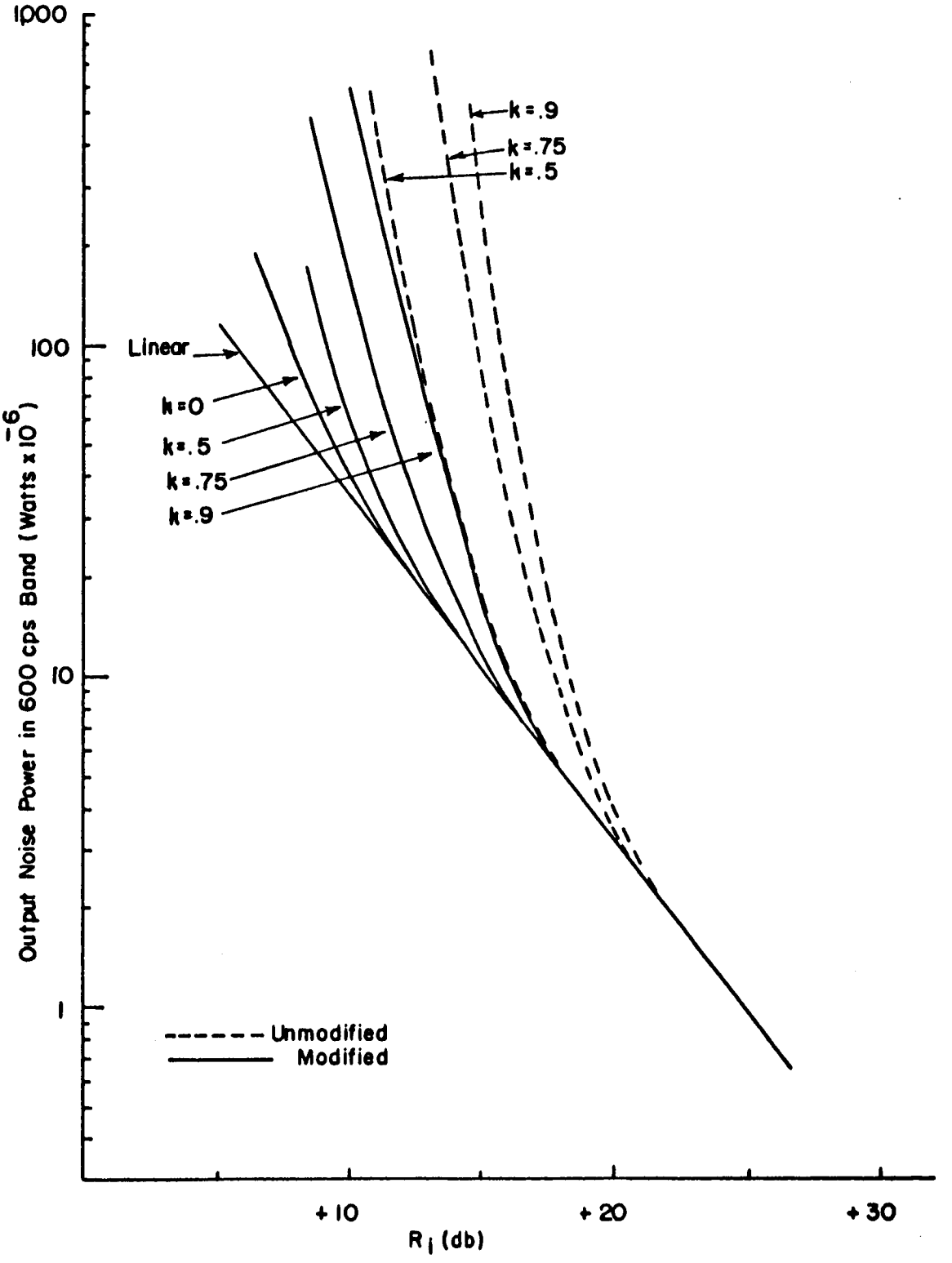

Figure 5.13. Output Noise Power of a First Order Tanlock System in a 600 cps Band ($\Delta\omega=0$)

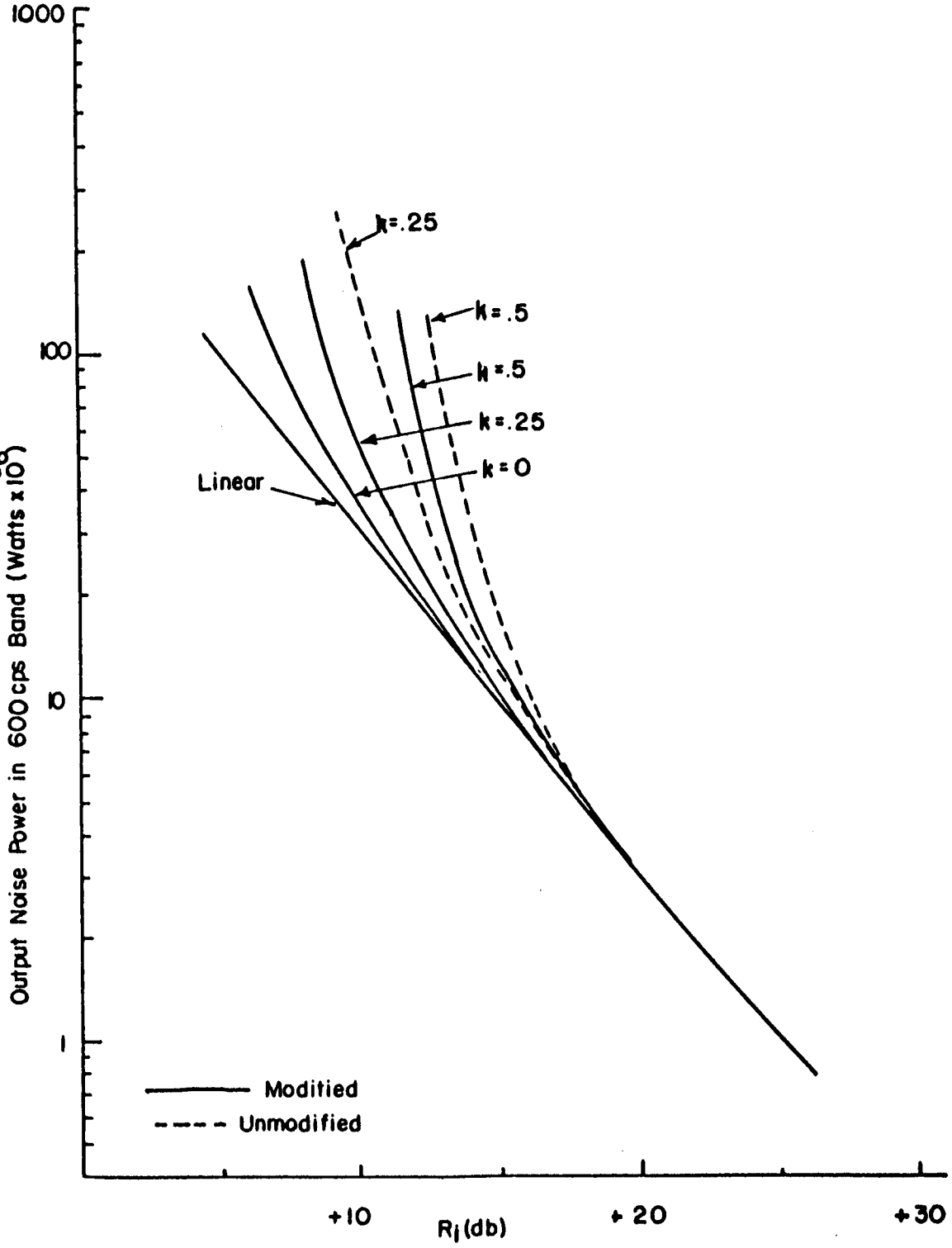

Figure 5.14. Output Noise Power of a First Order Tanlock Squared System in a 600 cps Band ($\Delta\omega=0$)

modified and unmodified systems exists. However, the difference is much less for the tanlock squared case.

5.7. Threshold

Throughout the literature discussion of the threshold of phase lock loops, is vague. But the onset of spikes at the output below some CNR is a common property of all such systems. Because of this and its ease of measurement the level of spike activity is proposed to be the most precise definition for threshold. It is extremely useful for comparing various phase lock loop systems and is independent of modulation or loop filter.

Shown in Figure 5.15 is the threshold performance of all the first order experimental systems in terms of rate of cycle-slipping (spikes/sec.) vs. R_i with no modulation present ($\Delta\omega=0$). In the range of measurements, the curves are uniformly spaced giving an excellent measure of the difference in threshold amongst the various systems.

The loss in threshold for the modified tanlock (k=.9) amounted to 5.0 db, while the loss for tanlock squared (k=.5) was 5.1 db. The loss for other values of k lie appropriately in between. An unmodified tanlock threshold curve (k=.75) is shown and its threshold is 3.6 db worse than the modified curve for the same k.

For the Fokker-Planck model (k=0), Viterbi[17] has found the expected number of spikes/sec., $\bar{S}$, vs. R_i for $\Delta\omega = 0$ to be

$$\bar{S} = \frac{2f_N}{\pi} e^{-4 R_i} \qquad (5.5)$$

This curve is also plotted on Figure 5.15. Only a small difference exists between it and the experimental result. Considering the

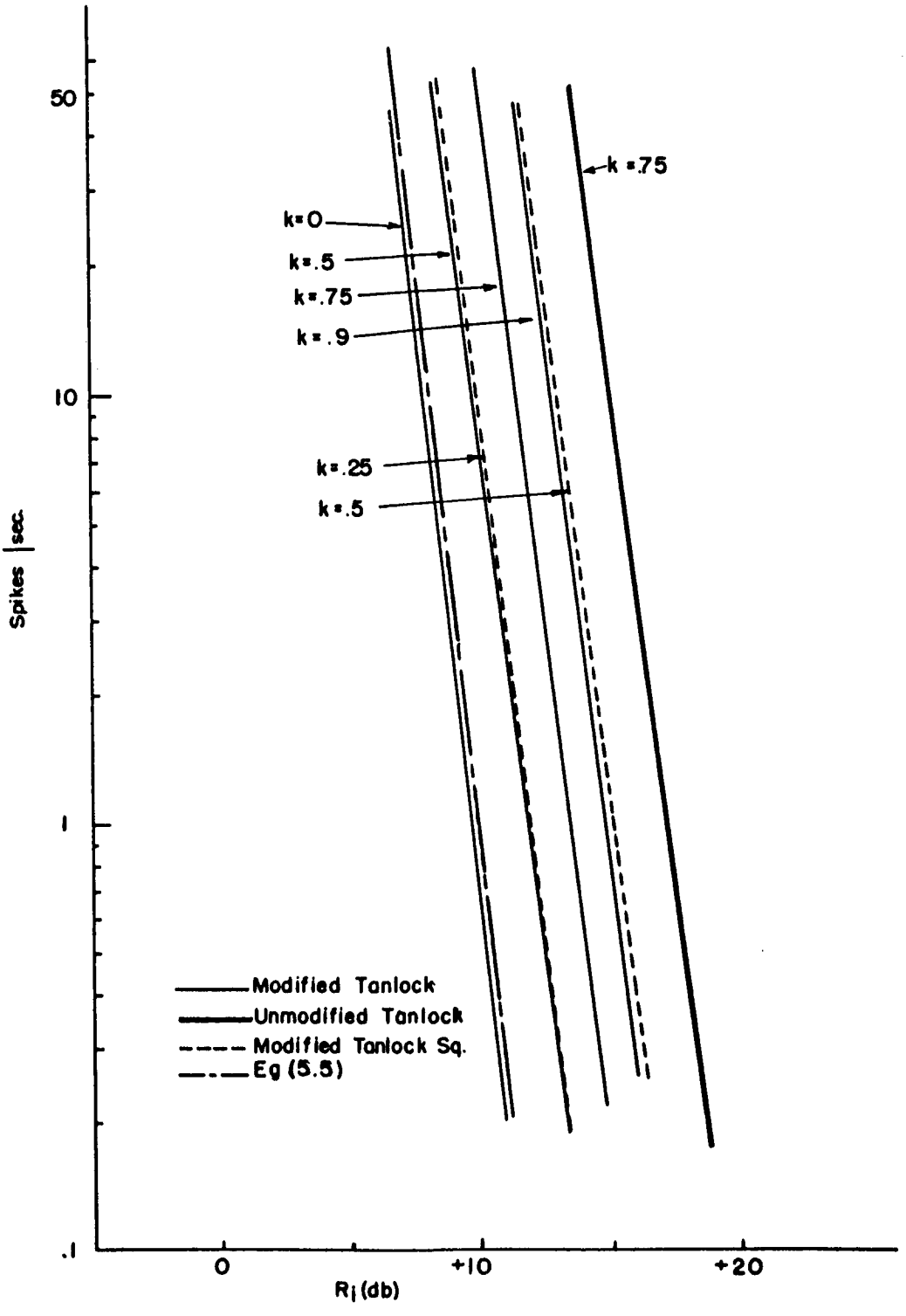

Figure 5.15. Threshold Curves for a First Order Tanlock and Tanlock Squared System ($\Delta\omega=0$)

sensitivity of (5.5) to small errors in f_N or N_o, performance is extremely good.

Thus it would appear that spike activity is a good predictor of threshold for these systems, the level chosen being a function of the use of the system. Only a 4db difference in R_i exists between a rate of 100 spikes/sec. and 1 spike/sec. This is important as it can be used to place upper and lower bounds on the threshold. The dynamic range used in taking the measurement was large. Below a rate of .5 spikes/sec., the length of time required to obtain a good statistical sample was considered too long compared to the short term stability of the system. Above 100 spikes/sec., the system was not considered to be useful because it was rarely in synchronism.

The threshold effect is not limited to the noisy case only. Whenever the instantaneous value of the carrier frequency exceeds the open loop gain, the loop loses synchronism. Such a condition can occur due to a static shift in the carrier, a modulating signal or both. To keep the loop synchronized requires that

$$\Delta\omega + \Delta\omega_{mp} \leq \Delta\omega_{max} \tag{5.6}$$

be satisfied, where $\Delta\omega_{mp}$ is the peak deviation due to the modulating signal.

When (5.6) is violated by sine wave modulation, the output signal essentially breaks up or distorts. An excellent example of the breakup effect is seen in Figure 5.16 where $\omega_m = 2\pi \cdot 50$ rad./sec. The result is symmetrical because $\Delta\omega = 0$ and thus (5.6) is violated equally in both directions. If $\Delta\omega \neq 0$, the result is asymmetrical in the direction of $\Delta\omega$.

The breakup effect appears to be the same as if impulses were added to the output signal. They are attributable to the 2 π cycling of the unsynchronized system. The longer the time that condition (5.6) is violated the more impulses appear.

Provided the signal rate, ω_m, is within the loop bandwidth, the breakup is caused only by excessive frequency deviation

$$\Delta\omega_m = \omega_m m_f \tag{5.7}$$

not the signal rate. As seen from (5.6) the maximum allowable deviation for the first order case is equal to $\Delta\omega_{max}$ when $\Delta\omega=0$, and is proportionately reduced for $\Delta\omega\neq 0$.

In Figure 5.17 is a plot of the fundamental of the signal output

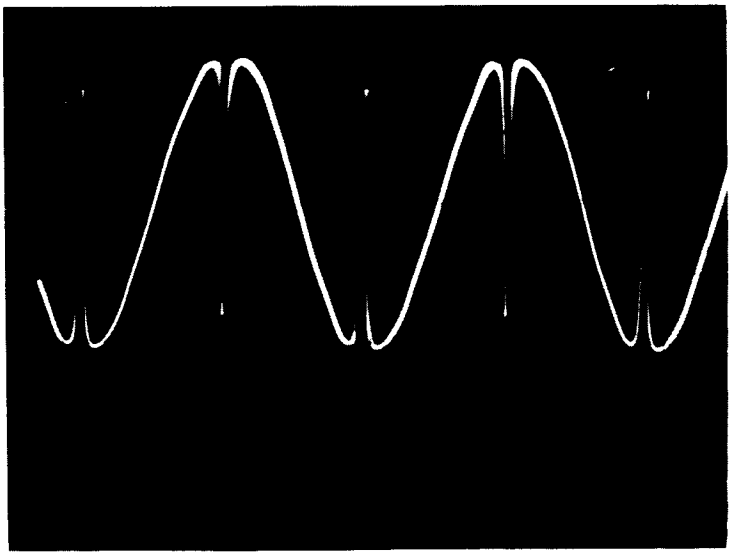

Figure 5.16. Scope Picture of Output Signal Breakup — No Noise Present.

voltage, $e_o$rms, vs. the modulation voltage, $e_i$rms, ($\Delta\omega=0$). The output

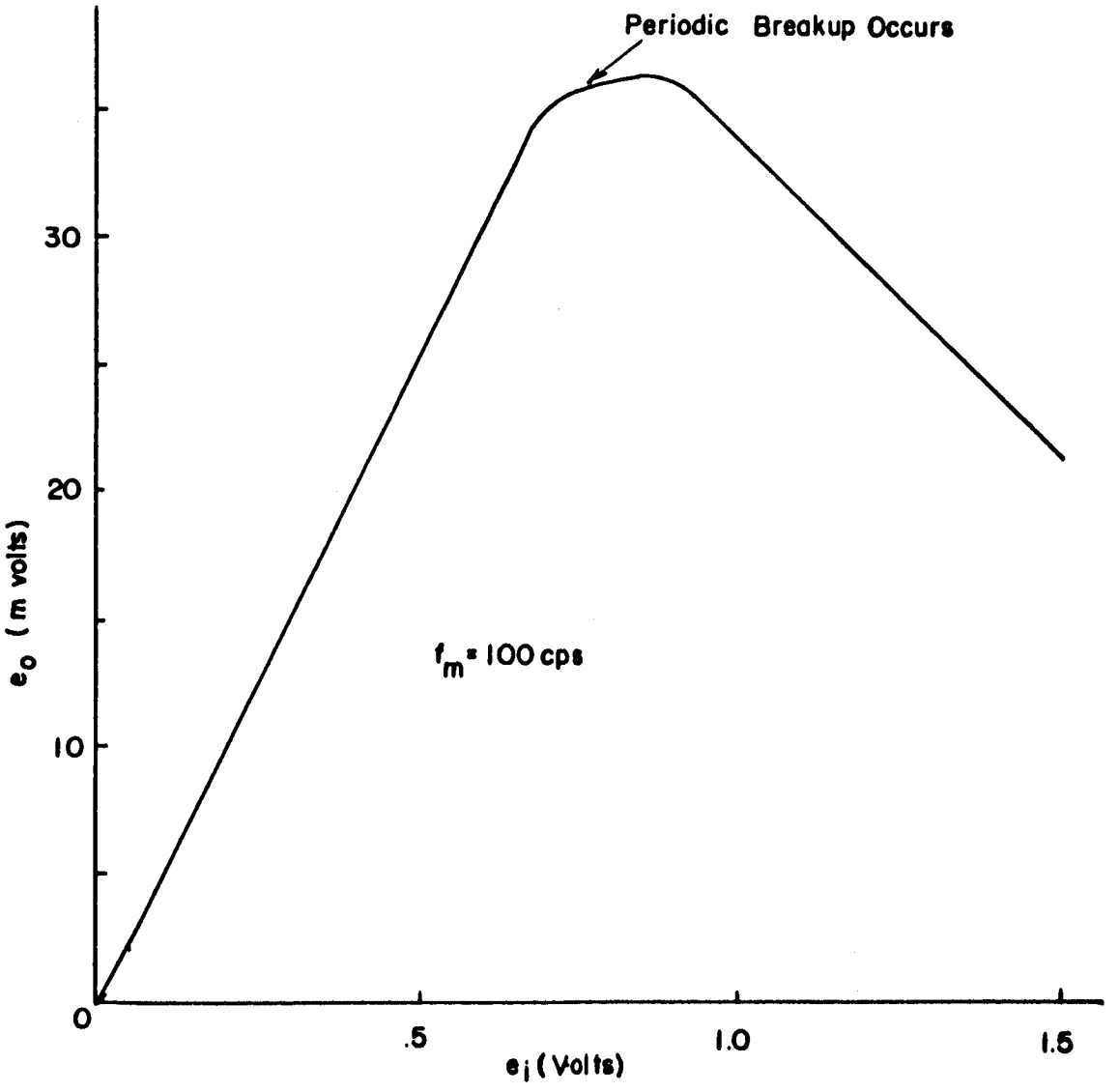

Figure 5.17. Graph of e_o vs e_i — First Order System ($\Delta\omega=0$)

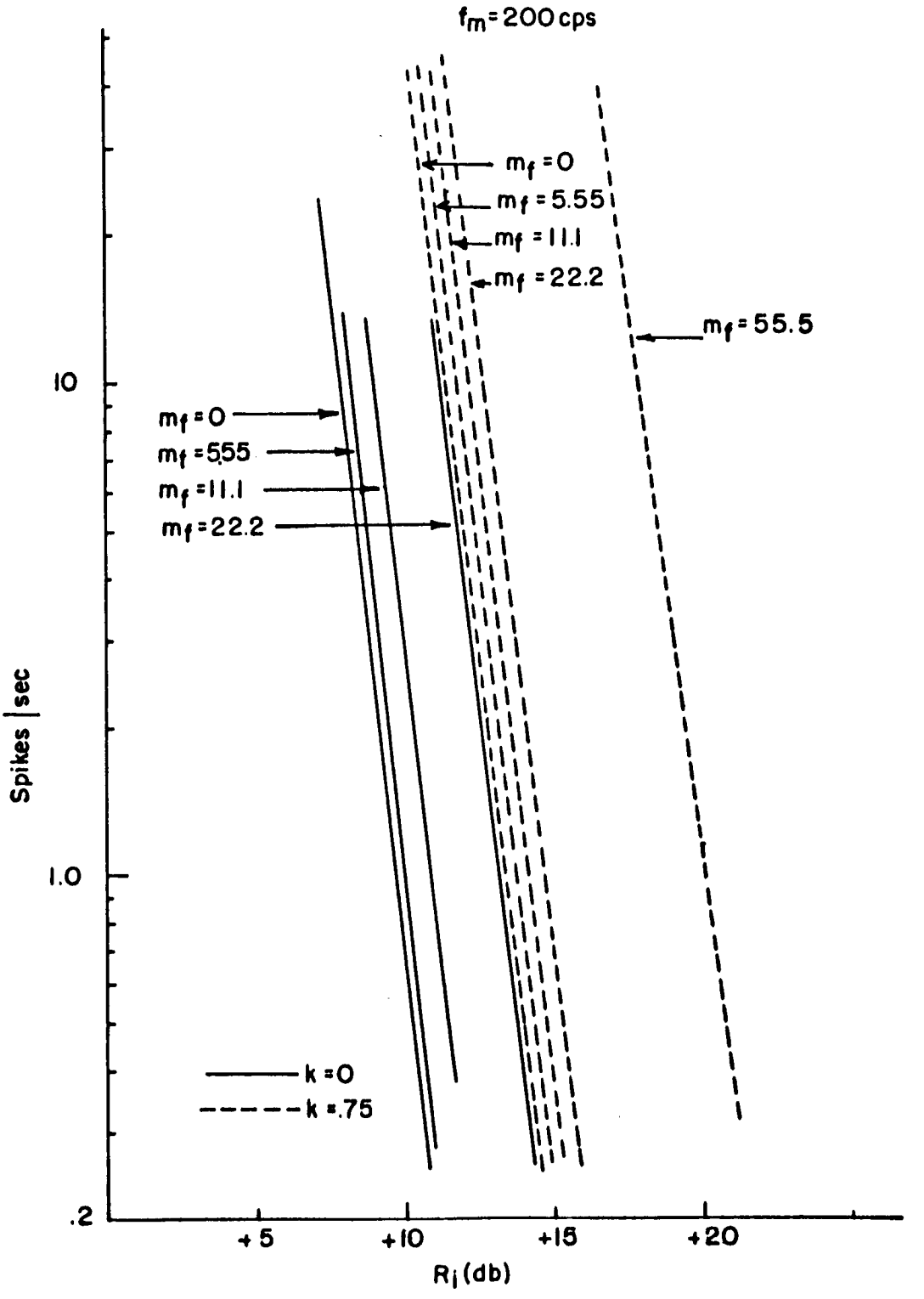

Figure 5.18. Threshold Curve with Sinusoidal Modulation of a Simple First Order Loop ($\Delta\omega$=0)

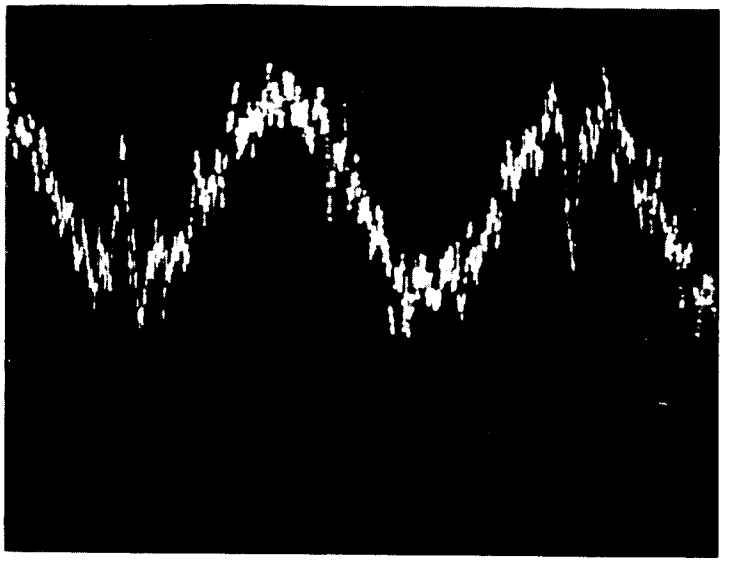

Figure 5.19. Scope Picture of Output Signal Breakup – Noise Present

increases linearly as the input until breakup occurs, then as the input increases still further the power in the fundamental frequency decreases. The remaining power goes into the harmonics of the fundamental because of the non-linear distortion that is introduced in cycle-slipping. The more cycles slipped, the less power in the fundamental.

The only difference between the output spikes in the modulated carrier, no noise case and unmodulated carrier, noisy case is that in the former the spikes occur periodically, in the latter they are random.

It is obvious then that any modulation of the carrier will tend to make the threshold poorer than that shown in Figure 5.15. Therefore a series of threshold curves were run for the modified tanlock system (k=0 and .75) with the modulated carrier. The results for a sine wave modulation of 200 cps is shown in Figure 5.18.

As the modulation index, m_f, increases the threshold drops but the extended lock range of k=.75, permits a much larger deviation than for

k=0. In either case the drop in threshold for m_f=11.1 was 1.1 db, while for m_f=22.2 it was 3.5db. The degradation is not proportional to m_f. As long as the modulation rate is within the loop bandwidth, the loss of threshold should only be a function of $\Delta\omega_m$.

A picture of the breakup of an output signal due to noise and the resulting impulses is shown in Figure 5.19 for $\omega_m=2\pi$ 50 rad./sec. In this case the breakup is not periodic but random, but the probability of a cycle slip is greatest at the peaks of the signal.

5.8. Design Criteria

The previous sections make it obvious that threshold is being traded for improved lock range and synchronization time in the high CNR region. It is therefore worthwhile to ask whether the use of the modified tanlock or tanlock squared systems is justifiable, since they are considerably more complex and expensive.

One way to answer this question is to extend the bandwidth of the simple system so as to obtain the same lock range as each of the tanlock and tanlock squared systems. This is equivalent to normalizing the input CNR to L. R. rather than f_N. By replotting Figure 5.15 in this fashion we obtain Figure 5.20. It can be seen that in fact the threshold of the modified systems improves as k increases getting as high as +1.1 db for k=.9 tanlock and +1.05 for k=.5, tanlock squared. Figure 5.20 indicates the various improvements. The noise bandwidths are no longer the same for the different systems now. Thus in fact these systems do have a higher threshold for a given lock range than does the simple loop. But it can be concluded that the improvements for the n^{th} order systems do not increase proportionately with n.

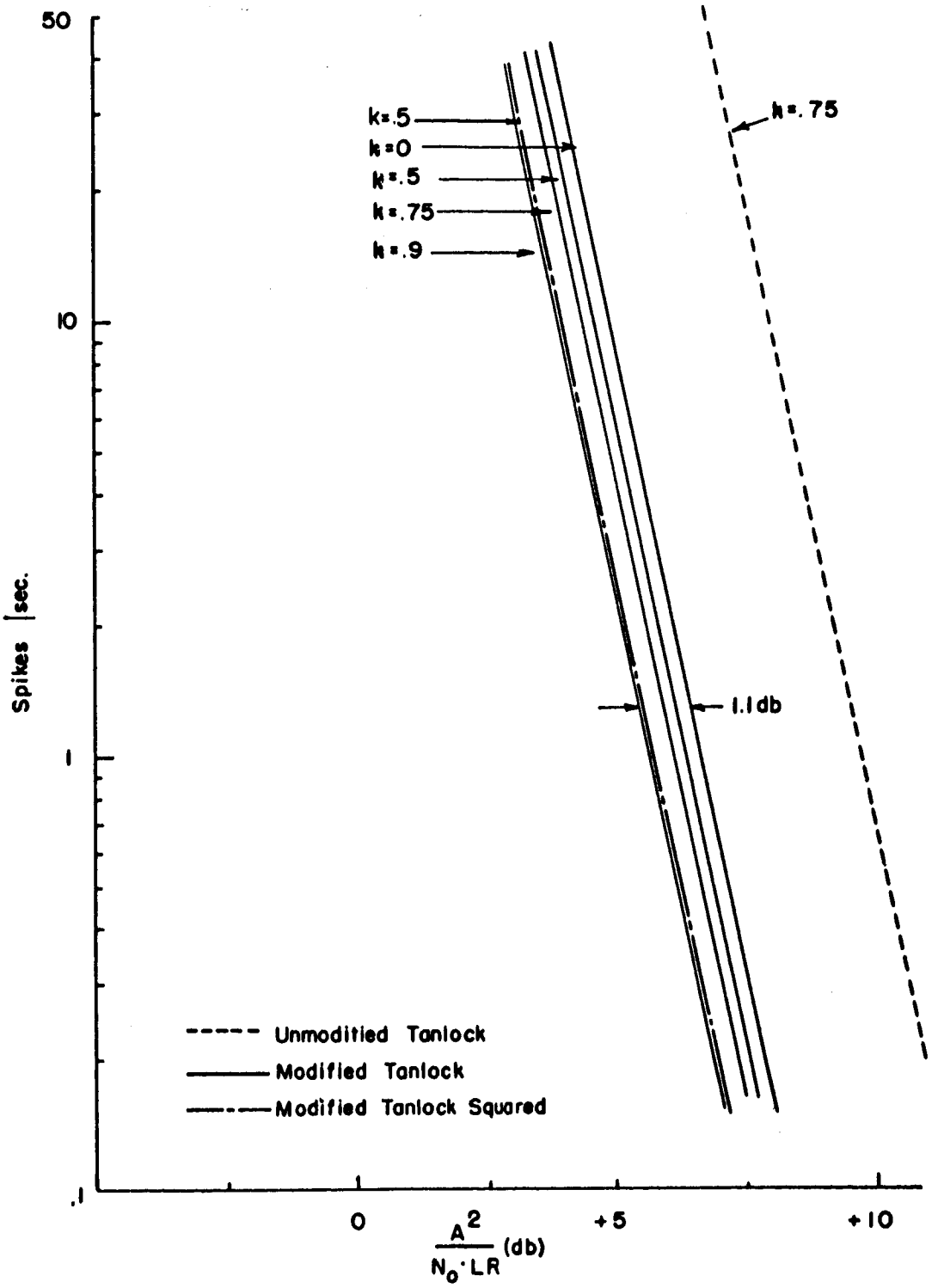

Figure 5.20. Threshold Curves for the First Order Tanlock System of Figure 5.15 Renormalized to the Lock Range

If the output of the loop is to be further processed, then it is advantageous to know the additional energy/spike that can be expected for a given R_i. This information can easily be obtained from Figures 5.13 and 5.15.

VI. EXPERIMENTAL RESULTS — SECOND ORDER SYSTEMS

Chapter 6 begins with a brief discussion of the types of filters used in the experimental evaluation of second order phase lock loop systems. Application of previously mentioned systems verification follows. The experimental results are then divided into two sections, each dealing with one type of filter. The order of presentation follows the established list of criteria. A summary is given at the end so that the basic results might more easily be applied.

6.1. Discussion of Filters

Due to the many variations that can be introduced into the system by allowing G(s) to be other than unity, only special cases of the Type II and Type IIIa filters of Table 2.1 were considered in this investigation. The choice of these two cases is based on several considerations. For practical purposes, the Type II filter finds use in phase lock loops used as AGC Amplifiers. It is unique since the noise bandwidth is the same as that of a first-order loop if the open loop gains are identical and the position of the pole of the filter only affects the damping. For a noisy input, the phase variance is the same as that of the first order case. The study of this filter gives a unique opportunity to see if additional simple filtering in the loop affects any of the criteria of interest.

The Type III or imperfect integrating filter is the most general

form that can be used for a second order system. It is generally operated under the assumptions of (2.29) for many applications involving carrier tracking systems. No exact solutions of this system are available for either deterministic or stochastic signals and the interdependency of the parameters makes a judicious choice difficult. However, several sample cases were examined in this work.

Not all of the general tanlock systems were tested in the second order case. It is sufficient to show that the results stay in the same relative position as those of the first order case for similar values of k. Other cases can then be interpolated from the complete study of Chapter 5. Thus for the Type II filter, values of k=0 and the modified tanlock, k=.75, were used while for the Type IIIa filter only k=0 was evaluated.

6.2. Systems Verification

Once the desired characteristic of the phase comparator has been formed and the correct filter inserted into the loop, the tests of (5.1), (5.3) and (5.4) can all be performed. These were frequently done and the results were the same as those already reported in Chapter 5.

One caution in the use of (5.3) is necessary for the second order systems. In general, depending on the loop parameters, the capture range will be less than the lock range. Thus if the loop operation is such that it is outside the capture range but within the lock range and loses synchronization, then synchronism can only be returned by shifting the carrier back within the capture range. This means that

when using a f.m. modulated signal, not only must the deviations be within the lock range but the modulation rate must be such that the system can track the deviation over the entire stable range. With this condition observed (5.3) is easily accomplished.

Before any criteria were evaluated the frequency response of both the inserted filters, G(s), and the entire loop itself was checked as outlined in Sec. 4.3.6. In each case the results indicated excellent correlation between the measured and the design values.

The experimental investigation was limited to a look at the effect of damping on the performance of systems with a fixed noise bandwidth and consideration was given to underdamped, critically damped and overdamped cases. A discussion of the results for each type of filter used will be done separately in the following.

6.3. Type II Filter

6.3.1. Equivalent Linear Noise Bandwidth

A circuit diagram of the Type II or RC filter is given in Figure 6.1. A complete list of the values and parameters which can easily be calculated from Table 2.1, are given in Table 6.1. It should be noted that

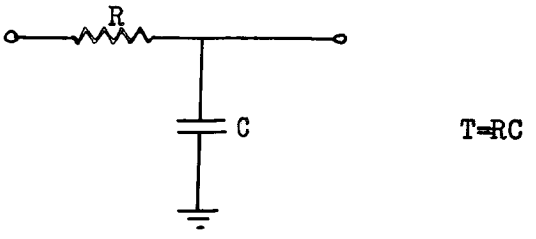

Figure 6.1. Circuit for Type II Filter.

Table 6.1

Parameter Values of the Experimental System Using a Type II Filter

	k = 0			k = .75		
R (ohm)	9300	9300	9300	8200	8200	8200
C (μfd)	.01254	.0063	.0016	.0147	.0074	.0019
K(rad/sec)	4330	4330	4330	4330	4330	4330
f_N (cps)	345	345	345	345	345	345
ξ	.707	1	2	.707	1	1.91

the value of R was slightly different for the k=0 and k=.75 cases due to a change in the attenuation of the signal path necessary for easy implementation. No other system changes were made.

For all cases the equivalent linear noise bandwidth was 345 cps, the same value used in the first order case. Thus comparisons are considerably simplified. All results are plotted vs. the normalized input signal to noise ratio R_i. Three values of damping, ξ = .707, 1.0 and 2.0 were used.

6.3.2. Lock Range

The relationship between the lock range and the capture range is important in interpreting results for the second order system. The steady state lock range curves described previously cannot be taken above the capture range. This is because once a noise peak causes a loss of synchronism, the system cannot restabilize since it was in a conditionally stable region to begin with. Thus the maximum value

(no noise) of these curves will be CR rather than LR.

For this simple RC filter, the capture range and the damping is only a function of the pole position. No difference between LR and CR was found in the laboratory for values of $\xi = 1$ and $\xi = 2$, but when ξ was reduced to .23, CR = .52 LR. This is a significant change, a result due to the sharp peaking in the response curve.

Figure 6.2 is a plot of the maximum lock range vs. R_i for the modified tanlock (k=0 and .75) using a criteria of 30 spikes/sec. The first order system resulting for each has been plotted for reference purposes. It is clear that as ξ increases the curves slowly approach that of the first order case. The difference in lock range is not significant between the first and second order system except in the important threshold region where considerable improvement is obtained.

The results are not surprising since the small signal responses of the first and second order cases become very similar within the 3db bandwidth as ξ gets large. The large peak of the response as ξ gets smaller is what actually helps to improve the lock range until the CR begins to change significantly from LR at a value of about $\xi = \frac{1}{\sqrt{2}}$. Once the latter condition occurs, the actual lock range curves drop below those shown. Thus $\xi = 1$, critical damping is an ideal operating point.

6.3.3. Output Noise Power

A plot of the output noise power (VCO input) in a 600 cps band is shown in Figures 6.3 and 6.4 for the k=0 and k=.75 cases respectively. The first order plots are given for comparison purposes and it is seen

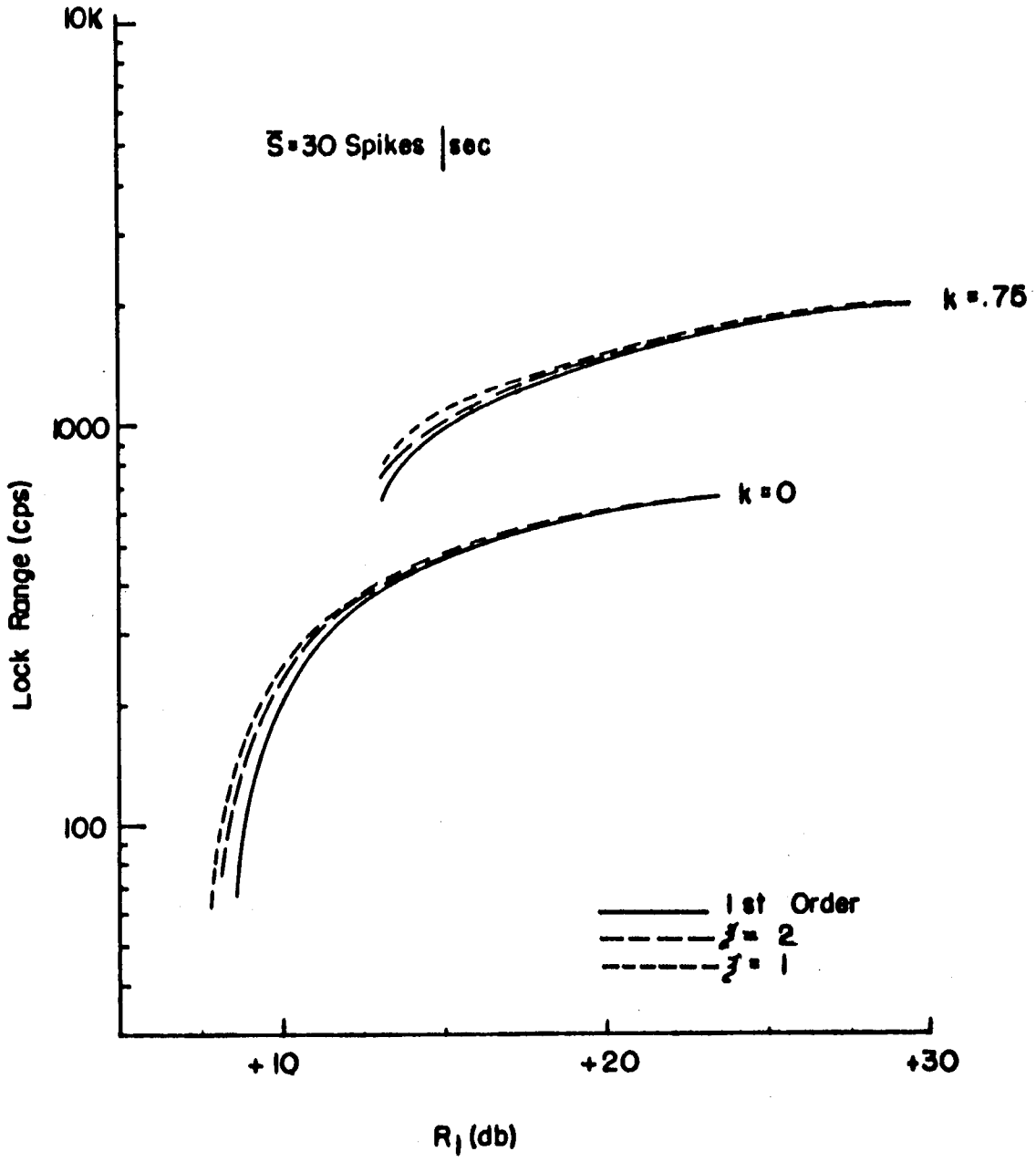

Figure 6.2. Dynamic Lock Range Curves for Second Order Tanlock System Using a Type II Filter

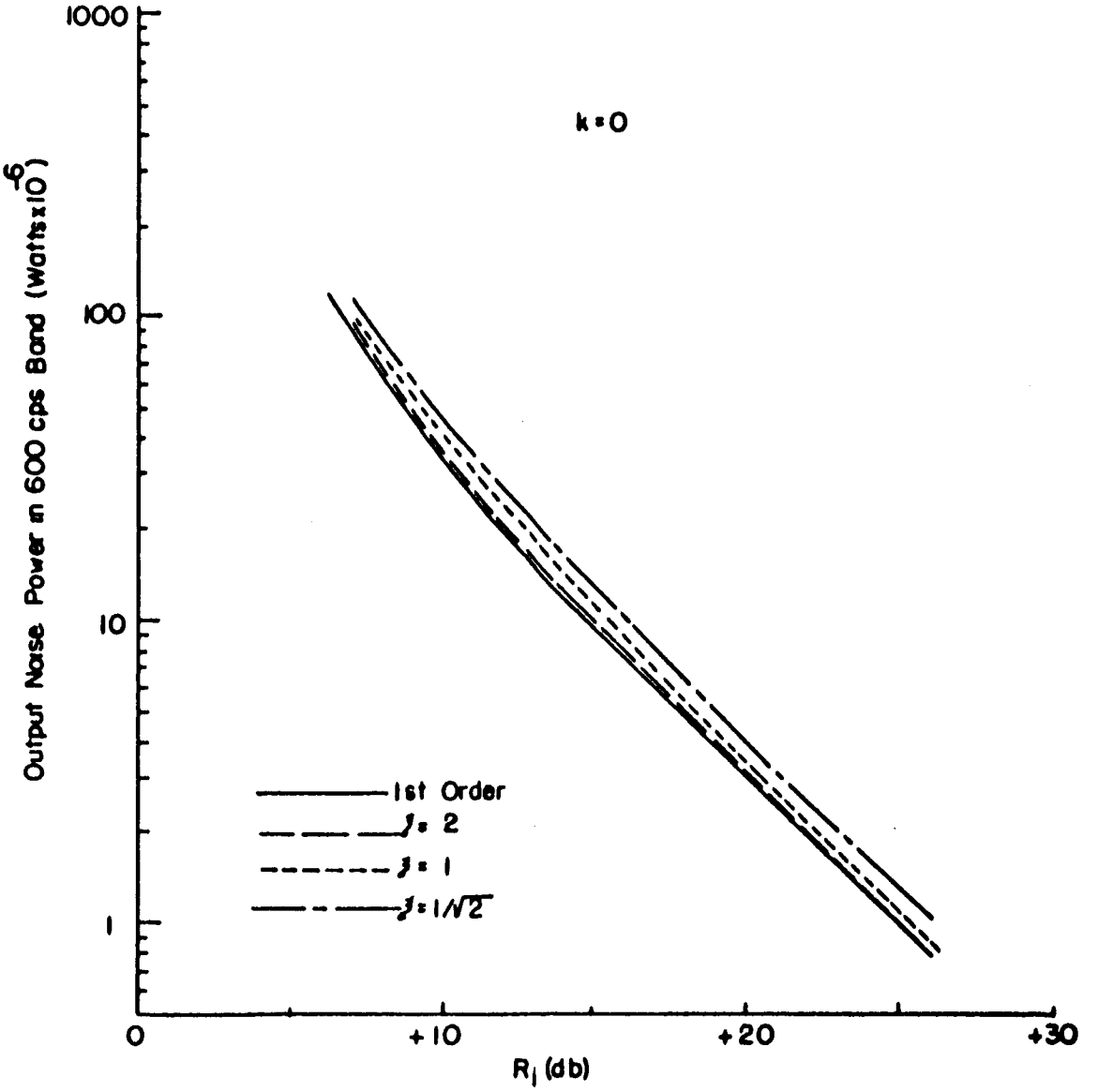

Figure 6.3. Output Noise Power in a 600 cps Band of a Second Order Tanlock System Using a Type II Filter ($\Delta\omega=0$)

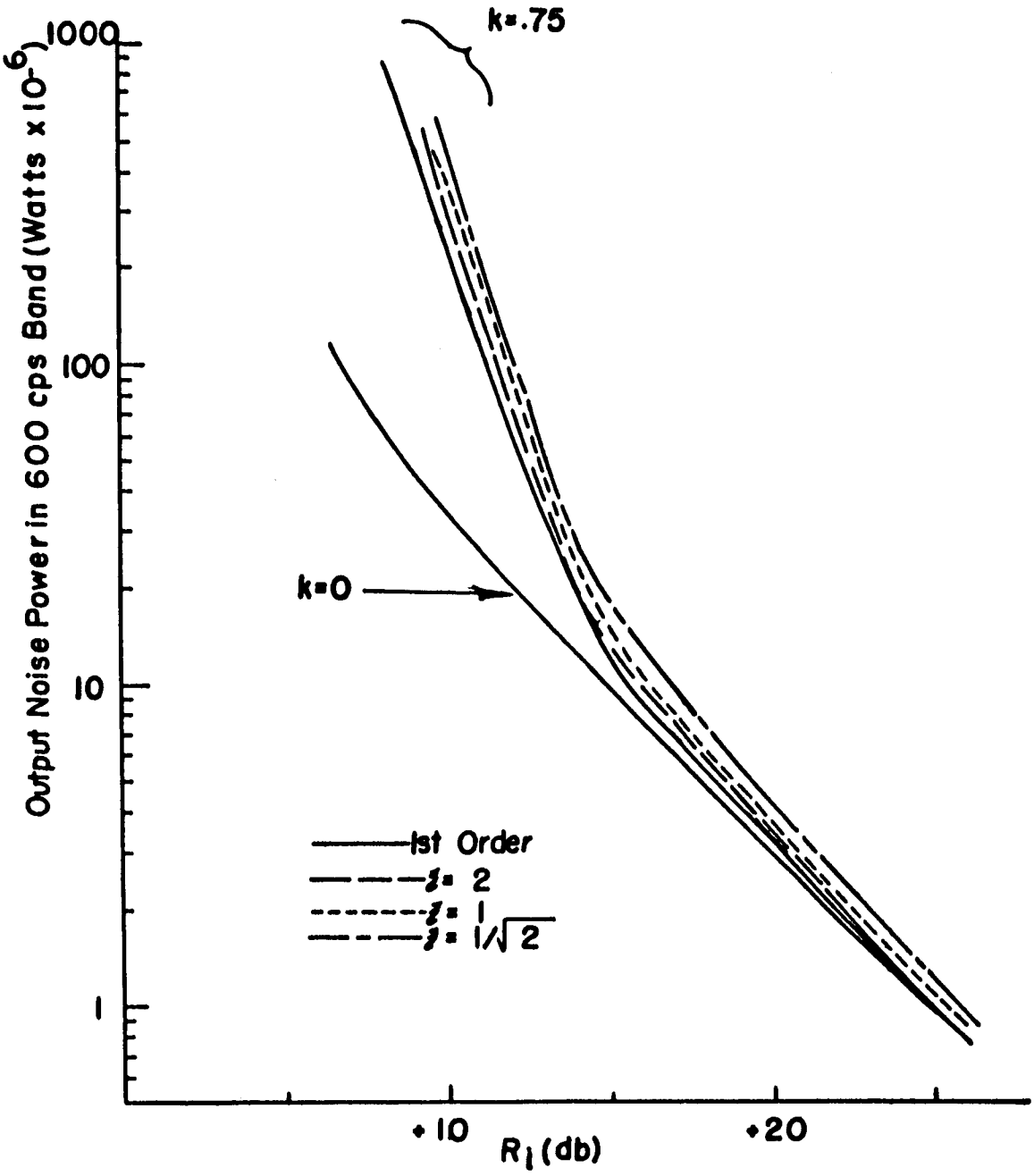

Figure 6.4. Output Noise Power in a 600 cps Band of a Second Order Tanlock System Using a Type II Filter ($\Delta\omega=0$)

that the results are consistent with those in Chapter 5. The slopes of both cases for the respective ξ are identical in the high CNR region indicating that the small signal parameters of each system were the same.

It is noted that as ξ decreases, the noise for a given R_i increases. Because 600 cps is very close to the 3db point of the response, as ξ decreases the peak of the response curve increases, increasing the noise power in a given band. If a smaller band were measured the effect would be much less. If the total noise were measured no difference would occur because each f_N is the same.

6.3.4. Threshold

Using the rate of cycle slipping as a measure of threshold behavior ($\Delta\omega=0$), it is clearly seen in Figure 6.5 that the critically damped case ($\xi=1$) shows a slight improvement over the first order case. It amounts to .3db for k=0 and .26 db for k=.75. For $\xi=2$ the first and second order cases are almost indistinguishable, a result consistent with the lock range measurements shown previously. It is significant that for $\xi=\frac{1}{\sqrt{2}}$, the threshold decreases over the first order case.

These results indicate that an optimum value of damping, $\xi=1$, exists for the best threshold performance as defined here, verifying the results of other authors such as Jaffe and Rechtin[10] and Schilling[13] investigating similar situations. The poor performance of the underdamped case is a result of the capture range beginning to differ significantly from the lock range. This has the effect of making the spikes become interdependent, thus they occur in bursts rather than singly. As CR separates further from LR this phenomena becomes more pronounced.

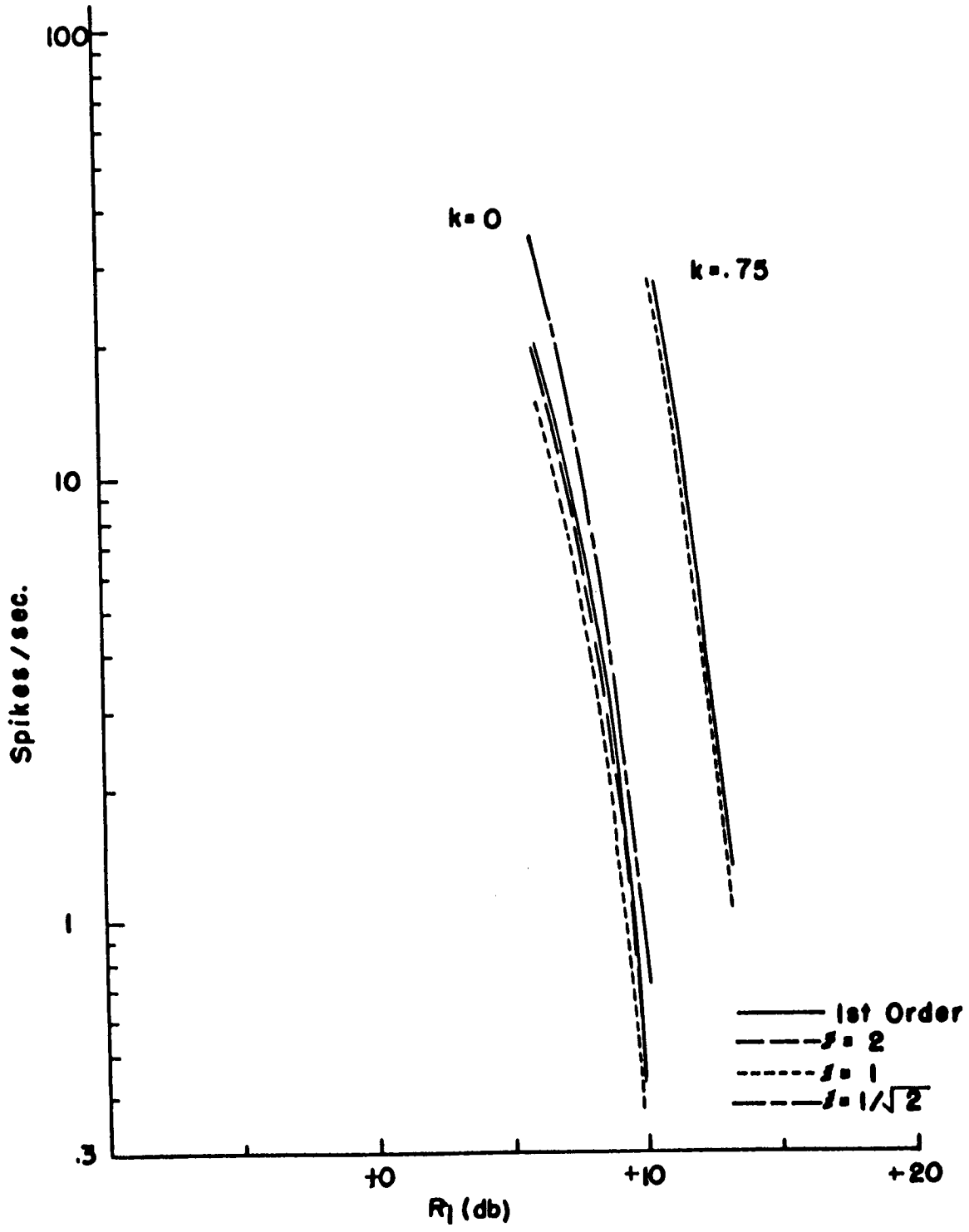

Figure 6.5. Threshold Curves for a Second Order Tanlock System Using a Type II Filter ($\Delta\omega=0$)

6.4. Type III Filter

6.4.1. Equivalent Linear Noise Bandwidth

A circuit diagram of the Type III filter used appears in Figure 6.6 and a table of values and parameters is listed in Table 6.2.

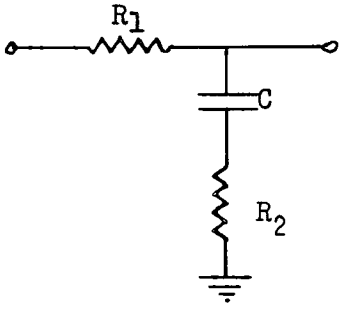

$T_1 = R_2 C$

$\gamma T_1 = (R_1 + R_2) C$

Figure 6.6. Circuit for Type III Filter

Table 6.2

Parameter Values of the Experimental System Using a Type III Filter

	D	E	F	D'
R_1(ohm)	730	730	730	730
R_2(ohm)	6580	6580	6580	6580
C(μfd)	1.37	2.34	3.90	2.74
γ	10	10	10	10
K(rad/sec)	20,000	23,450	25,750	20,000
f_N(cps)	228	228	228	194
ξ	.74	1	1.35	1
ω_n(rad/sec)	225	186	158	159

The implementation of this filter under the conditions of (2.29)

were rather difficult to achieve in the experimental system. Due to bandwidth considerations the value of K was restricted to 25,000 rad./sec. or less. Thus it was impossible to have

$$f_N = 345 \text{ cps}$$

and

$$\gamma = \gg 1 \tag{6.1}$$

as desired. As a compromise, values of

$$f_N = 228 \text{ cps}$$

and

$$\gamma = 10 \tag{6.2}$$

were used. Material presentation was not affected, since all plots have been normalized to f_N by using the parameter R_i. For this particular filter, both K and the capacitor, C, were changed to obtain the desired values of damping. Only the k=0 case was considered.

6.4.2. Lock Range

For the design values of the Type IIIa filter listed in Table 6.2, the capture range of the system was considerably less than the lock range. Therefore no lock range measurements with noise were made outside the capture range.

Figure 6.7 is a graph of the lock range curves (k=0) vs. R_i for ξ= .74, 1 and 1.32 (D,E, and F, Table 6.2). The value of f_N was kept constant. Clearly the lock range decreases sharply as ξ decreases as was expected from the results of the RC filter. But the separation of the curves is also quite significant. The first order case is given for comparisons. Based on the same f_N, the second order system has a higher threshold for a given lock range capability below +9.75db, but will be better above this value.

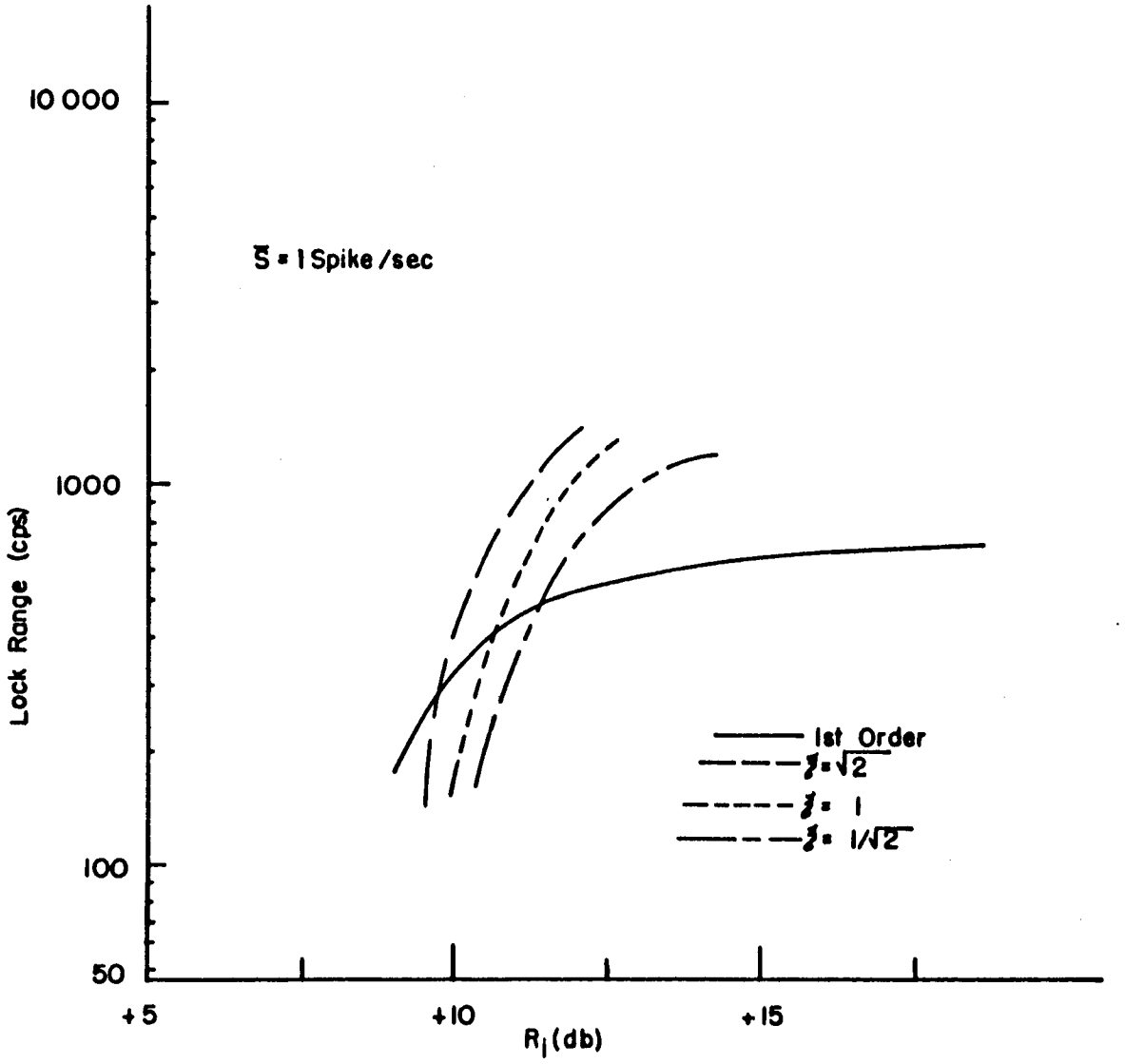

Figure 6.7. Dynamic Lock Range Curves for a Second Order Simple System Using a Type III Filter

Table 6.2 indicates that K increases as ξ increases. If the curves are normalized to K instead of f_N, they become much closer together though the larger values of ξ are still clearly better. However, no valid comparison can now be made with the first order case, since under this condition it is far superior. Only one spike/sec. was used for this measurement because of the difficulty in maintaining enough stability to get consistent readings for values near the capture range.

6.4.3. Output Noise Power

The output noise power in 400 and 600 cps bands is plotted (D,E,F) in Figures 6.8 and 6.9 respectively. The noise increases as ξ decreases for a given R_i as previously discussed. The noise outputs are less for a given R_i when compared with Figure 6.2 since the f_N is less and the noise power is now distributed over a much larger band.

6.4.4. Threshold

The threshold curves ($\Delta\omega=0$) for this filter are shown in Figure 6.10. It is apparent that the larger ξ is the better the threshold performance for systems having the same f_N. A check on the validity of using f_N for comparisons was made for the fourth set (D') of parameters listed in Table 6.2. The loop gain was constrained to be 20,000 rad./sec. so that for $\xi=1$, the value of f_N was 194 cps. By plotting this result vs. R_i on Figure 6.10 it can be seen that it is almost coincident with curve E, $\xi=1$. This was considered ample evidence that f_N is the valid criteria for comparing the second order systems also.

The threshold curve for the first order case has also been plotted on Figure 6.10. It has a better threshold performance than any of this

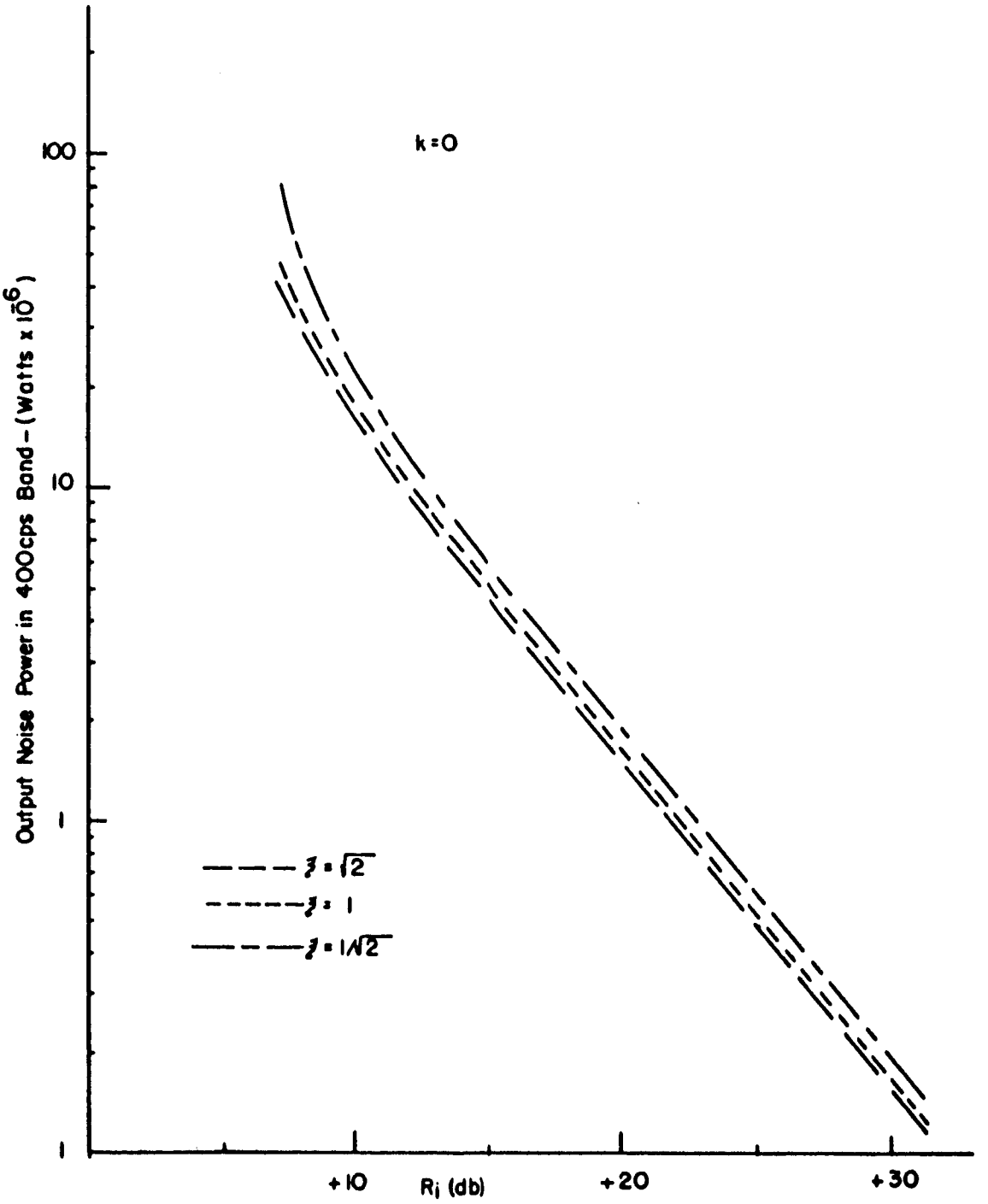

Figure 6.8. Output Noise Power in a 400 cps Band of a Second Order Simple System Using a Type III Filter ($\Delta\omega=0$)

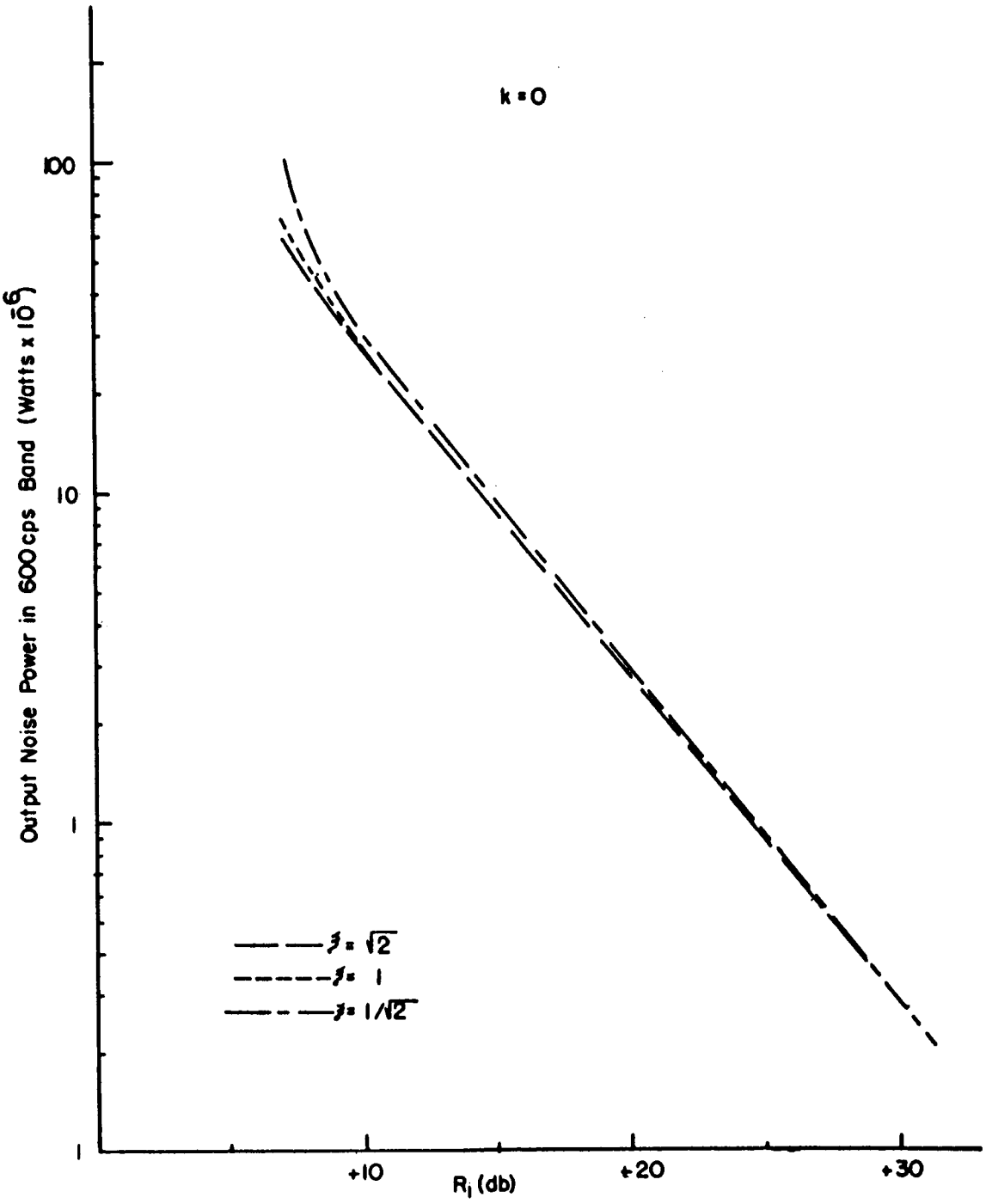

Figure 6.9. Output Noise Power in a 600 cps Band of a Second Order Simple System Using a Type III Filter ($\Delta\omega=0$)

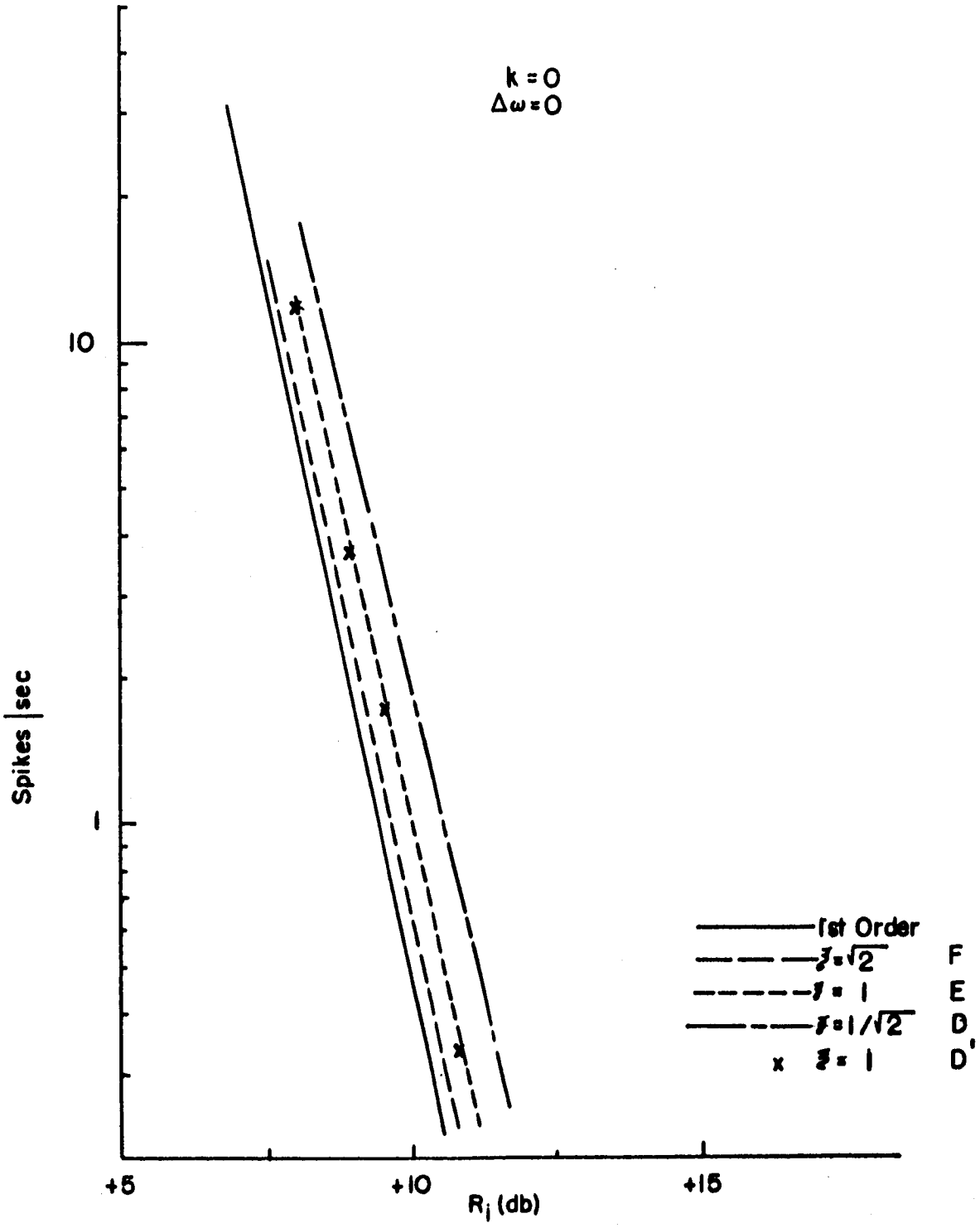

Figure 6.10. Threshold Curves for a Second Order Simple System Using a Type III Filter ($\Delta\omega=0$)

type second order case. A loss of .7db occurs if $\xi=1$ but as ξ gets larger, the two cases approach each other. Again bursts of pulses appear, getting more frequent as ξ gets smaller. This appears to be the main reason for the higher threshold caused by this type of filter.

6.5. Summary

From the experimental results it is evident that both the type of filter and the damping of a second order system have significant effects on performance. If the lock range and capture range of the system are comparable, improvement in both lock range and threshold performance can be obtained and the critical damping case ($\xi=1$) appears to be optimum. In other cases where CR is considerably less than LR (Type IIIa), some loss in threshold is found but this can be traded for a gain in lock range above a certain value of R_i. Again $\xi=1$, seems to be a good compromise, but the designer must be more critical in considering the application.

Thus in fact second order systems do have slightly better performance than the equivalent first order systems based on the criteria herein evaluated.

The results of this chapter can be extrapolated to the general tan-lock system, by using the results of Chapter 5. Thus it was not necessary to redo all the data for the second order system, spot checks being sufficient to verify this conclusion.

VII. EXPERIMENTAL RESULTS – LIMITER

This chapter presents experimental results where a limiter is used in conjunction with a first order phase lock loop. Comparisons are made with results of Chapter 5. Performance of the limiter alone is also included.

7.1. Background

The previous chapters have all been concerned with the performance of fixed bandwidth phase lock loops. The carrier was of fixed amplitude and the CNR varied by changing the noise level only. Such a procedure enabled us to take a look at the fundamental loop operation.

Frequently these systems are operated in conjunction with external control units such as an AGC system or a limiter. The purpose is to reduce the carrier level as noise increases so that the bandwidth of the system is reduced. Thus over a large range of CNR the value of the phase error increases more slowly, permitting a lower threshold occurrence. Jaffe and Rechtin[10] and Gilchriest[11] showed that the limiter was a sub-optimum way of minimizing the mean square phase error of a loop due to a combination of signal and noise. An AGC system was shown to be a much poorer method.

For practical reasons it is advantageous to use a limiter to keep

the noise and signal levels within reasonable bounds. Furthermore, it is hoped that because of the suppression of the noise peaks and induced bandwidth changes, that the system will perform as well or better than the same system under the same conditions without the limiter.

With this in mind, a limiter was added to the overall system shown in Figure 4.1. The purpose was to compare system performance with that of a loop with no limiter.

7.2. Limiter Performance

The limiter design consisted of two high gain amplifiers each followed by a double diode clamp (see Figure B.3). A low impedance output was provided by an emitter follower. The output of both stages was hard limited by a 30mv signal at the input and the output level was $\pm$ .5 volts. A 50 mv signal was used in all tests insuring that signal and noise would be hard limited for all values of CNR. The linearity of the system without the diodes was excellent and the frequency response well over 700kc.

In general it can be assumed that the total output power of the limiter[26] in a band centered at the signal frequency is constant, i.e.,

$$S_p + N_p = K \tag{7.1}$$

If it is assumed that

$$\frac{S_p}{N_p} = a \frac{S_i}{N_i} \tag{7.2}$$

where a = constant

then it follows from (7.1) and (7.2) that

$$N_p = \frac{K}{a\frac{S_i}{N_i} + 1} \tag{7.3}$$

and

$$S_p = \frac{K\, a\left(\frac{S_i}{N_i}\right)}{a\frac{S_i}{N_i} + 1} \tag{7.4}$$

To measure the output signal component and the noise centered about it, the test set up of Figure 7.1 was used. The input signal

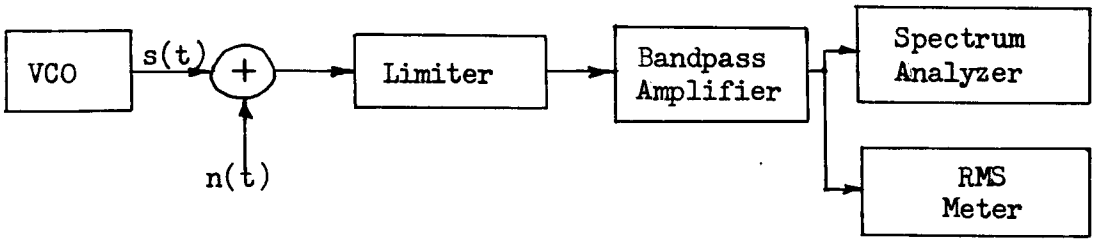

Figure 7.1. Block Diagram of Limiter Test System.

and noise are easily measured since the system is linear to this point. At the output, a spectrum analyzer was used to measure the output signal component and an rms meter measured the total power.

A plot of the signal power and noise power in a narrow band centered at 450 kc vs CNR is shown in Figure 7.2. It can be seen that the results are similar in shape to those given by (7.3) and (7.4), though the output power was not quite constant over the entire range of CNR. No attempt was made to band limit the input noise so its spectrum ran from 100cps to 500kc. The effect of this additional noise at the input is to essentially add additional energy at the carrier frequency as well as noise in the center band.

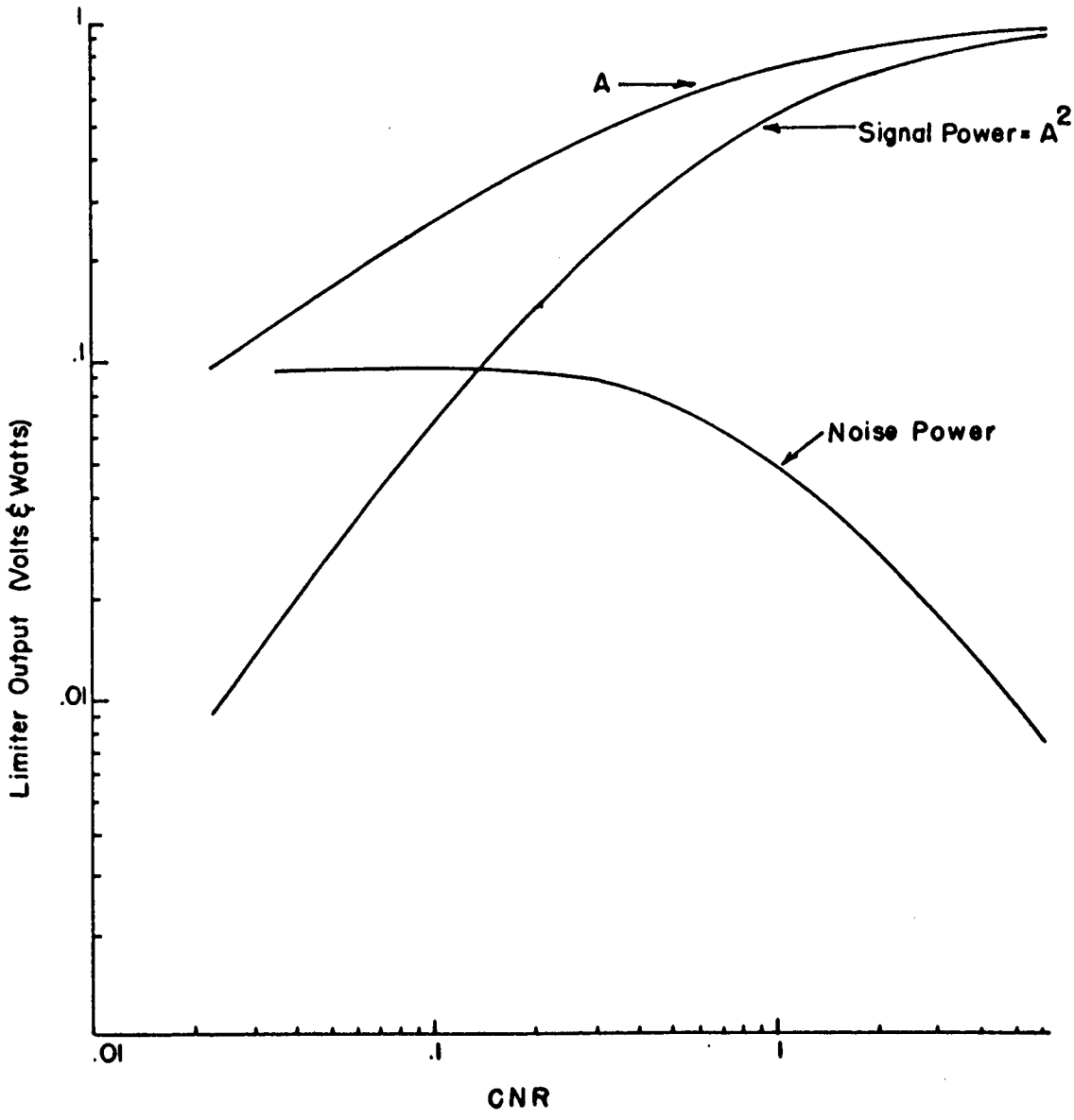

Figure 7.2. Signal and Noise Responses of a Narrowband Limiter

7.3. System Performance

Several of the performance curves previously described in Chapter 5 were rerun for the first order tanlock system preceded by a limiter. These are described below. Since the limiter effectively prevents the amplitude of the noise from exceeding that of the peak signal, no modification of the tanlock system is necessary for these measurements. It should be noted that only the special case of $\Delta\omega=0$, with no modulation was considered in this section.

7.3.1. Equivalent Linear Noise Bandwidth

With no noise present, the loop was adjusted to have a noise bandwidth of f_N=345cps. This was to make comparisons between systems with and without a limiter. A value of f_N=610cps was also used to check systems with a different bandwidth.

7.3.2. Lock Range

The lock range curves vs CNR are shown in Figures 7.3 and 7.4 respectively for a 10 spike/sec. criteria. The relative position of the curves is maintained though the respective improvements of the various systems decreases throughout the entire measurement range of 40 db. The curves seem to converge at very low CNR. The lack of a threshold is apparent and these curves should be compared to those of Figure 5.8 where no limiter was used. The curves do become linear, which is caused by the fact that the signal is now decreasing linearly with CNR.

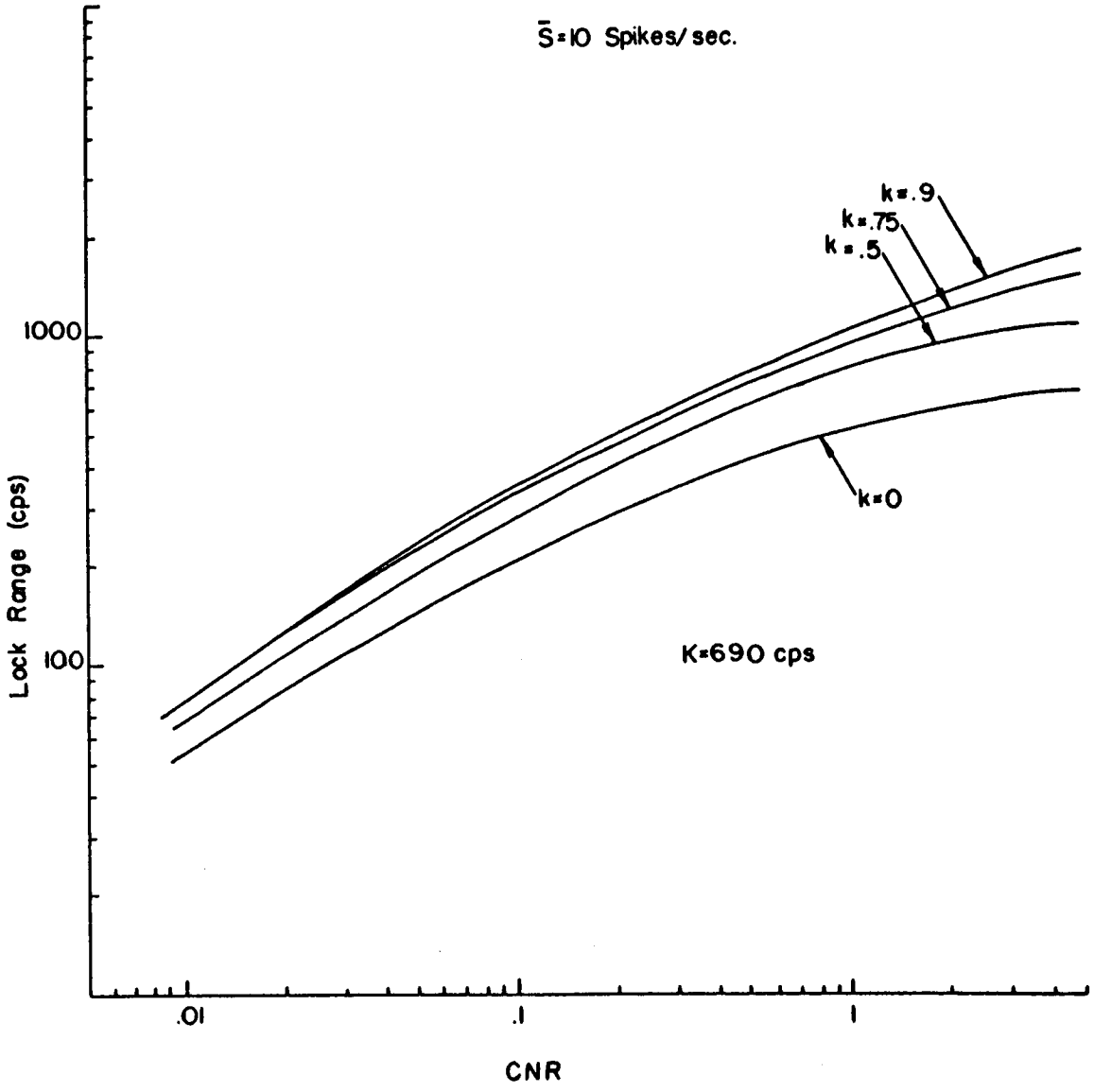

Figure 7.3. Dynamic Lock Range Curves for a Combination Limiter, First Order Tanlock System

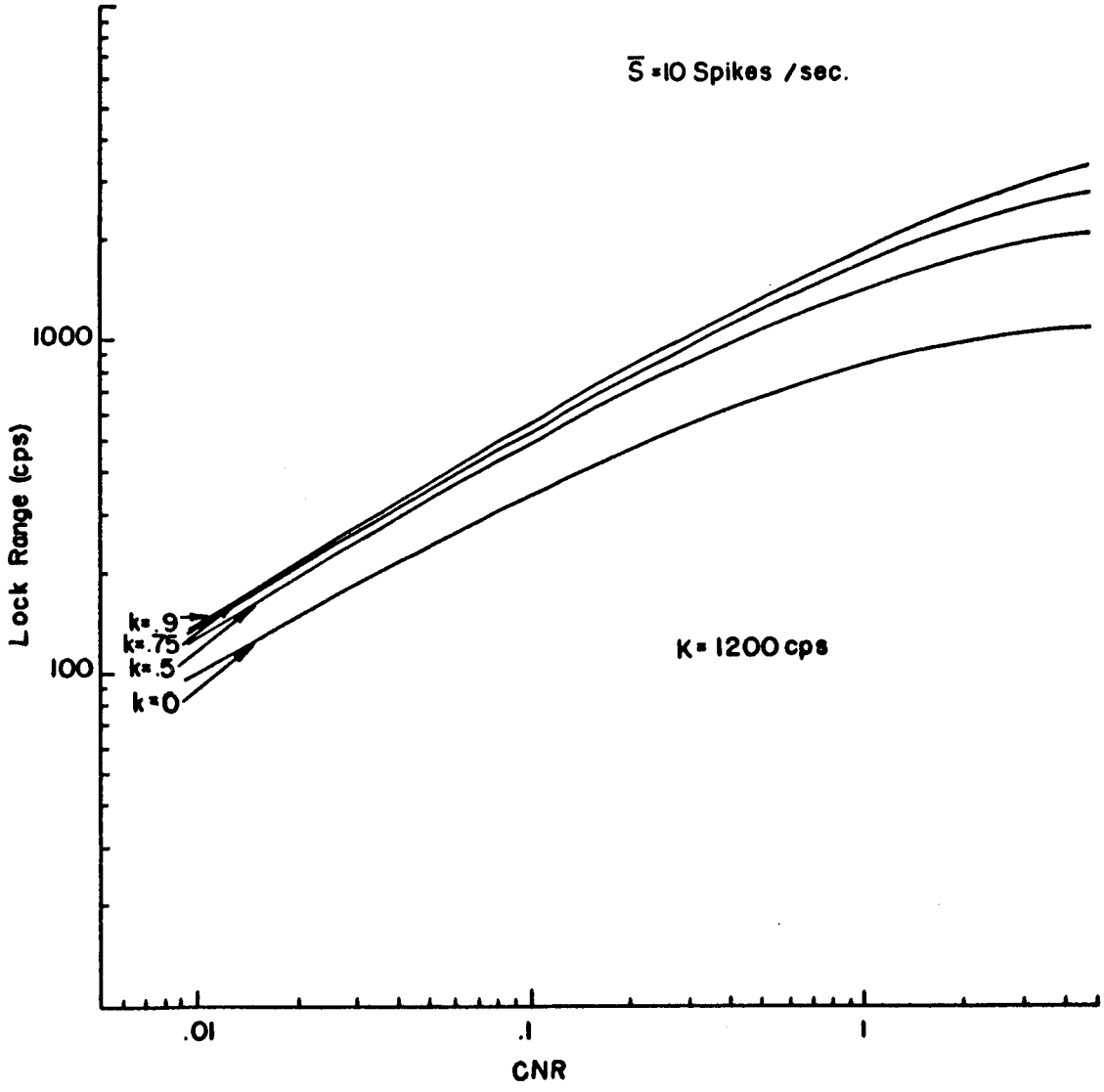

Figure 7.4. Dynamic Lock Range Curves for a Combination Limiter, First Order Tanlock System

7.3.3. Output Noise Power.

In the linear region, above the threshold of the limiter, all systems have approximately the same output power as expected; see Figures 7.5 and 7.6. However, when $\Delta\omega=0$, no threshold-spikes-appear because of the limiter. As a result it would be expected that the noise continues to increase linearly with CNR. Due to the fact that the bandwidth of the system is continually decreasing, however, the overall result is to maintain the output power fixed below a certain CNR. This point is a little higher for the higher bandwidth system because of the fixed measuring band at the output. The higher the value of k, the larger the output noise, though the differences are not very great.

7.3.4. Threshold.

No spike phenomena for $\Delta\omega=0$ was observable regardless of the noise bandwidths used or the level of input noise. However, clearly cycles are slipped by varying $\Delta\omega$ slightly from zero as was seen by the lock range curves of Figures 7.3 and 7.4.

This effect can be explained by studying Figure 7.2. As CNR decreases the signal level, A, measured in rms volts, decreased, causing a proportionate reduction of the loop bandwidth. Though the output noise of the limiter is not flat, it might be assumed after the narrowband filter that the noise into the loop is flat. The value of R_i (5.5) calculated at the limiter output can be found based on f_N for each input signal to noise ratio. These are listed in Table 7.1 for the k=0 case. As can be seen, R_i, though decreasing with CNR, never reaches the threshold level of the universal curve of Figure 5.15. Thus no spikes will occur for $\Delta\omega=0$.

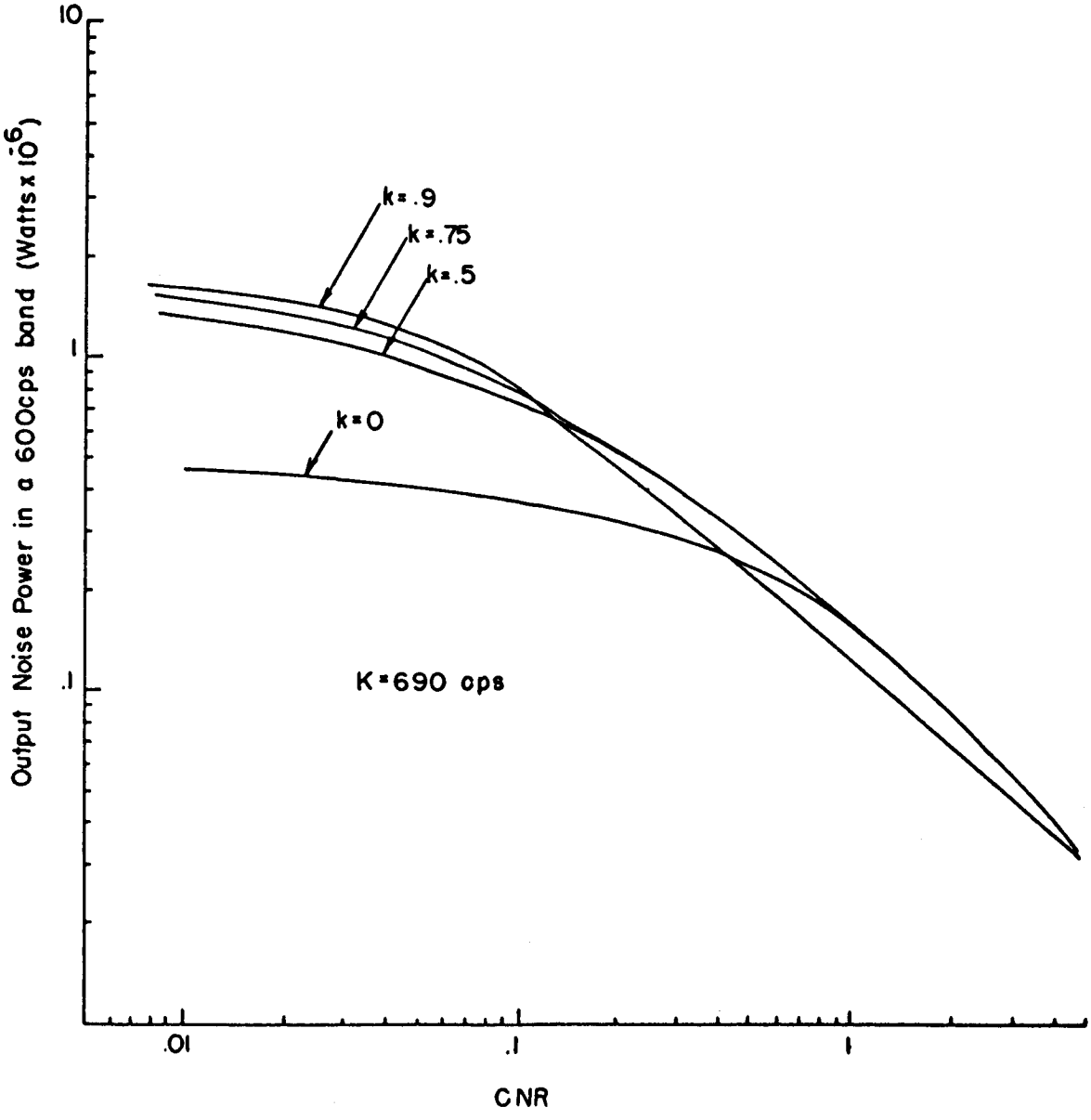

Figure 7.5. Output Noise Power in a 600 cps Band of a Combination Limiter, First Order Tanlock System ($\Delta\omega=0$)

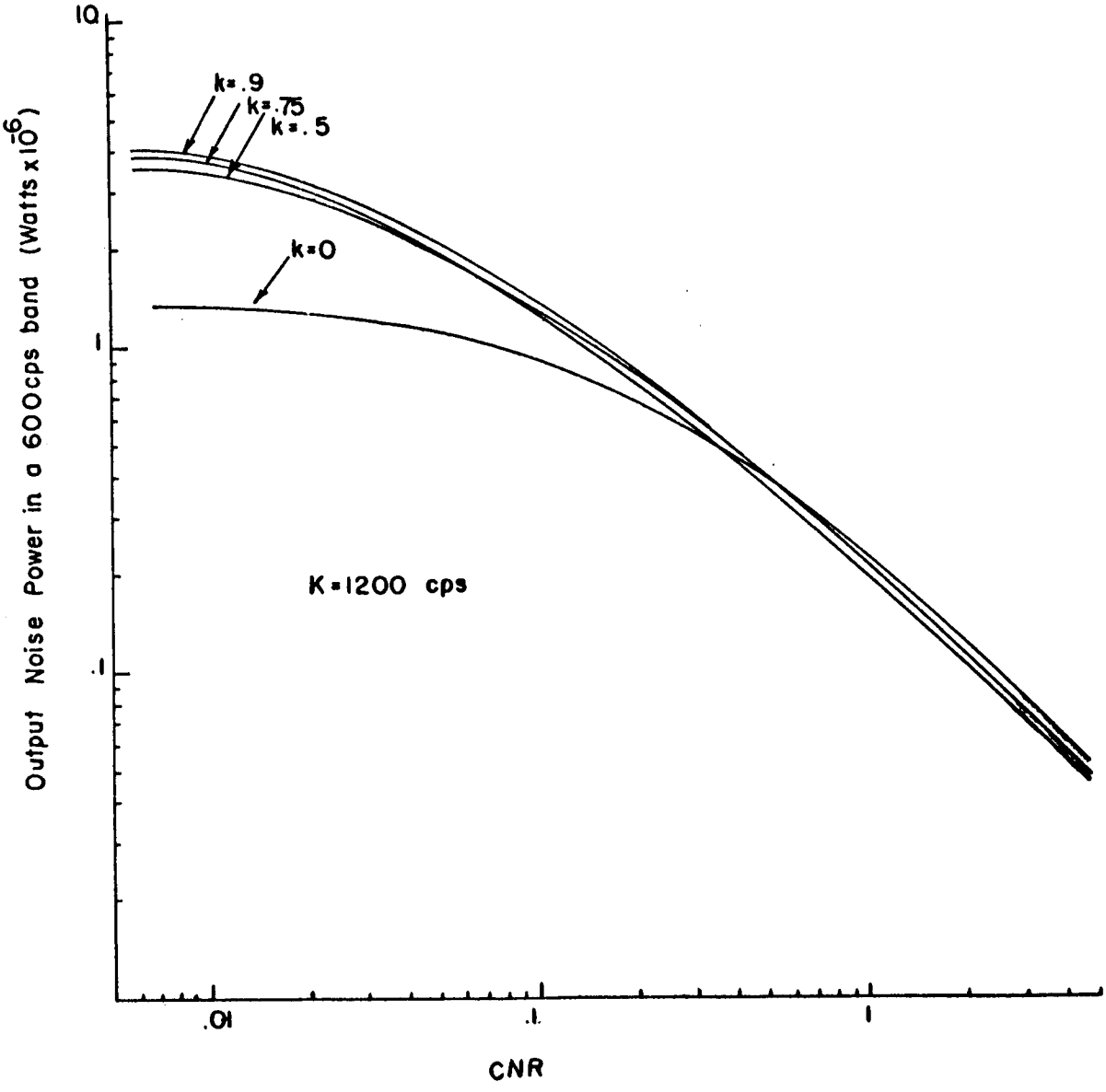

Figure 7.6. Output Noise Power in a 600 cps Band of a Combination Limiter, First Order Tanlock System ($\Delta\omega=0$)

Table 7.1

Parameter Values of a First Order Experimental System Using a Limiter (k=0)

CNR	A	f_N	R_i(db)
∞	1.0	345	∞
4.71	.93	321	45.9
2.27	.855	295	43.1
.641	.608	210	33.3
.333	.490	169	30.85
.19	.380	131	29.7
.125	.310	107	27.55
.0666	.235	81	27.1
.0284	.145	50	24.7
.0154	.1	34	23.1
.0083	.075	25	22.0

7.4. Conclusions

In order to adequately compare the first order systems, with and without a limiter, the measured criteria must be compared on the basis of the same R_i at the receiver input. In the former case R_i must be measured at the limiter input, not at the detector input as is done in the latter case.

Figure 7.7 is a replot of Figures 5.8 and 7.3 vs. the parameter R_i measured at the receiver input. It appears that for a given R_i, the system without a limiter has a better lock range performance even though it has a threshold. This also means that a much higher modulation index

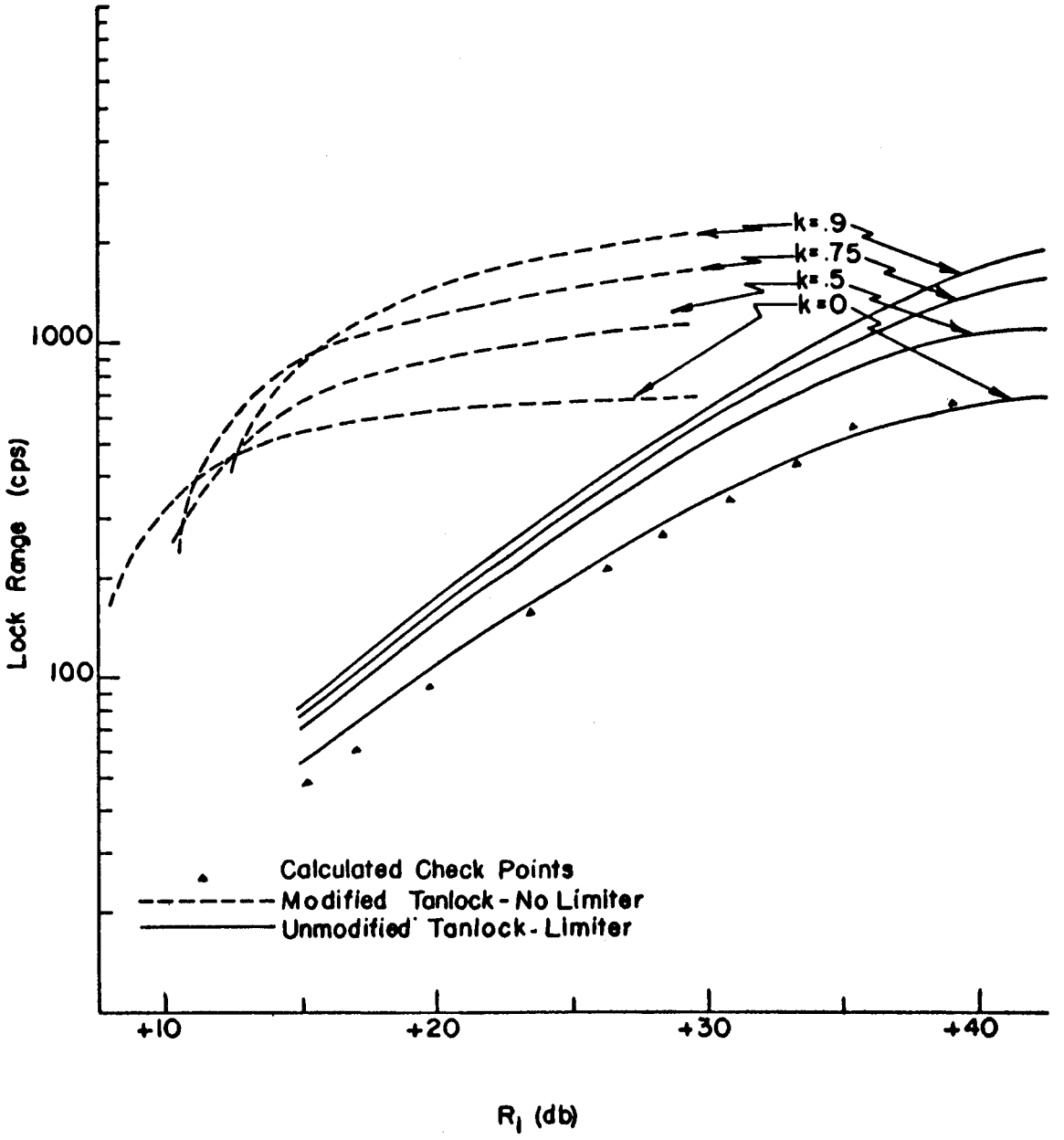

Figure 7.7. Comparison of the Dynamic Lock Range Curves of a First Order Tanlock Loop with and without a Limiter

for a given ω_m can be obtained using the system without a limiter.

As a check on the validity of the limiter results, a few points were calculated from Figure 5.8 for the various f_N's of Table 7.1. These points lie quite close to the actual measured curve indicating the consistency of the experimental results. It should be noted that the spike rate for the two cases is different, but the results would not be significantly changed if they were the same.

VIII. THE THRESHOLD PHENOMENA

This chapter attempts to clarify the threshold problem of phase lock loops. A definition of the threshold is given which is precise but general enough to include all systems. A thorough discussion of the causes and effects of spikes is also included. Statistical evidence is then presented to verify the conclusion that the spikes follow a poisson distribution.

8.1. Causes of Threshold

Most non-linear systems when subjected to signal and noise will exhibit a threshold at some value of CNR. This threshold has been defined as the point where some chosen index of performance, usually the output signal to noise ratio, exhibits a knee in the curve. This is generally where the performance deviates significantly from that which is expected if the system were linear. At best this definition is ambiguous in many situations.

From this research effort it is concluded that for threshold in systems like the phase lock loop containing a periodic non-linearity, the most meaningful definition is the level of spike activity at the output. It is very precise, accurate and easy to measure. It also seems very natural since once spikes begin to appear, they increase rapidly for only small changes in CNR. Furthermore the use of this

criteria is independent of the loop filter, the modulation and the spectrum of the input noise though the CNR where the threshold occurs is not. It is also the most efficient method of comparing any system which exhibits the spike phenomena.

The cause of these spikes is due to momentary losses of synchronism which cause the system to restabilize $2\pi n$ ($n=\pm1,\pm2,\ldots$) radians from its previous stable point. Each complete cycle of 2π radians causes one spike at the output. The polarity of the spike depends on the direction moved. If $\Delta\omega=0$, positive and negative pulses are equally probable. A thorough analogy of this phenomena with a pendulum is given by Charles[22]. The description of the spikes as impulses can only be considered approximate, since most of the energy is contained in the equivalent noise bandwidth of the loop (see Figure 5.12).

Consider a phase lock loop with noise and no signal. Loss of lock will be caused by a noise peak forcing the phase error to exceed its maximum stable value. For a first order system, the spikes occur at independent, random intervals following a poisson distribution (see Section 8.3). In second order systems, if LR and CR are comparable, the spikes occur at independent, random times. As soon as CR differs significantly from LR, the spikes begin to occur in bursts of varying length, but as Charles[22] points out the bursts appear to follow a poisson distribution.

As modulation increases, the occurrence of spikes or bursts of spikes tend to occur more frequently for a given CNR. They are also more likely to occur at the peak deviation of the signal, thus developing a strong dependence on the modulation. In the limit, the

signal alone can cause spikes without noise.

8.2. Effects of Threshold

The threshold point of a system can be termed the value of CNR below which the system cannot be used for its design function. At the onset of threshold, the output noise in some information band was seen to increase more rapidly. This is explained by the additional energy created by the spikes. When a modulating signal is present, cycle slipping causes the signal energy to be spread over a large band. The result is that the output noise power increases, and the output signal power decreases, thus causing a large drop in the output signal to noise ratio. This latter effect, the signal breakup, has not been previously mentioned in the literature.

It should also be noted that below and in the region of the threshold, the slope of the output signal to noise ratio will vary for a phase lock system of the same bandwidth. This is because the spike energy is not distributed uniformly in the low frequency region and thus the information band strongly influences the noise power measurement. Similarly the deviation for a f.m. or p.m. signal influences the noise power measurement.

8.3. Statistical Analysis of Spike Phenomena

Before a threshold model of the loop can be developed, it is desirable to know some of the statistics of the spike occurrences for the first order systems due to noise alone. Both Lindsey[18] and Schilling[23] have assumed that if the noise at the input is gaussian, the pulses follow a poisson distribution. Though Rice[24]

shows that this is true for the output spikes of a discriminator, there has been no evidence to show that this is true for phase lock loop systems. Evidence is now presented to verify that the necessary conditions for this hypothesis are true within the limits of the tests performed.

A strip recording of about 300-600 spikes for the tanlock system (k=0, .5, .75 and .9 $\Delta\omega$=0) were taken at specific values of CNR with no signal present. A sample of one strip appears in Figure 8.1. Three basic tests listed below were then performed on each set of data in an attempt to establish the statistics of the spikes,

(1) An Interval Histogram, a distribution of the intervals between successive spikes.

(2) A Joint Interval Histogram, a joint distribution or autocorrelation of two successive spike intervals.

(3) A Chi-Square Test, which tests the hypothesis that the samples come from a specified distribution.

8.3.1. Interval Histogram

By measuring the interval between successive spikes for a given set of conditions an interval histogram similar to that of Figure 8.2 can be drawn. In this typical case, k=0, and R_i=+8.49db. A dead space of .0049 sec. is plainly shown, while all the other intervals were arbitrarily chosen to be .0195 sec.

The dead space is explained by the fact that it takes a finite time to cycle through 2π radians, this being the minimum time possible between any two pulses. The total number of pulses are measured, since the positive and negative pulses are equally probable ($\Delta\omega$=0).

A much simpler method of plotting this data is to choose a fixed

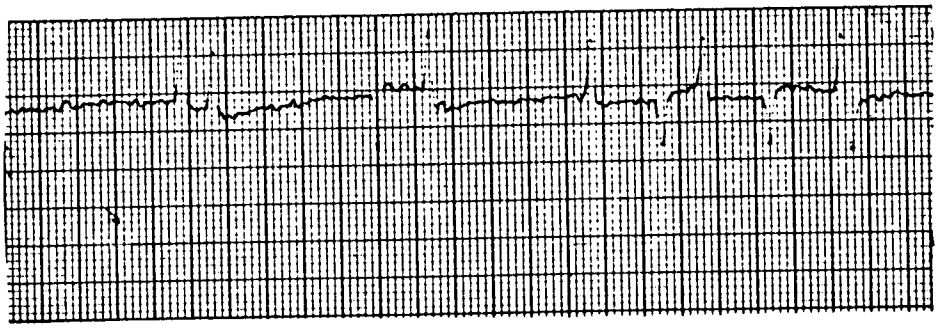

Figure 8.1. Sanborn Recording of the Filtered Output Signal of a First Order Loop (k=0) Showing Cycle Slipping Spikes

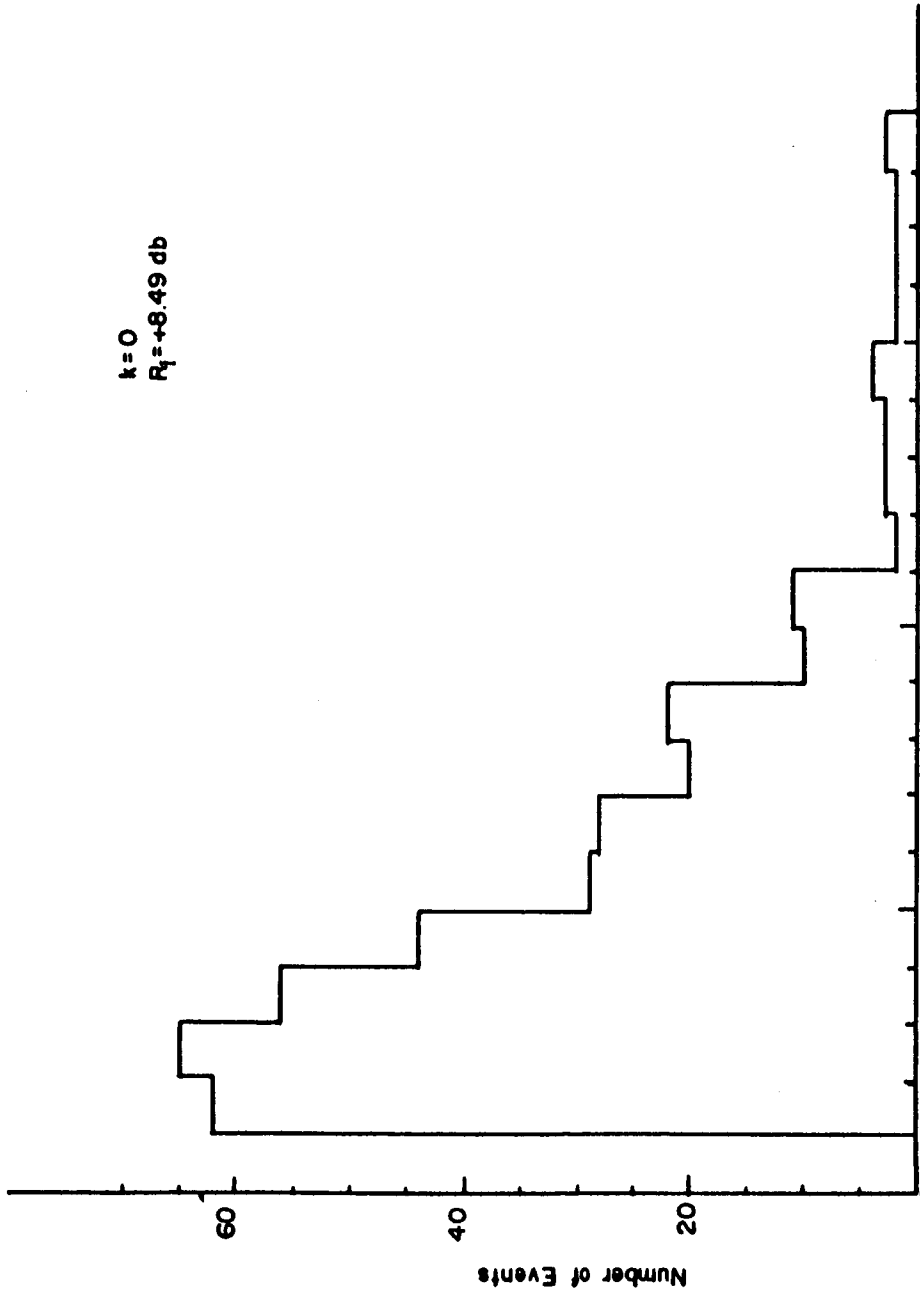

Figure 8.2. Typical Interval Histogram of Cycle Slipping Spikes

interval of time on the recording and then count the number of pulses occurring in each interval. Then by counting the number of intervals, n_j, for a specified number of pulses, j, the discrete distribution of Figure 8.3 is obtained. Using this particular formulation it is much easier to apply the Chi-Square Test.

A set of distribution graphs is shown in Figure 8.4 for values of k=0, .5, .75 and .9. The average value of the distribution is easily obtained as

$$\hat{\lambda} = E(j) = \frac{\sum_{j=o}^{r} j \cdot n_j}{\sum_{j=o}^{r} n_j} \qquad (8.1)$$

where r = number of data intervals and

$$n = \text{total number of points} = \sum_{j=o}^{r} n_j$$

The histograms all appear to follow a poisson distribution whose density function is

$$p(j) = \frac{e^{-\lambda} \lambda^j}{j!} \qquad (8.2)$$

By using the value of $\hat{\lambda}$, found in (8.1), (8.2) is also plotted in Figures 8.4, 8.5. The theoretical densities for poisson processes fit the experimental ones quite well.

8.3.2. Joint Interval Histogram

By measuring the time intervals between all pairs of adjacent pulses, a typical joint interval histogram, Figure 8.6, can be drawn. The number of dots in each square represent the third dimension or height of the plot. In this case k=.5 and the intervals were equal to .4 sec.

The distribution appears to be symmetrical about the 45° axis, a

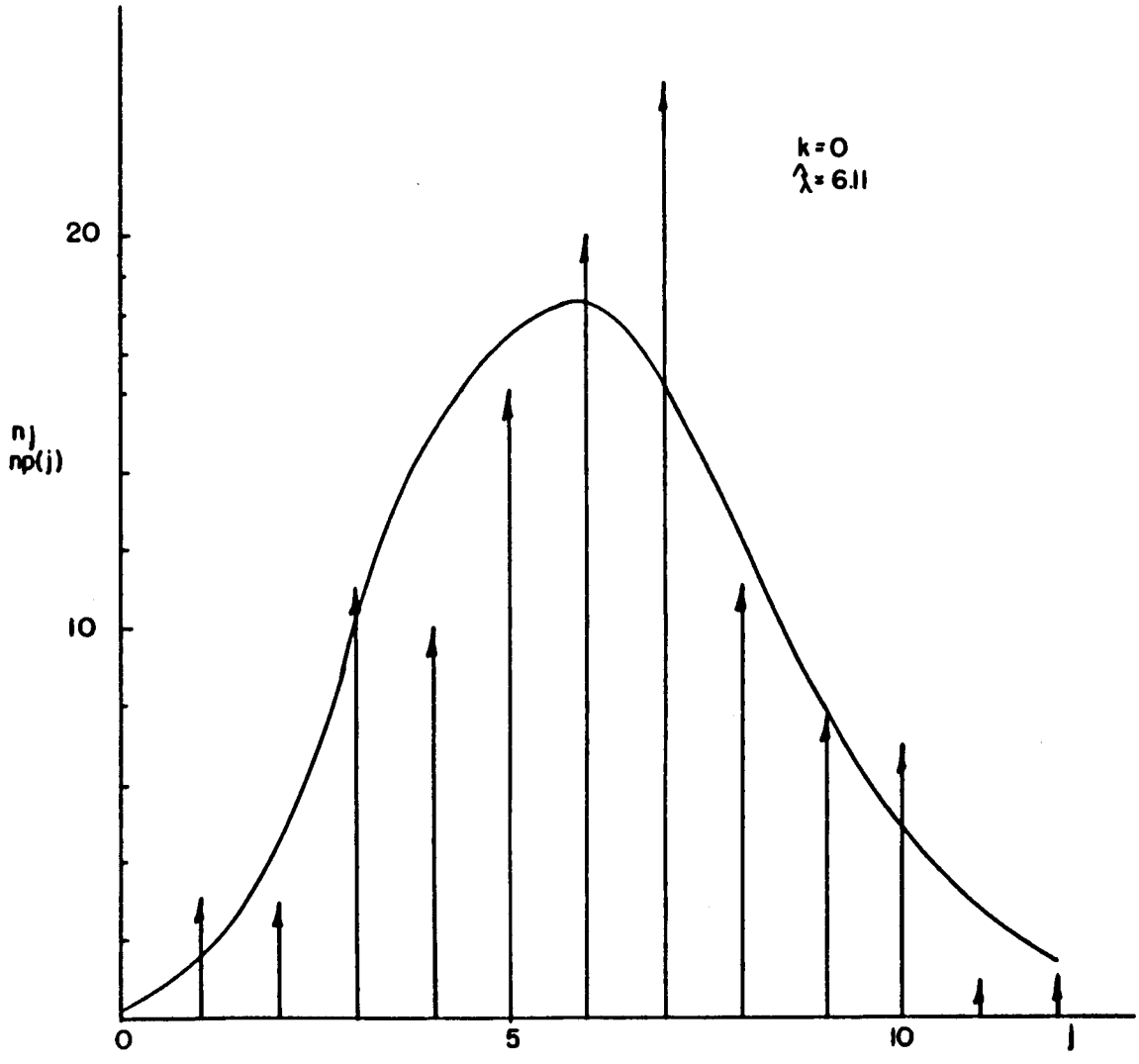

Figure 8.3. Distribution Graph of Cycle Slipping Spikes (k=0)

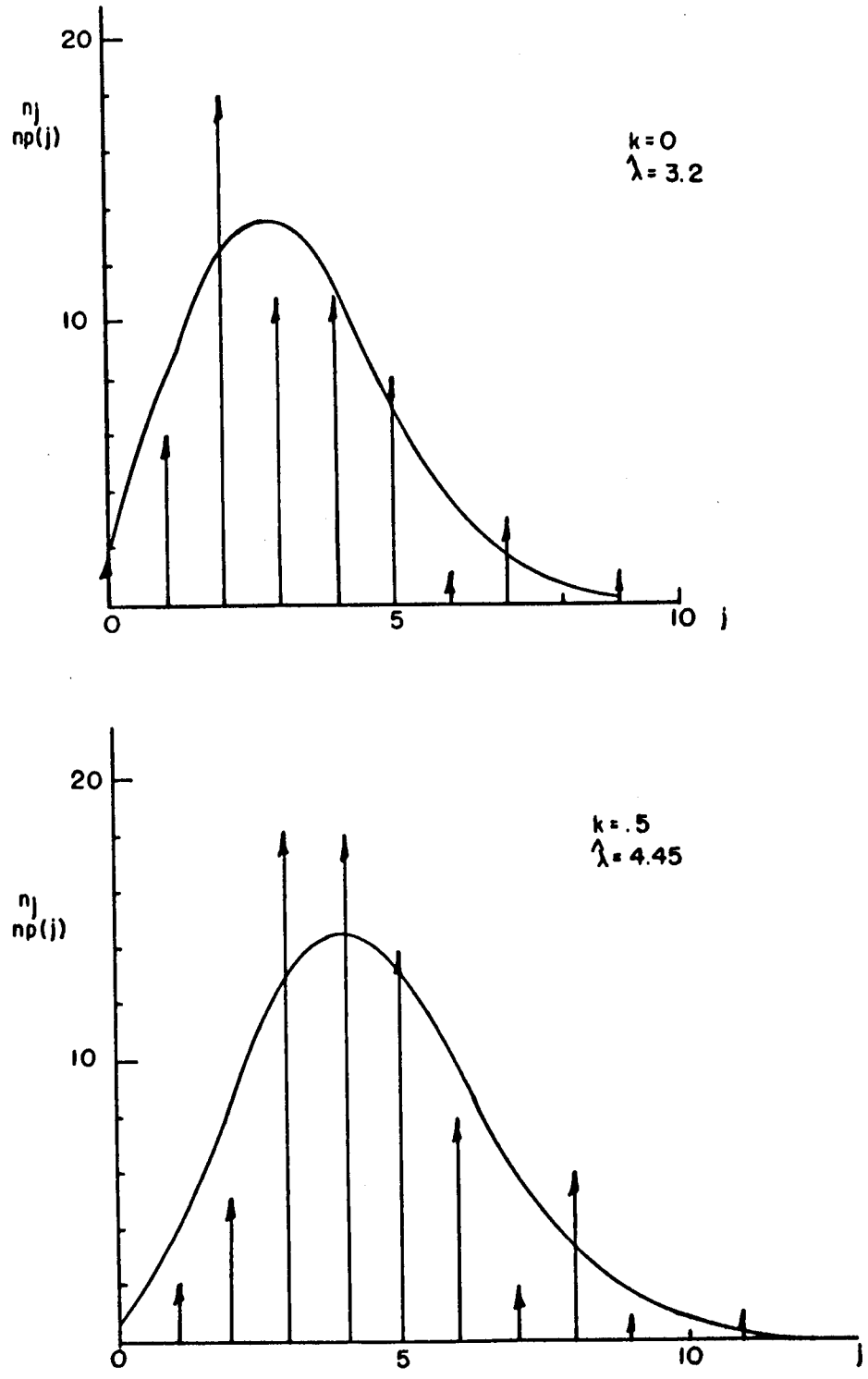

Figure 8.4. Distribution Graph of Cycle Slipping Spikes for Several First Order Tanlock Systems Showing Theoretical Poisson Distributions (k=0, .5)

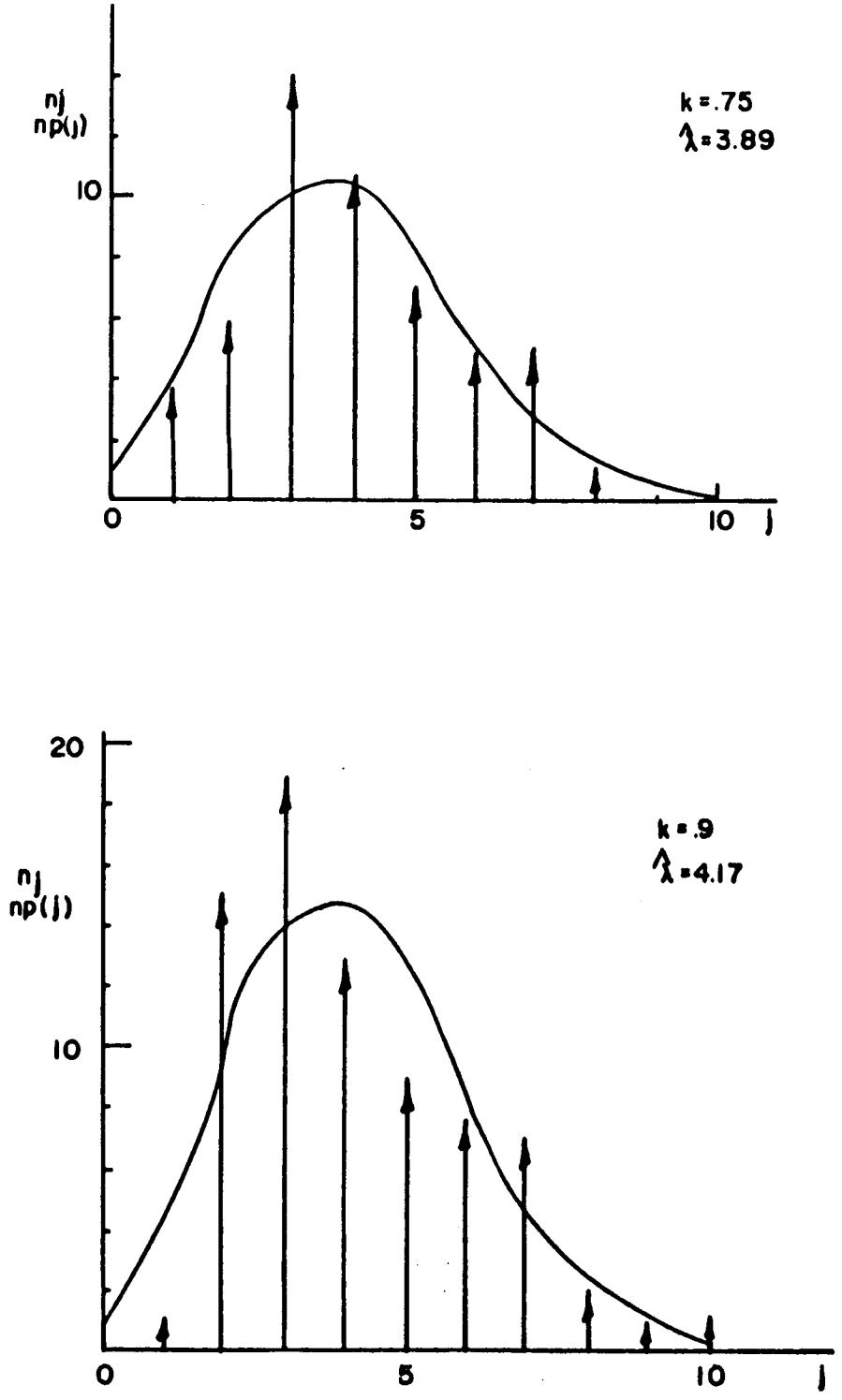

Figure 8.5. Distribution Graph of Cycle Slipping Spikes for Several First Order Tanlock Systems Showing Theoretical Poisson Distributions (k=.75, .9)

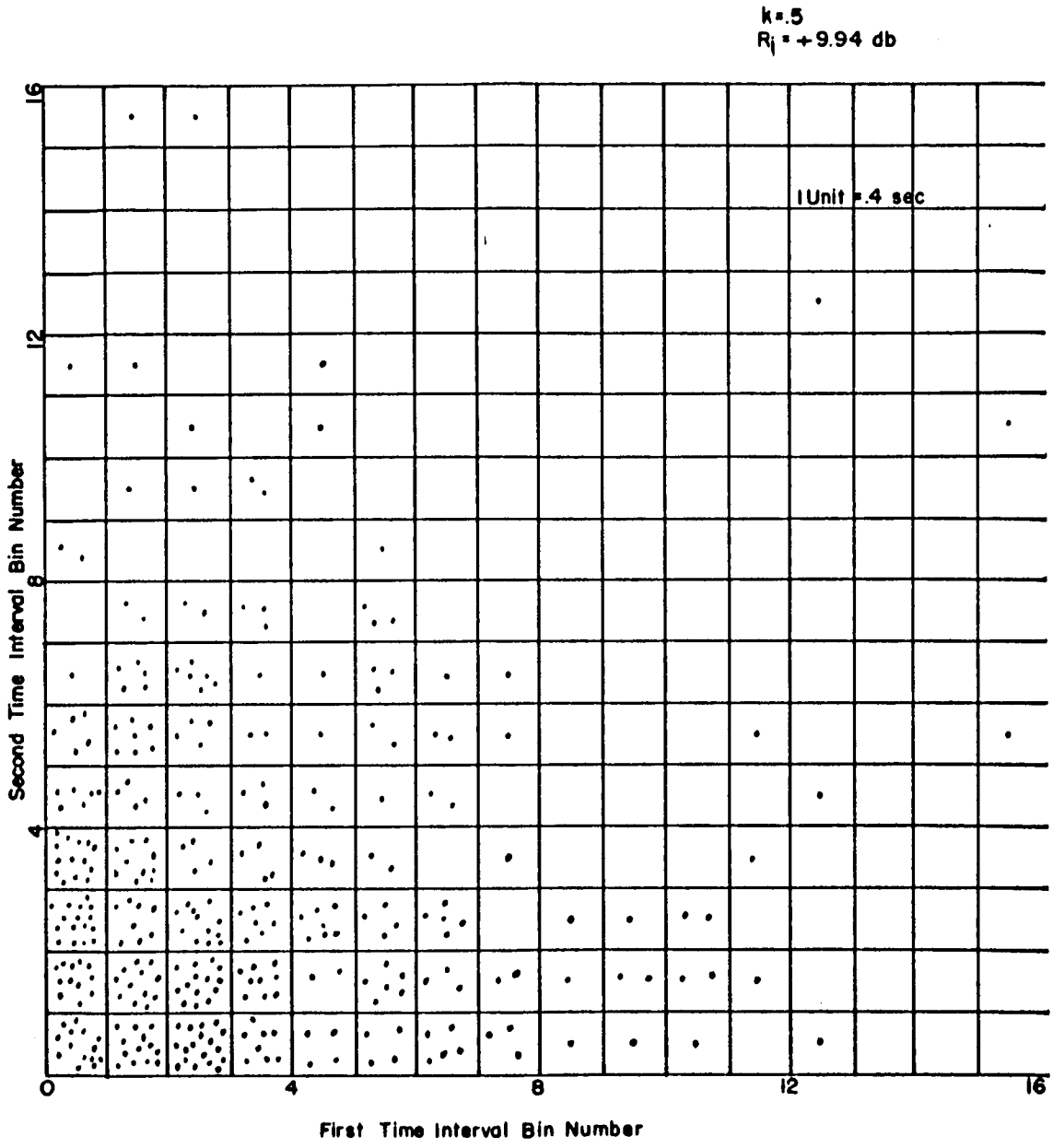

Figure 8.6. Typical Joint Interval Histogram (k=.5)

necessary condition for independence. A cross section through any row or column, indicates uniformity and the rows and columns near zero have the same density function indicating that they are independent of position. Not enough samples are available to carry this result much past the fourth or fifth interval. No clusters of pulses occur so that no burst phenomena, like in certain second order cases, is present. Thus a satisfaction of these necessary conditions leads to the conclusion that the pulses occur independently in the noise only case ($\Delta\omega=0$). These results are typical of all phase lock loop systems with a periodic nonlinearity.

8.3.3. Chi-Square Test

The use of the Chi-Squared significance test for this problem involves an application of Theorem 12.4.2 found in Fisz.[25] We are to test the experimental distribution against the assumed poisson distribution. Since the one parameter, λ, is unknown, it must be estimated by a maximum likelihood estimate. For the poisson distribution this is the same as $\hat{\lambda}$ of (8.1). The statistic

$$\hat{\chi}^2 = \sum_{j=1}^{r} \frac{(n_j - n\pi_j)^2}{n\pi_j} \tag{8.3}$$

where π_j = probability of the value j occurring must then be calculated. The test

$$P\left\{ \chi_\mu^2 \geq \hat{\chi}^2 \right\} > a \tag{8.4}$$

where a is the level of significance generally .01 or .05 is then made. If (8.4) is true then the hypothesis that the samples come from the assumed distribution is accepted with a certain degree of assurance.

Otherwise the hypothesis must be rejected.

Table 8.1 is a tabulation of (8.3) and (8.4) along with the degrees of freedom $\mu=r-2$, for the data given in Figures 8.3 and 8.4. In each case the hypothesis test was positive by a wide margin. Thus it

Table 8.1

Tabulation of Results of Chi-Square Test on Cycle Slipping Pulses

k	$\hat{\lambda}$	$\hat{\chi}^2$	$P\{\chi^2_\mu \geq \hat{\chi}^2\}$	μ
0	6.11	6.101	.52	7
0	3.2	3.418	.33	3
.5	4.45	7.757	.1	4
.75	3.89	1.863	.65	3
.9	4.17	2.844	.60	4

is believed that the pulses are independent and follow a poisson distribution. This conclusion is valid for the first order modified and unmodified tanlock systems as well as the second order systems which do not exhibit the burst phenomena.

IX. CONCLUSIONS

9.1. Conclusions

The experimental research effort was extremely successful in every respect. Relative comparisons were easily made amongst the systems considered. It can be concluded that not only does the non-linear phase comparator affect performance but some improvements can be obtained over the simple sine comparator.

Based on a fixed bandwidth criteria, it is clear as shown in Section 5.7 that the threshold for the modified tanlock and tanlock squared comparators increased as k increased, i.e., as the system became more non-linear. If, however, loop design is based on a fixed lock range criteria, then the threshold actually decreases as k increases (See Figure 5.20).

No significant differences were observed between the modified tanlock and tanlock squared comparators for the same lock range. However, if Figures 5.13 and 5.14 are compared it can be seen that the unmodified tanlock squared had a lower threshold than the unmodified tanlock, a result predicted by the Fokker-Planck Model.

The results of Chapter 6 show that under certain conditions the insertion of filtering into the closed loop can improve certain performance criteria. From this it might be inferred that systems of order greater than 2 might even do better. The generally accepted use of critical camping in second order systems was shown to be a

desirable design criteria.

It is felt that a significant contribution was made in the establishment of universal curves for lock range and threshold. These curves should prove extremely useful to designers desiring to use these systems in the future.

The simple definition of threshold given in terms of spikes/sec. and the ease with which it can be measured is a most worthwhile result. A close study of the results presented in Chapters 5 and 6 show this definition to be independent of loop filter, modulation and comparator. The choice of the threshold, which can be made from the curves given, is based on the designers ultimate use of the particular system.

Finally the statistical distribution of the spikes, shown in Chapter 8 to be poisson for the first order loop and special cases of the second order loop should prove useful to those attempting to model the threshold behavior.

9.2. Recommendations for Future Study

Since the Fokker-Planck Model fails to make an accurate prediction of the threshold for certain classes of non-linearities, it would be desirable to pursue other methods of attack. One of these might be the generalized Kolomogorov Equations where the Markov assumption is not necessary.

This would have the effect of placing the threshold phenomena on a more mathematical foundation. It would also enable an optimization procedure to be used to find the nonlinear phase comparator giving the best performance in some sense. Finally it might enable an easier

evaluation of higher order systems to be made, avoiding the tedious but rewarding experimental approach.

Finally it would be advantageous to compare the above results with systems which perform similar functions. These might include discriminators and frequency feedback systems. Since a theoretical approach would be as difficult as that for phase lock loops, an extensive experimental study should prove worthwhile.

B I B L I O G R A P H Y

BIBLIOGRAPHY

1. Gruen, W. J., "Theory of AFC Synchronization," Proc. IRE, Vol. 41, pp. 1043-1048, August, 1953.

2. Cahn, C. R., "Piecewise Linear Analysis of Phase Locked Loops," PGSET, Vol. 8, No. 1, pp. 8-13, March, 1962.

3. Baker, T. S., "Analysis of the Synchronization of an Automatic Phase Control System," Ph.D. Thesis, Harvard Univ., January, 1965.

4. Rey, T. J., "APC: Theory and Design," Proc. IRE, Vol. 48, No. 10, pp. 1760-71, October, 1960.

5. Viterbi, A. J., "Acquisition and Tracking Behavior of Phase Locked Loops," Vol. X, B.P.I. Symposia Series, pp. 583-620, April, 1960.

6. Richman, D., "Color-Carrier Reference Phase Synchronization in NTSC Color Television," Proc. IRE, Vol. 42, pp. 106-133, January, 1954.

7. Byrne, C. J., "Properties and Design of the Phase Controlled Oscillator with a Sawtooth Comparator," B.S.T.J., Vol. 41, No. 2, pp. 559-602, March 1962.

8. Goldstein, A. J., "Analysis of the Phase-Controlled Loop with Sawtooth Comparator," B.S.T.J., Vol. 41, No. 2, pp. 603-633, March 1962.

9. Robinson, L. M., "Tanlock: A Phase Lock Loop of Extended Tracking Capability," Proc. National Winter Conference on Military Electronics, Los Angeles, Calif., pp. 396-421, February, 1962.

10. Jaffe, P. and Rechtin, R., "Design and Performance of Phase Lock Circuits Capable of Near Optimum Performance Over a Wide Range of Input Signal and Noise Levels," PGIT, Vol. 1, No. 1, pp. 66-76, March, 1955.

11. Gilchreist, C. E., "Application of the Phase Lock Loop to Telemetry As a Discriminator Tracking Filter," PGTRC, Vol. 4, No. 1, pp. 20-35, June, 1958.

12. Margolis, S. G., "The Response of a Phase Locked Loop to a Sinusoid Plus Noise," PGIT, Vol. 3, No. 2, pp. 136-142, June, 1957.

A P P E N D I X A

13. Schilling, D. L., "Response of an Automatic Phase Control System to F. M. Signals and Noise," Brooklyn Polytechnic Institute Rpt. #PIBMRI-1040-62, June, 1962.

14. Van Trees, H. A., "Functional Techniques for the Analysis of the NonLinear Behavior of Phase Locked Loops," Proc. IEEE, Vol. 52, No. 8, pp. 894-911, August, 1964.

15. Booton, R. C., "The Analysis of Non Linear Control Systems with Random Inputs," Proc. of Non-Linear Circuit Symposium, BPI, pp. 369-392, April, 1953.

16. **Develet**, J. A., "A Threshold Criterion for Phase Lock Demodulation," Proc. IRE, Vol. 51, No. 2, pp. 349-356, February, 1963.

17. Viterbi, A. J., "Phase Locked Loop Dynamics in the Presence of Noise by Fokker-Planck Techniques," Proc. IRE, Vol. 40, No. 8, pp. 1737-1753, December, 1963.

18. Lindsey, W. C., "Investigation of Second Order Phase Locked Loops by Fokker-Planck Methods," JPL Space Programs Summary, Vol. 4, No. 37-30, pp. 262-268, December, 1964.

19. Lehan, F. W. and Parks, R., "Optimum Demodulation," IRE Convention Record, Part 8, pp: 101-103, March, 1953.

20. Youla, D. C., "The Use of Maximum Likelihood in Estimating Continuously Modulated Intelligence Which Has Been Corrupted by Noise," PGIT, Vol. 1, No. 3, pp. 90-105, March, 1954.

21. Van Trees, H. A., "An Introduction to Feedback Demodulation," MIT Lincoln Lab., Group Rpt. No. 64G-5, August, 1963.

22. Charles, F. J., "A Model Distribution for the Phase-Error in Second Order Phase Lock Loops," PGCS, Vol. 15, No. 1, Oct. 1966.

23. Schilling, D. L., and Billig, J., "A Comparison of the Threshold Performance of the Frequency Demodulator Using Feedback and the Phase-Locked Loop," Brooklyn Polytechnic Institute Report #PIBMRI-1207-64, May 1964.

24. Rice, S. O., "Noise in FM Receivers," Chapter 25, Time Series Analysis, Edited by M. Rosenblatt, John Wiley, 1963.

25. Fisz, M., Probability and Mathematical Statistics, John Wiley, New York, N. Y., 1963.

26. Springett, R. C., "A Note on Signal-to-Noise and Signal-to-Noise Spectral Density Ratios at the Output of a Filter-Limiter Combination," JPL Space Programs Summary, Vol. 4, No. 37-36, pp. 241-244.

27. Uhran, J. J., and Lindenlaub, J. C., "The Effect of Phase Detector Characteristics on Phase Lock Loop Design Parameters," Short Paper, IEEE International Symposium on Information Theory," UCLA February, 1966.

APPENDIX A

This section includes items measured in conjunction with the many tests discussed and referred to in Chapter 4 but not included therein.

Table A-1

Frequency Response of the Philbrick Analog Divider and Multiplier

e_1(rms)	e_2(d.c)	E	Divide Mode f_3(KC)	Multiply Mode f_3(KC)
1.0	2.0	1	64	27
1.0	2.0	2	52	50
1.0	2.0	3	54	69
1.0	2.0	5	54	80
1.0	1.0	1	30	26
1.0	1.0	2	29	51
1.0	1.0	5	36	90
1.0	.5	1	14.9	26
1.0	.5	2	15.2	51
1.0	.5	5	42	90
1.0	.2	1	7.6	26
1.0	.2	2	15.4	53
1.0	.2	5	43	90
.1	.2	5	7	--
.5	.2	5	22	--

f_3 = -3 db point.

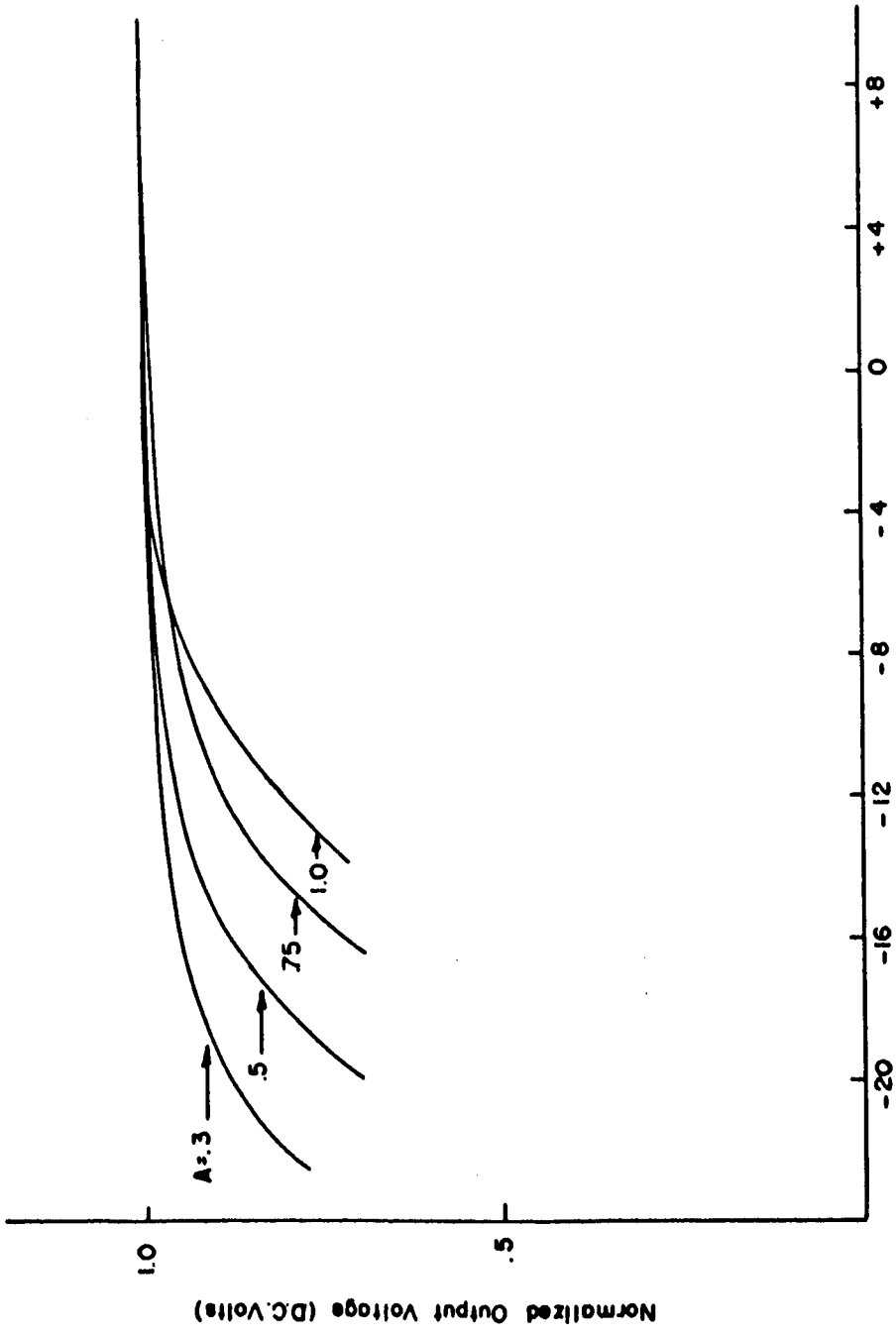

Figure A.1. Output Noise Power of System Multipliers in a 100 cps Band vs. Input Noise Power for Various Input Signal Levels

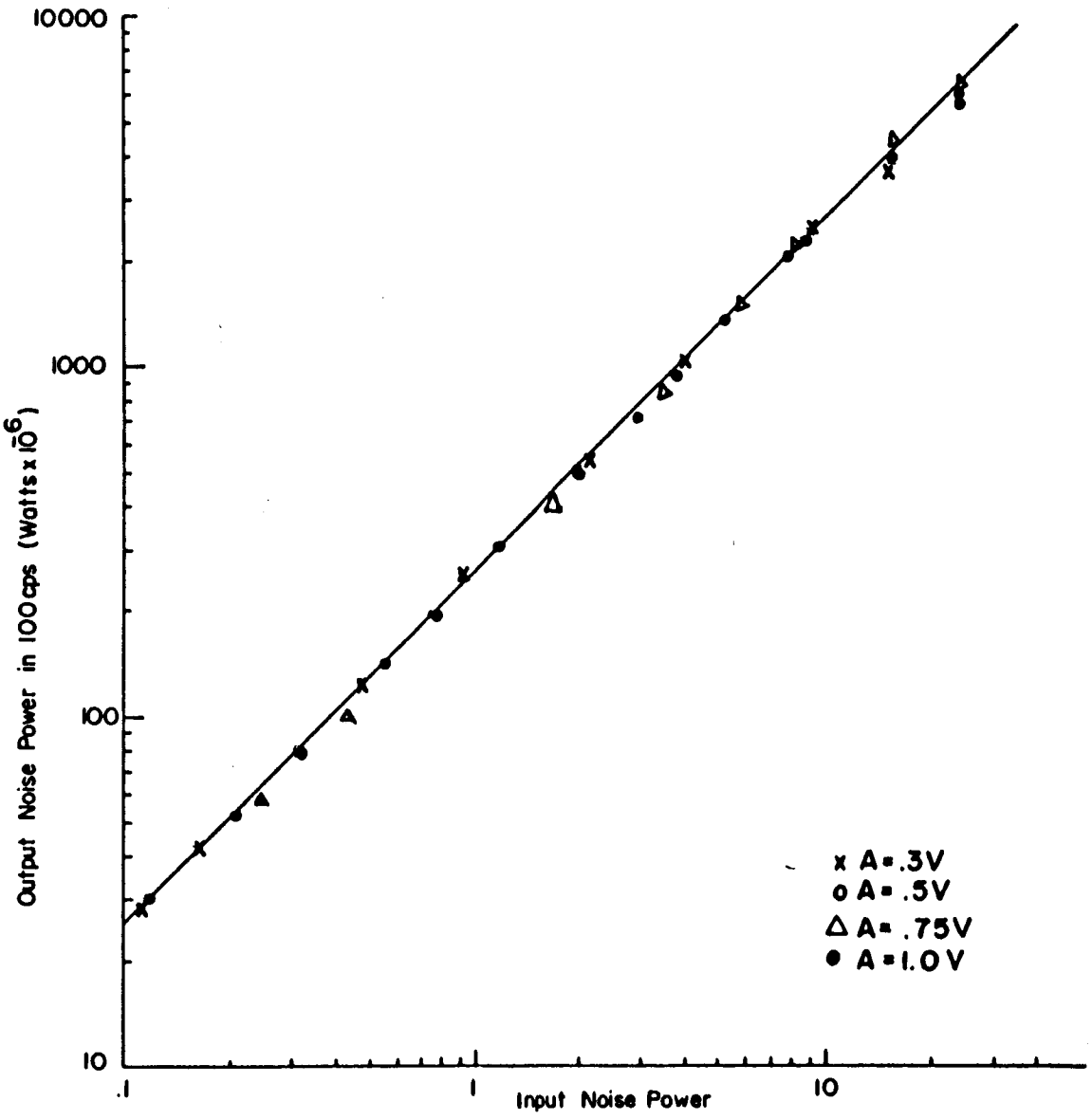

Figure A.2. Output Noise Power of System Multipliers in a 100 cps Band vs. Input Noise Power for Various Input Signal Levels

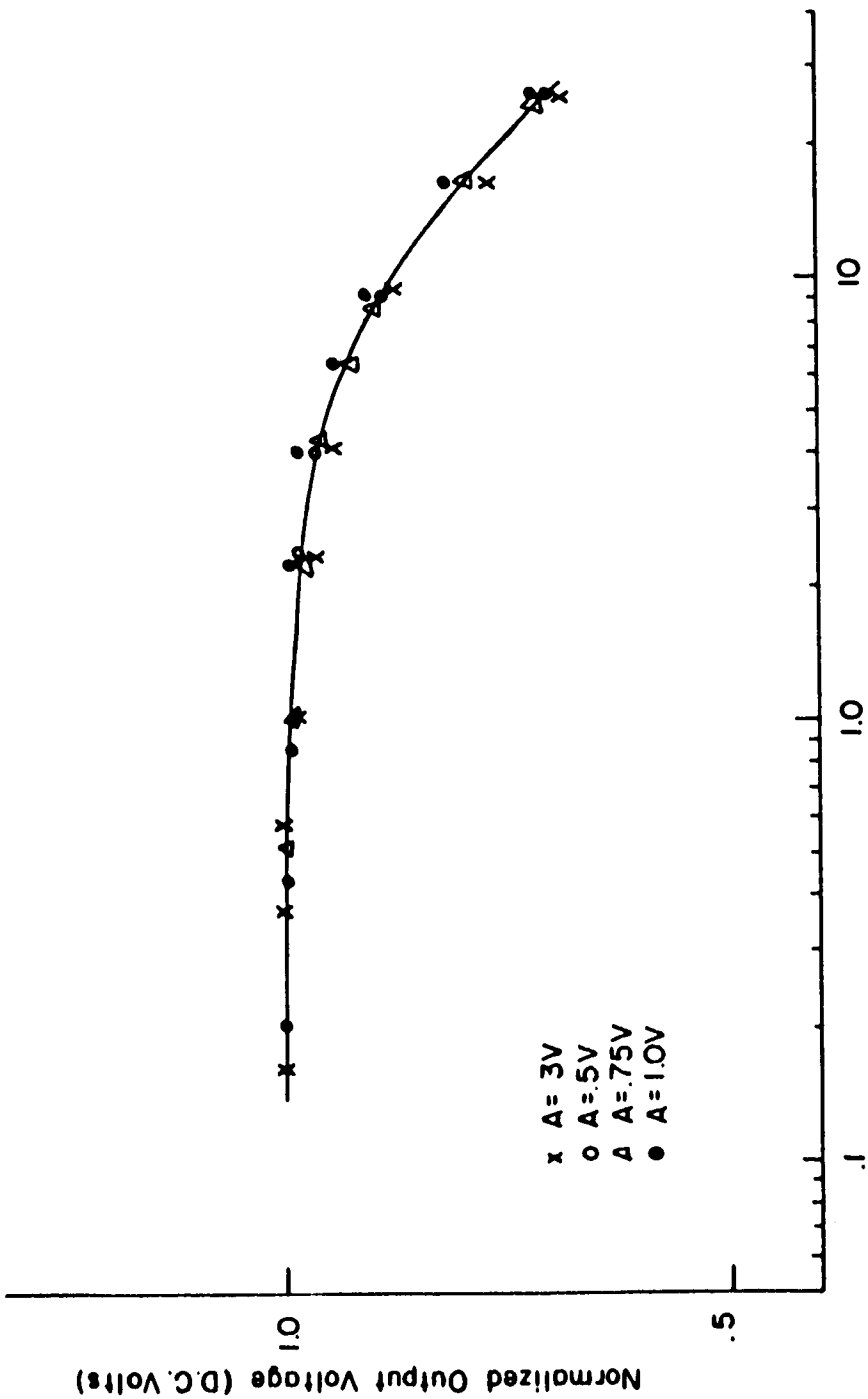

Figure A.3. D.C. Output Voltage of System Multipliers vs. Total Input Power for Various Input Signal Levels

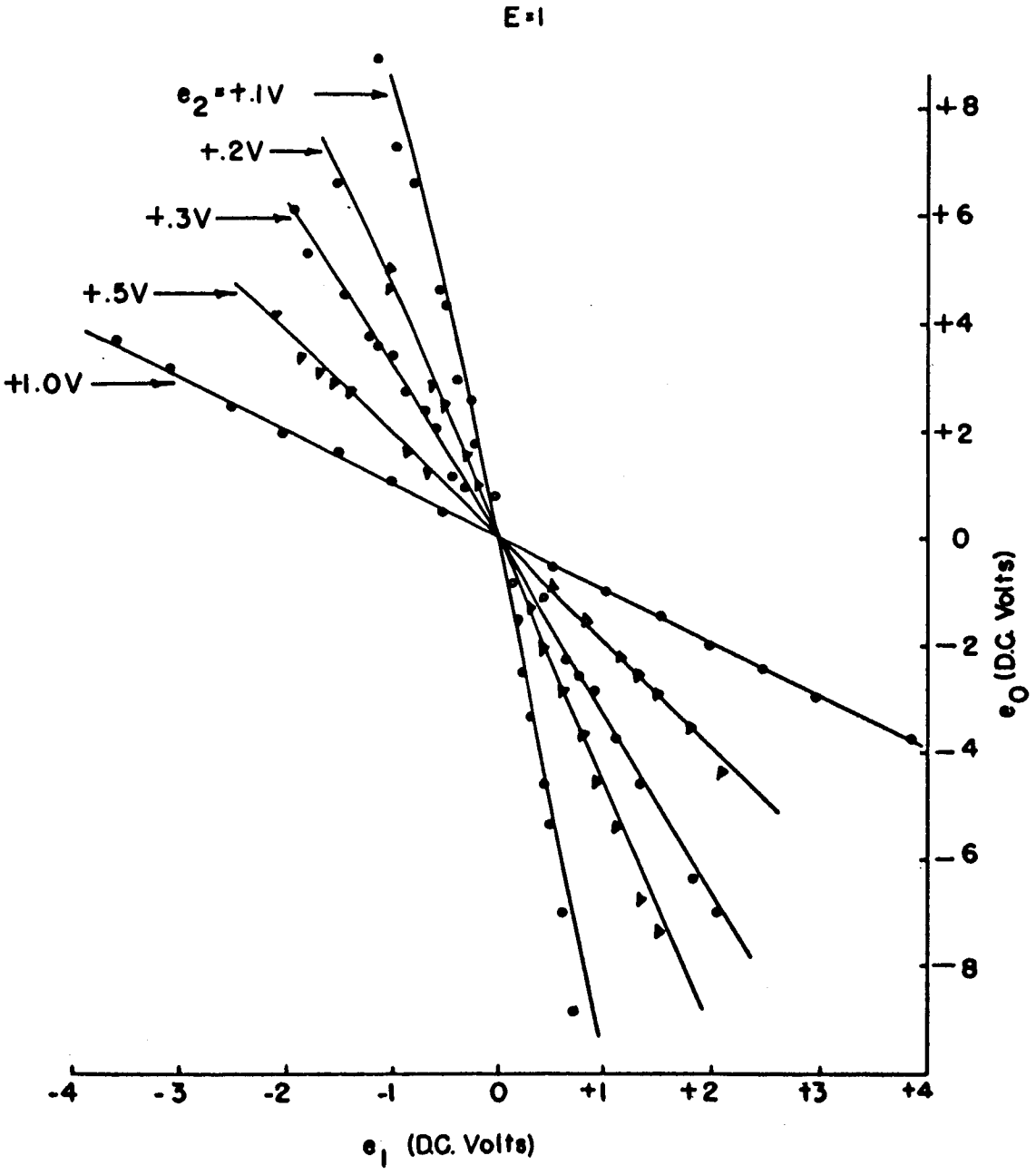

Figure A.4. Signal Response of Analog Divider for Various Values of the Denominator Signal

A P P E N D I X B

APPENDIX B

Appendix B includes the circuit and component diagrams for the entire experimental system used. All component values have been given and the transistor and diode types specified. It should be noted that all values of resistance are in ohms and capacitors in μμf unless otherwise specified. All coils were wound with No. 28 SEW.

Individual sections of the system are given in Figures B.1 through B.7 and the entire layout in Figure B.8. The special circuits used to measure spike activity are given in Figure B.9.

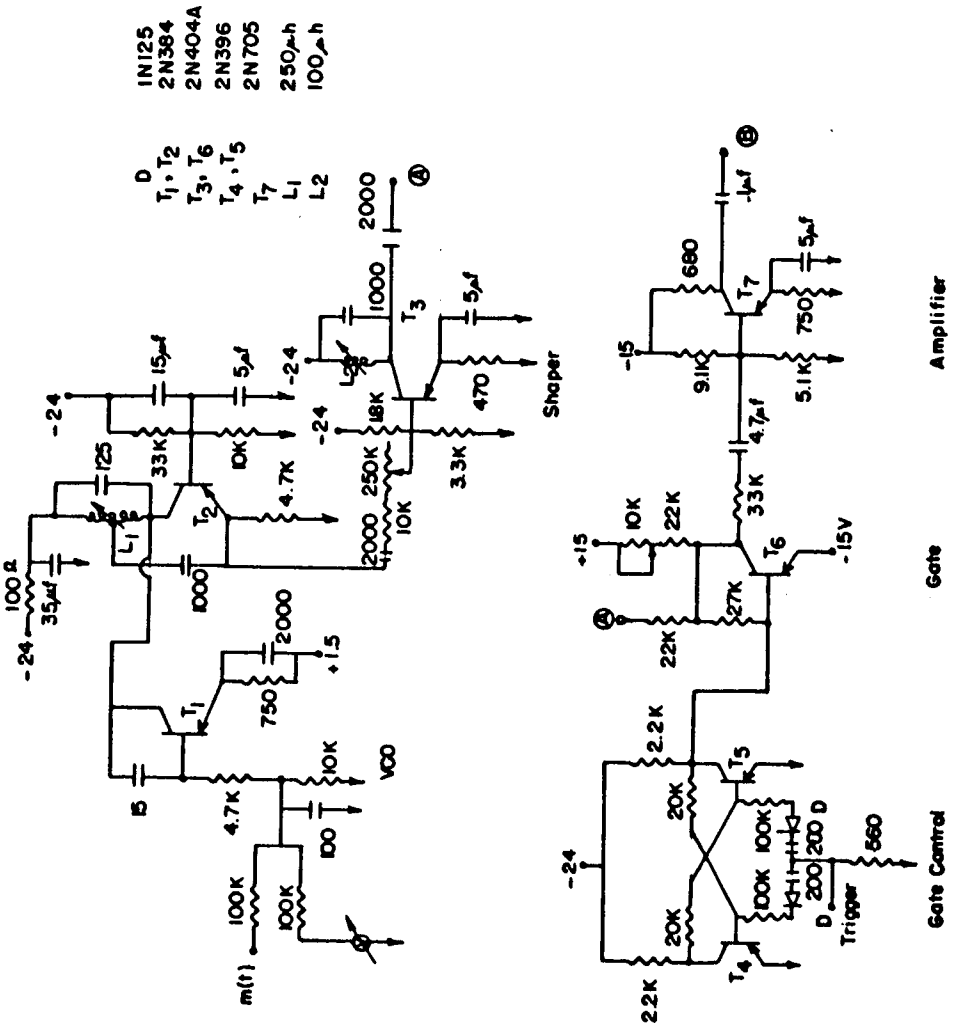

Figure B.1. Transmitter and Gate

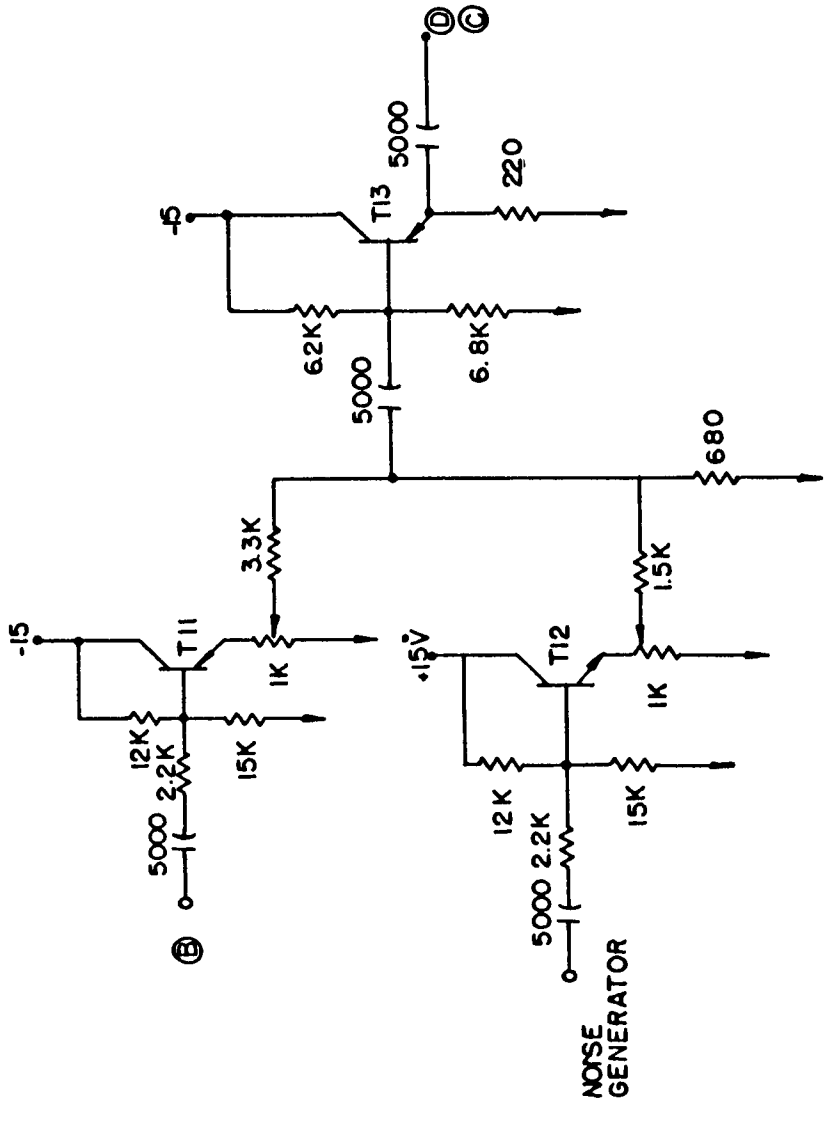

T11 2N404A

T12 2N1893

T13 501M

Figure B.2. Signal and Noise Adder

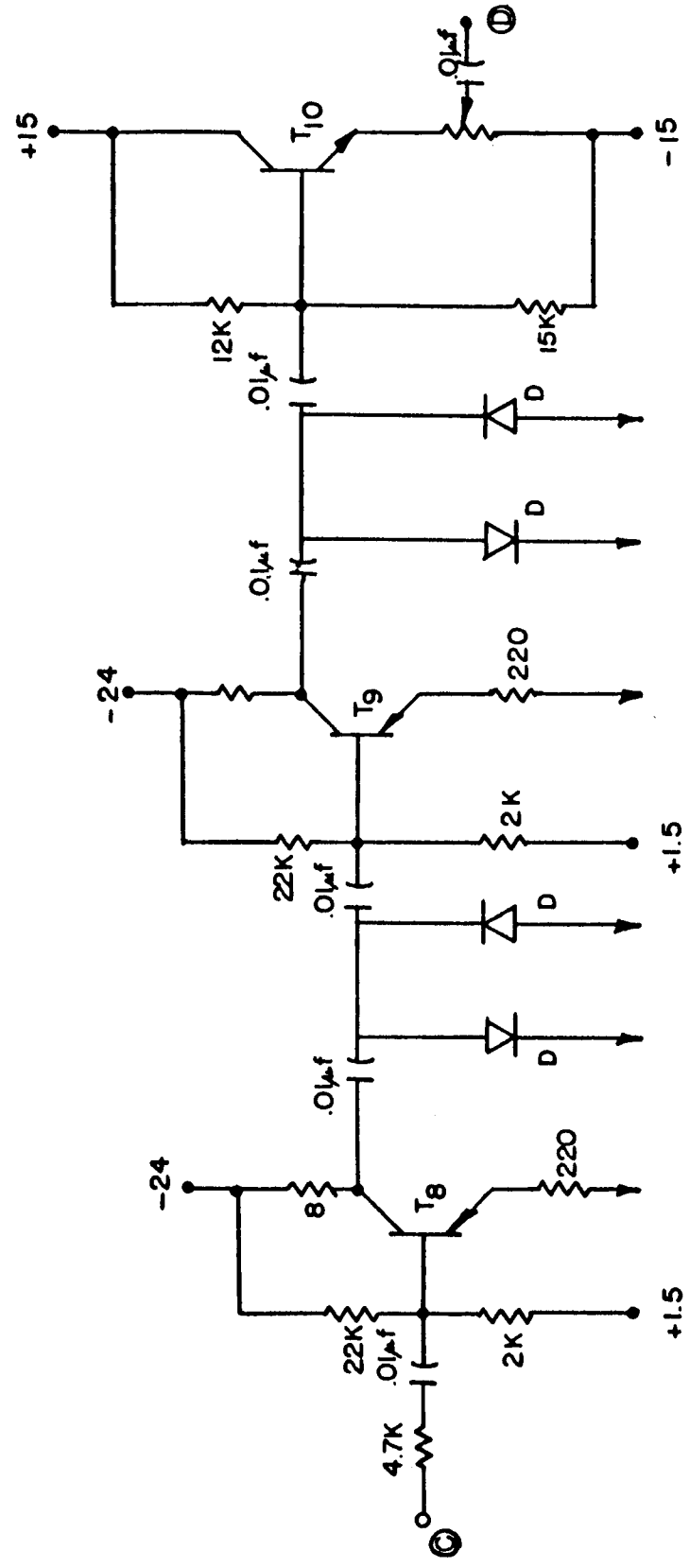

D 1N1305
T_8, T_9 2N404A
T_{10} 2N1893

Limiter

Figure B.3. Limiter

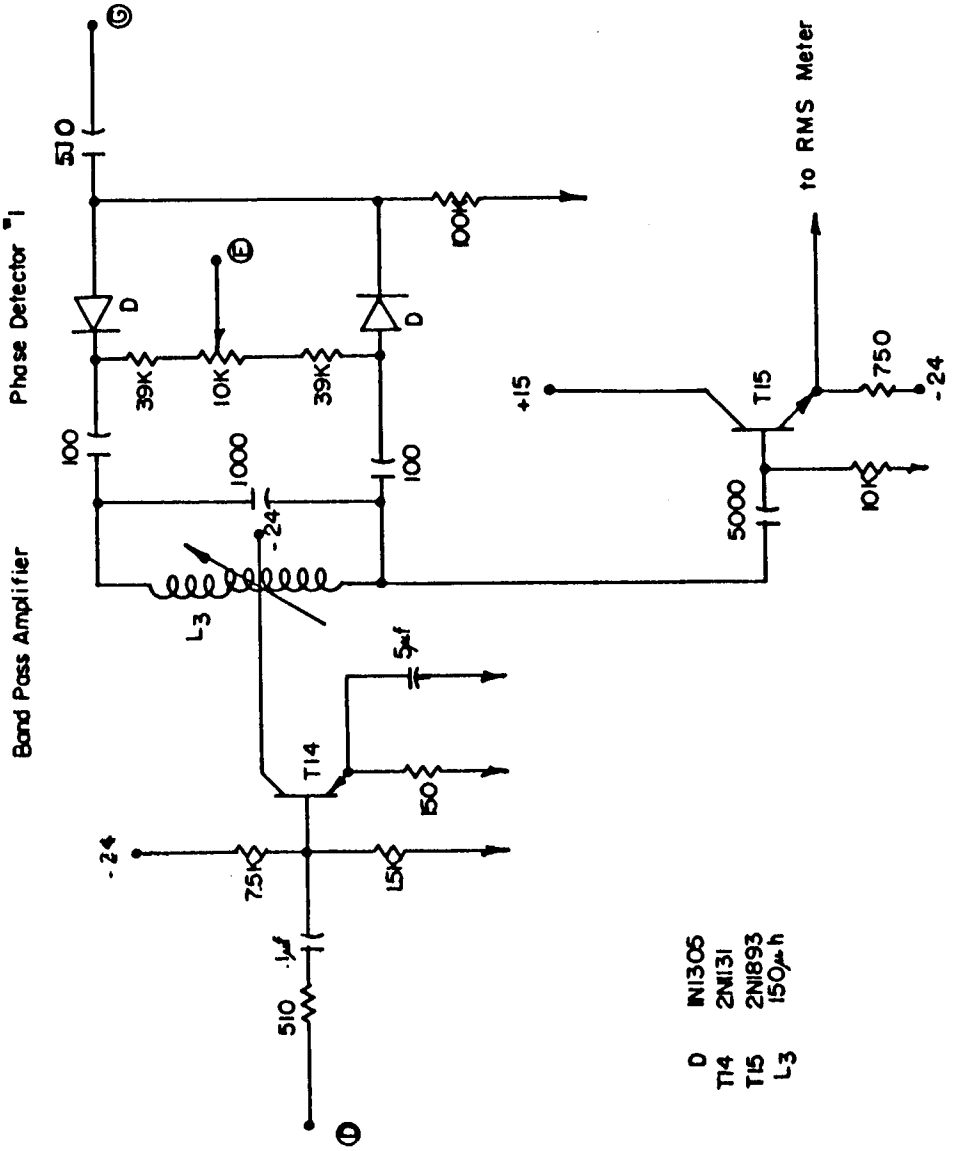

Figure B.4. Phase Detector #1

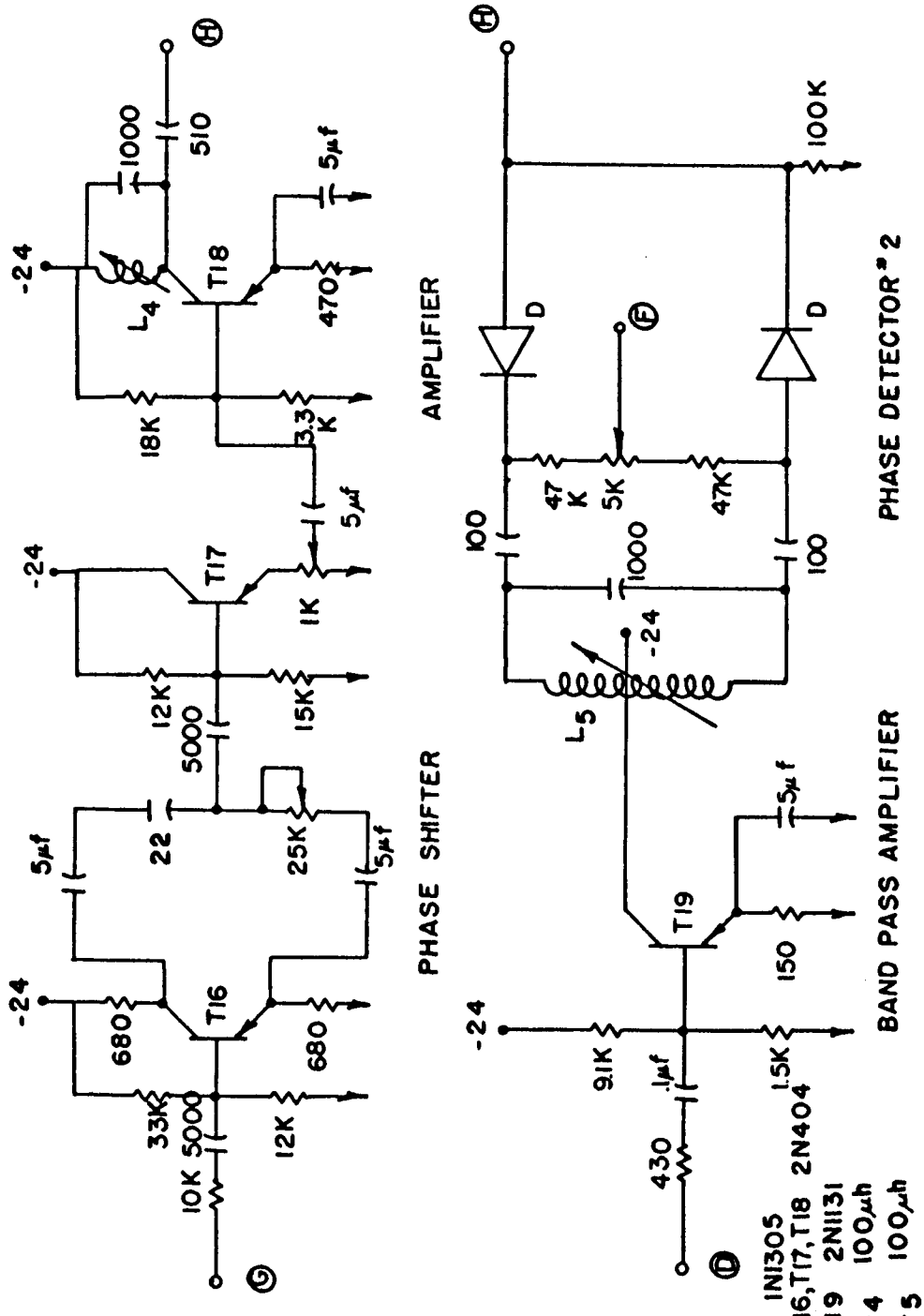

Figure B.5. Phase Shifter and Phase Detector #2

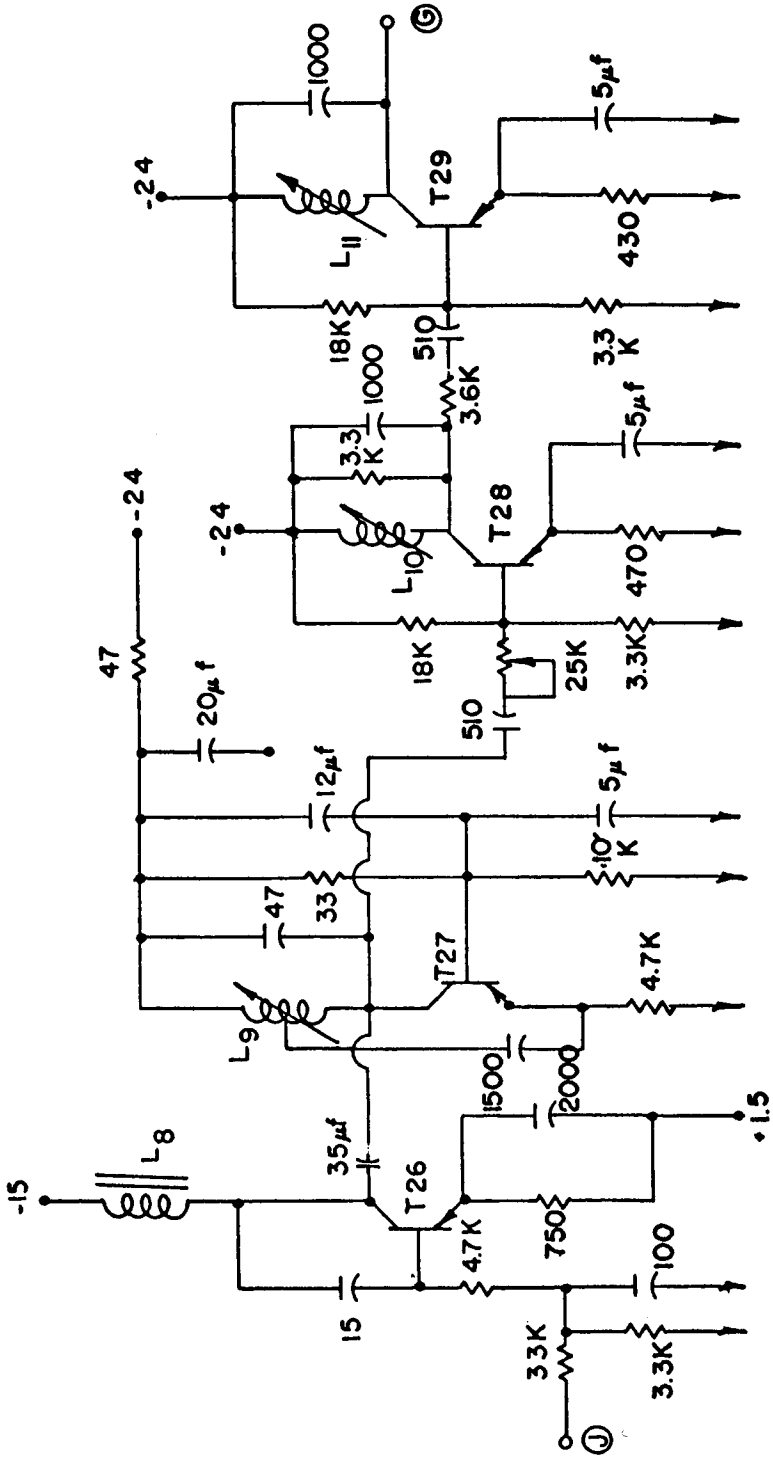

Figure B.6. Receiver VCO

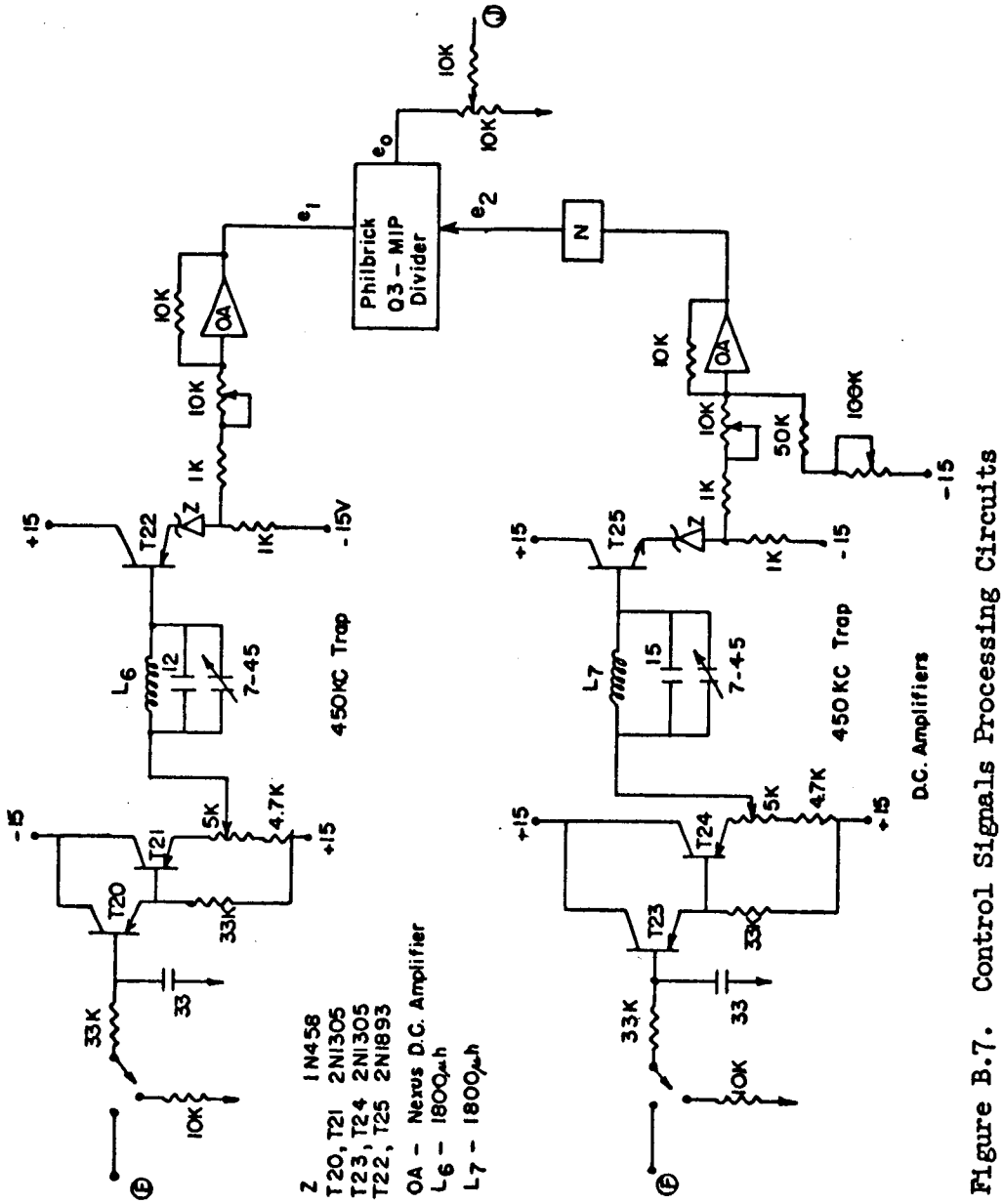

Figure B.7. Control Signals Processing Circuits

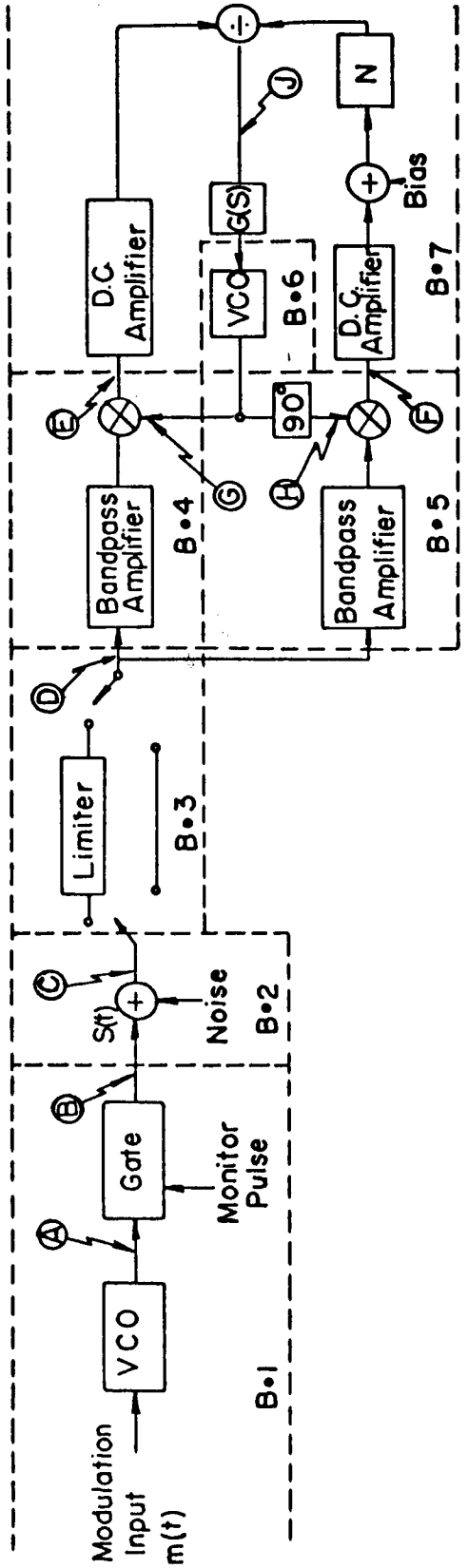

Figure B.8. Block Diagram of Experimental System

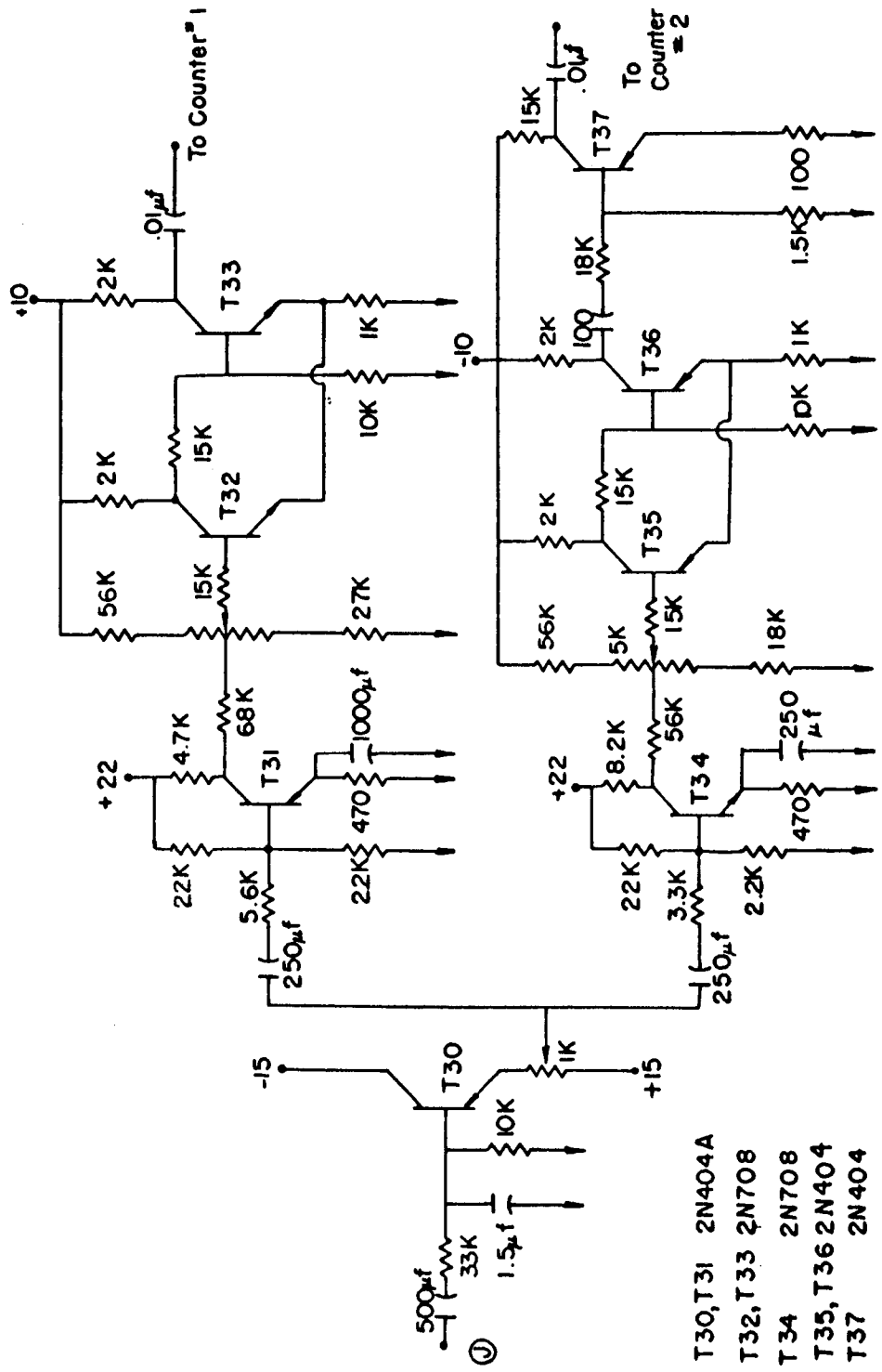

Figure B.9. Spike Detecting Circuits

RECENT RESEARCH PUBLICATIONS
SCHOOL OF ELECTRICAL ENGINEERING
PURDUE UNIVERSITY

TR-EE65-1 **PERFORMANCE OF EASILY IMPLEMENTED ERROR REDUCTION TECHNIQUES**
J. C. Hancock and R. G. Marquart, Contract No. AF 33(657)-10709; PRF 3474-61-780, January 1965.

TR-EE65-2 **UNSUPERVISED LEARNING RECEIVERS FOR BINARY CHANNELS WITH INTERSYMBOL INTERFERENCE.**
J C. Hancock and R. W. Chang. Contract No. NSF-GP-2898; PRF 3955-50-285, January 1965.

TR-EE65-3 **INVESTIGATION OF OPTIMIZATION OF ATTITUDE CONTROL SYSTEMS, VOL. I.**
R. Sridhar, G. C. Agarwal, R. M. Burns, D. M. Detchmendy, E. H. Kopf, Jr., and R. Mukundan. Contract No. JPL-950670/SUBNAS 7-100, PRF No. 3807-55-285, January 1965.

TR-EE65G4 **INVESTIGATION OF OPTIMIZATION OF ATTITUDE CONTROL SYSTEMS, VOL. II.**
R. Sridhar, G. C. Agarwal, R. M. Burns, D. M. Detchmendy, E. H. Kopf, Jr., and R. Mukundan. Contract No. JPL-950670/SUBNAS 7-100, PRF No. 3807-55-285, January 1965.

TR-EE65-5 **SOLID STATE MICROWAVE POWER RECTIFIERS.**
R. H. George. Contract No. AF30(602)3481, PRF No. 411-53-285, February 1965.

TR-EE65-6 **SEQUENTIAL DECISIONS, PATTERN RECOGNITION AND MACHINE LEARNING.**
K. S. Fu and C. H. Chen. Contract No. NSF G-2183, PRF 3810, PRF 3373 - David Ross Grant, April 1965.

TR-EE65-7 **PRESSURE SENSITIVITY OF ALLOYED P-N JUNCTIONS**
H. W. Thompson, Jr. Contract No. N123(953)35011A, PRF 3832-53-2859. June 1965.

TR-EE65-8 **A STUDY OF STOCHASTIC AUTOMATA AS MODELS OF ADAPTIVE AND LEARNING CONTROLERS.**
K. S. Fu and G. T. McMurtry. Contract No. NSF G-2183; PRF 3810; June 1965.

TR-EE65-9 **SPEECH ANALYSIS.**
G. W. Hughes and J. F. Hemdel. Contract No. AF19(628)-305 with Air Force Cambridge Research Labs., Bedford, Massachusetts; PRF 3080-53-285.

TR-EE65-10 **ADVANCED CONTROL TECHNIQUES APPLIED TO LARGE FLEXIBLE LAUNCH VEHICLES VOLUME I.**
J. E. Gibson, V. Haas, J. C. Hill, L. E. Jones, A. S. Morse, S. Murtuza, A. M. Steinberg. Contract No. NASA 8-11416; NASAMSFC, Huntsville, Alabama; PRF 4005-52-285.

TR-EE65-11 **ADVANCED CONTROL TECHNIQUES APPLIED TO LARGE FLEXIBLE LAUNCH VEHICLES VOLUME II.**
J. E. Gibson, V. Haas, J. C. Hill, L. E. Jones, A. S. Morse, S. Murtuza, A. M. Steinberg. Contract No. NASA 8-11416; NASAMSFC, Huntsville, Alabama; PRF 4005-52-285. July 1965.

TR-EE65-12 **ADAPTIVE AND LEARNING CONTROL SYSTEMS-FINAL REPORT.**
J. E. Gibson and K. S. Fu. Contract No. AF AFOSR 62-531; Air Force Office of Scientific Research; PRF 3123-57-285; July 1965.

TR-EE65-13 **ANALYSIS AND DESIGN OF NONLINEAR CONTROL SYSTEMS-FINAL REPORT.**
J. E. Gibson, Principal Investigator; J. B. Pearson, Principal Investigator; Authors-J. B. Pearson, J. R. Rowland, G. N. Saridis, and P. H. Swain. Contract No. AF 29(600)-3566, Air Force Missile Development Center, Holloman Air Force Base; PRF 3304; August 1965.

TR-EE65-14 **AN ADAPTIVE PATTERN RECOGNITION MACHINE USING NEURON-LIKE ELEMENTS.**
K. S. Fu and W. C. Lin. Contract No. NSF Grant GP-2183; PRF 3810-50-285; August 1965.

TR-EE65-15 **ESTIMATION OF PROBABILITY DENSITY AND DISTRIBUTION FUNCTIONS.**
G. R. Cooper and J. A. Tabaczynski. Contract No. NSF Grant G-18997; PRF 2974; August 1965.

TR-EE65-16 **LOWER BOUNDS ON THE THRESHOLDS OF SUBHARMONIC OSCILLATIONS.**
D. R. Anderson and T. N. Trick. Contract No. National Science Foundation Grant GK26; PRF 4108, September 1965.

TR-EE65-17 **AN APPLICATION OF STOCHASTIC AUTOMATA TO THE SYNTHESIS OF LEARNING SYSTEMS.**
K. S. Fu and R. W. McLaren. Contract No. National Science Foundation Grant GP-2183; PRF 3810, September, 1965.

TR-EE65-18 **A UNIFIED N-PORT SYSTEM THEORY**
L. O. Chua and B. J. Leon, National Science Foundation Grant GK-26, PRF 4180, September, 1965.

TR-EE65-19 **ON RECEPTION OF SIGNALS FOR CHANNELS HAVING MEMORY**
J. C. Hancock and R. W-L. Chang, National Science Foundation Grant GP-2898, PRF 3955, October, 1965.

RECENT RESEARCH PUBLICATIONS
SCHOOL OF ELECTRICAL ENGINEERING
PURDUE UNIVERSITY

TR-EE65-20 LEARNING THEORY APPLIED TO COMMUNICATIONS
Dwight F. Mix and John C. Lindenlaub, Air Force Contract AF33(615)-2620, PRF #4218-53-285, October, 1965

TR-EE65-21 LEARNING PROBABILITY SPACES FOR CLASSIFICATION AND RECOGNITION OF PATTERNS WITH OR WITHOUT SUPERVISION
E. A. Patrick and J. C. Hancock, National Aeronautics and Space Administration Contract NsG-553 PRF #3823-52-285, November, 1965

TR-EE66-1 TOWARD BRAIN MODELS WHICH EXPLAIN MENTAL CAPABILITIES – (Report No. I)
R. J. Swallow, Support: E. E. Department Research

TR-EE66-2 ON THE ASYMPTOTIC STABILITY OF FEEDBACK CONTROL SYSTEMS CONTAINING A SINGLE TIME-VARYING ELEMENT
Z. V. Rekasius and J. R. Rowland, NASA Institutional Grant (SUB-UNDER NRG 14-005-021) PRF #4220-52-285, January, 1966

TR-EE66-3 ANALOGUE DEMODULATION ON A FINITE TIME INTERVAL
J. C. Hancock and P. W. Brunner, NSF Grant #GP-2898, PRF #3955-50-285, April, 1966

TR-EE66-4 STEADY STATE ANALYSIS OF LINEAR NETWORKS CONTAINING A SINGLE SINUSOIDALLY VARYING ELEMENT.
B. J. Leon and J. V. Adams, Grant #GK26, PRF #4108-50-285, May, 1966

TR-EE66-5 CYBERNETIC PREDICTING DEVICES
A. G. Ivakhnenko and V. G. Lapa. Translated by Z. J. Nikolic, April, 1966

TR-EE66-6 ON THE STOCHASTIC APPROXIMATION AND RELATED LEARNING TECHNIQUES
K. S. Fu, Y. T. Chien, Z. J. Nikolic and W. G. Wee, National Science Foundation GK-696, PRF #4502, April, 1966

TR-EE66-7 JOINTLY OPTIMUM WAVEFORMS AND RECEIVERS FOR CHANNELS WITH MEMORY
J. C. Hancock and E. A. Quincy, NSF GP-2898, PRF 3955 and NASA NSG-553, PRF 3823, June 1966

TR-EE66-8 AN ADAPTIVE PATTERN RECOGNIZING MODEL OF THE HUMAN OPERATOR ENGAGED IN A TIME VARYING CONTROL TASK
K. S. Fu and E. E. Gould, National Science Foundation Grant GK-696; PRF #4502, May, 1966

TR-EE66-9 ANALYSIS OF A WIDEBAND RANDOM SIGNAL RADAR SYSTEM
G. R. Cooper and Ronald L. Gassner, National Science Foundation Grant GK-189 PRF #4243, August, 1966.

TR-EE66-10 OPTIMAL CONTROL IN BOUND PHASE-COORDINATE PROCESSES
J. Y. S. Luh and J. S. Shafran, NASA/JPL No. 950670, PRF #3807, July, 1966

TR-EE66-11 ON THE OPTIMIZATION OF MIXTURE RESOLVING SIGNAL PROCESSING STRUCTURES
J. C. Hancock and W. D. Gregg, NSF GP-2898;-PRF #3955; NASA NGR-15-005-021;-PRF #4219, October, 1966.

TR-EE66-12 OPTIMAL CONTROL OF ANTENNA POINTING SYSTEM
J. Y. S. Luh and G. E. O'Connor, Jr., NASA/JPL No. 950670; PRF #3807, August, 1966

TR-EE66-13 DESIGN OF LARGE SIGNAL SETS WITH GOOD APERIODIC CORRELATION PROPERTIES
G. R. Cooper and R. D. Yates, Lockheed Electronics Company, Contract #29951, PRF #4195, September, 1966

TR-EE66-14 A PRELIMINARY STUDY OF THE FAILURE MECHANISMS OF CdSe THIN FILM TRANSISTORS
R. J. Schwartz and R. C. Dockerty, U.S. Naval Avionics Facility, N0016366C0096 A02, PRF #4850-53-285, September, 1966

TR-EE66-15 REAL-TIME ESTIMATION OF TIME-VARYING CORRELATION FUNCTIONS
G. R. Cooper and W. M. Hammond, NSF Contract No. GK-189; PRF #4243-50-285, October, 1966

TR-EE66-16 ON THE FINITE STOPPING RULES AND NONPARAMETRIC TECHNIQUES IN A FEATURE-ORDERED SEQUENTIAL RECOGNITION SYSTEM
K. S. Fu and Y. T. Chien, National Science Foundation GK-696, PRF #4502, October, 1966

TR-EE66-17 FAILURE MECHANISMS IN THIN-FILM RESISTORS
H. W. Thompson, Jr. and R. F. Bennett, Naval Avionics Facility, Contract No. N0016366 C0096; Task Order No. A02, October, 1966

TR-EE66-18 DISTRIBUTION FREE, MINIMUM CONDITIONAL RISK LEARNING SYSTEMS
E. A. Patrick, Air Force Avionics Laboratory (AVWC), Contract AF 33 (615) 3768, November 1966